

**IZMIR KATIP CELEBI UNIVERSITY
GRADUATE SCHOOL OF NATURAL AND APPLIED SCIENCES**

**OPTIMIZATION OF FRICTION STIR SPOT WELDING PARAMETERS
WITH EXPERIMENTAL DESIGN METHOD AND INVESTIGATION OF THE
EFFECTS OF PROCESS PARAMETERS ON THE LAP JOINT STRENGTH
AND WELD MORPHOLOGY OF SIMILAR AND DISSIMILAR
THERMOPLASTICS: ACRYLONITRILE BUTADIENE STYRENE AND
POLYCARBONATE**

M.Sc. THESIS

Asil AYAZ

Department of Mechanical Engineering

DECEMBER 2019

IZMIR KATIP CELEBI UNIVERSITY
GRADUATE SCHOOL OF NATURAL AND APPLIED SCIENCES

**OPTIMIZATION OF FRICTION STIR SPOT WELDING PARAMETERS
WITH EXPERIMENTAL DESIGN METHOD AND INVESTIGATION OF THE
EFFECTS OF PROCESS PARAMETERS ON THE LAP JOINT STRENGTH
AND WELD MORPHOLOGY OF SIMILAR AND DISSIMILAR
THERMOPLASTICS: ACRYLONITRILE BUTADIENE STYRENE AND
POLYCARBONATE**

M.Sc. THESIS

**Asil AYZAZ
(Y180228009)**

Department of Mechanical Engineering

Thesis Advisor: Asst. Prof. Dr. Aydın ÜLKER

DECEMBER 2019

İZMİR KATİP ÇELEBİ ÜNİVERSİTESİ
FEN BİLİMLERİ ENSTİTÜSÜ

**DENEYSEL TASARIM YÖNTEMİ İLE SÜRTÜNME KARIŞTIRMA NOKTA
KAYNAK PARAMETRELERİNİN OPTİMİZASYONU VE PROSES
PARAMETRELERİNİN BENZER VE FARKLI TERMOPLASTİKLERİN
(AKRİLONİTRİL BÜTADİEN STİREN VE POLİKARBONAT)BİNDİRME
BAĞLANTI MUKAVEMETİNE VE KAYNAK MORFOLOJİSİNE
ETKİLERİNİN ARAŞTIRILMASI**

YÜKSEK LİSANS TEZİ

Asil AYZ
(Y180228009)

Makine Mühendisliği Ana Bilim Dalı

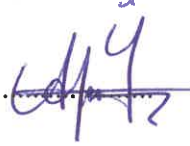
Tez Danışmanı: Dr. Öğr. Üyesi Aydın ÜLKER

ARALIK 2019

Asil AYAZ, a **M.Sc.** student of **IKCU Graduate School Of Natural And Applied Sciences**, successfully defended the thesis entitled “**OPTIMIZATION OF FRICTION STIR SPOT WELDING PARAMETERS WITH EXPERIMENTAL DESIGN METHOD AND INVESTIGATION OF THE EFFECTS OF PROCESS PARAMETERS ON THE LAP JOINT STRENGTH AND WELD MORPHOLOGY OF SIMILAR AND DISSIMILAR THERMOPLASTICS: ACRYLONITRILE BUTADIENE STYRENE AND POLYCARBONATE**”, which he prepared after fulfilling the requirements specified in the associated legislations, before the jury whose signatures are below.

Thesis Advisor :

Asst. Prof. Dr. Aydın ÜLKER
İzmir Katip Çelebi University

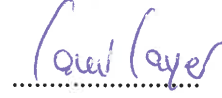
.....

Jury Members :

Assoc. Prof. Dr. Kutlay SEVER
İzmir Katip Çelebi University

.....

Assoc. Prof. Dr. Sami SAYER
Ege University

.....

Date of Submission : 27.11.2019

Date of Defense : 27.12.2019

To my family,

FOREWORD

First and foremost, I would like to thank my advisor, Asst. Prof. Dr. Aydın ÜLKER for their invaluable guidance, support, and encouragement during my studies at Izmir Katip Celebi University. I would also like to thank Assoc. Prof. Dr. Sami SAYER for the helpful discussion.

I would like to thank my parents Naci and Sultan AYZ and my brother Anıl AYZ for their support during my all life.

Finally, I would also like to my thanks to all my friends and colleagues at Izmir Katip Celebi University for helping me and keeping my spirits up.

December 2019

Asil AYZ

TABLE OF CONTENTS

	<u>Page</u>
FOREWORD	vii
TABLE OF CONTENTS	ix
ABBREVIATIONS	xiii
LIST OF TABLES	xv
LIST OF FIGURES	xvii
ABSTRACT	xxi
ÖZET	xxii
1. INTRODUCTION	1
2. POLYMERS	3
2.1 Classification of Polymers and Molecular Structures	5
2.2 Thermosets	7
2.3 Thermoplastics	8
2.4 ABS	10
2.5 PC	13
3. JOINING OF POLYMERS	17
3.1 Adhesives	18
3.2 Mechanical Fastening.....	19
3.3 Welding	20
4. FRICTION STIR WELDING AND FRICTION STIR SPOT WELDING ...	23
4.1 Friction Stir Welding.....	23
4.2 Friction Stir Spot Welding	24
4.2.1 Types of Friction Stir Spot Welding Process.....	25
4.2.1.1 Plunge type FSSW	25
4.2.1.2 Refill FSSW	26
4.2.1.3 Swing FSSW	27
4.2.1.4 Stitch FSSW	28
4.2.1.5 Pinless FSSW	28
4.2.2 Process Parameters.....	29
4.2.3 Tool design for Friction Stir Spot Welding	30
4.2.4 Mechanical properties, microstructure and macrostructure of Friction Stir Spot Welds	31
4.2.5 Material flow	33
4.2.6 Advantages and disadvantages of FSSW	34
4.2.7 Areas of applications.....	35
5. FRICTION STIR SPOT WELDING OF POLYMERS	37
6. OPTIMIZATION AND DESIGN OF EXPERIMENT	49
6.1 Modeling and Optimization Techniques	49
6.2 Design of Experiment.....	51
6.3 The Taguchi Approach.....	52
6.4 Background and Overview	53

6.5 Methodology.....	54
6.5.1 Defining the problem	55
6.5.2 Selection of parameters and number of levels	55
6.5.3 Selection of appropriate orthogonal array	56
6.5.4 Performing the experimental run.....	60
6.5.5 Statistical analysis and S/N ratio calculations.....	60
6.5.6 Confirmation test.....	63
6.6 Advantages and Disadvantages of Taguchi Method	63
7. EXPERIMENTS.....	65
7.1 Materials and Method.....	65
7.1.1 Acrylonitrile butadiene styrene (ABS) and Polycarbonate (PC)	65
7.1.2 Experimental setup for Friction Stir Spot Welding.....	66
7.1.3 Friction Stir Spot Welding Tool.....	67
7.2 Preliminary research and evaluation of experiments.....	67
7.3 Determination of FSSW Parameters and Levels for Taguchi Method.....	68
7.4 Selection of Taguchi Orthogonal Array	69
7.5 Experimental Design Matrix	70
7.6 Process Preparations.....	71
7.6.1 Manufacturing of sheets for FSSW.....	71
7.6.2 Fixing of the clamping apparatus	71
7.6.3 Setting of the FSSW tool.....	72
7.6.4 Fixing the (work adaptor plate) plates on the clamping apparatus	72
7.6.5 Setting of the operating parameters.....	73
7.7 Manufacturing of Welded Joints	74
7.7.1 Tool Rotation.....	74
7.7.2 Pre-Heating.....	75
7.7.3 Plunging	75
7.7.4 Stirring.....	76
7.7.5 Tool Retraction.....	76
7.7.6 Cooling and cleaning of the FSSW tool.....	76
7.7.7 Completion of experiments in the experimental design matrix	76
7.8 Characterization of Welded Joints - Lap Joint Shear Load Tests	77
7.8.1 Preparation of tensile test samples	77
7.8.2 Marking of Measuring Points of Tensile Test Samples	78
8. RESULTS.....	81
8.1 Results of Taguchi Methods for Lap Joint Shear Load	81
8.1.1 Signal-to-noise (S/N) ratio analysis	82
8.1.2 Response tables of S/N ratios and main effects plots.....	83
8.1.3 Response tables of means and main effect plots	87
8.1.4 Normal probability plot of residulas	91
8.1.5 Analysis of variance (ANOVA)	93
8.1.6 Fisher Test (F Test)	95
8.1.7 Contribution Rate of Welding Parameters	96
8.1.8 Optimum welding parameters	98
8.1.8.1 Optimum welding parameters and levels for ABS-ABS joints.....	99
8.1.8.2 Optimum welding parameters and levels for PC-PC joints	100
8.1.8.3 Optimum welding parameters and levels for ABS-PC joints	102
8.1.9 Calculations of optimum lap joint shear load for ABS-ABS, PC-PC and ABS-PC joints.....	104

8.1.10 Confirmation of experiments of FSSW of ABS-ABS, PC-PC and ABS-PC joints	105
8.1.11 Initial lap joint shear loads and improvements of ABS-ABS, PC-PC and ABS-PC joints	105
8.1.12 Calculations of initial lap joint shear loads of ABS-ABS, PC-PC and ABS-PC joints	110
8.1.13 Comparison of the results of ABS-ABS, PC-PC and ABS-PC joints ..	111
8.2 Visual examination and morphological analysis of welded joints of ABS-ABS, PC-PC, and ABS-PC	112
8.3 Effects of Process Parameters on Weld Strength for ABS-ABS, PC-PC and ABS-PC Joints.....	119
8.3.1 Effect of tool rotational speed	119
8.3.2 Effect of plunge depth	120
8.3.3 Effect of dwell time.....	121
8.4 Failure Modes of ABS-ABS, PC-PC and ABS-PC Joints	122
9. CONCLUSIONS	129
9.1 ABS-ABS joints	129
9.2 PC-PC Joints	130
9.3 ABS-PC Joints.....	131
REFERENCES.....	133
CURRICULUM VITAE.....	139

ABBREVIATIONS

HDA	: Housing Development Administration
ABS	: Acrylonitrile Butadiene Styrene
PC	: Polycarbonate
FSSW	: Friction Stir Spot Welding
FSW	: Friction Stir Welding
ICI	: Imperial Chemicals Industries
UV	: Ultraviolet
PE	: Polyethylene
PP	: Polypropylene
PA	: Polyamide
POM	: Polyoxymethylene
PEW	: Polyethylene wax
PBTF	: Poly (butylene 2,5-thiophenedicarboxylate)
PVC	: Polyvinyl Chloride (PVC)
PS	: Polystyrene (PS)
PMMA	: Polymethyl Methacrylate
PPO	: Polyphenylene
HIPS	: High Impact Polystyrene
3D	: Three Dimensional
SAN	: Styrene-Acrylonitrile
BPA	: Bisphenol A
CD	: Compact Disc
TWI	: The Welding Institute
SZ	: Stir Zone
PM	: Parent Material
TMAZ	: Thermomechanically Affected Zone
HAZ	: Heat Affected Zone
HDPE	: High Density Polyethylene
NC	: Neural Computing
GA	: Genetic Algorithm
RSM	: Response Surface Method
ANN	: Artificial Neural Networks
DOE	: Design of Experiments
TS	: Tabu Search
SA	: Simulated Annealing
OA	: Orthogonal Array
S/N	: Signal-to-Noise Ratio
ANOVA	: Analysis of Variance
CNC	: Computer Numerical Control
MSD	: Mean Square Deviation

LIST OF TABLES

	<u>Page</u>
Table 2.1 : Properties of crystalline and amorphous structures.	10
Table 3.1 : Classification of plastic joining methods [21].	18
Table 3.2 : Classification of plastic welding methods [25].....	20
Table 4.1 : Advantages of FSSW process [48].	34
Table 5.1 : Samples for different joint designs after tensile test [51].	39
Table 5.2 : Influence of tapered cylindrical pin on fractures [57].....	41
Table 6.1 : Selection of two-level orthogonal arrays [76].	58
Table 6.2 : Selection of three-level orthogonal arrays [76].....	58
Table 6.3 : Orthogonal arrays (three-level, L ₉) [72].	59
Table 6.4 : Orthogonal test arrays [78].	59
Table 7.1 : The main properties of ABS	65
Table 7.2 : The main properties of PC	65
Table 7.3 : Welding parameters and their levels for ABS-ABS joints	68
Table 7.4 : Welding parameters and their levels for PC-PC joints	69
Table 7.5 : Welding parameters and their levels for ABS-PC joints	69
Table 7.6 : L ₉ orthogonal array of welding parameters and levels for each joint	69
Table 7.7 : L ₉ orthogonal array for process parameters and their levels	70
Table 7.8 : L ₉ orthogonal array for process parameters and their levels	70
Table 7.9 : L ₉ orthogonal array for process parameters and their levels	71
Table 8.1 : Experimental results for lap joint shear load and calculated S/N ratios for ABS-ABS joints.	81
Table 8.2 : Experimental results for lap joint shear load and calculated S/N ratios for PC-PC joints.....	82
Table 8.3 : Experimental results for lap joint shear load and calculated S/N ratios for ABS-PC joints.....	82
Table 8.4 : Response table of S/N ratios (larger-is-better) for ABS-ABS joint.....	83
Table 8.5 : Response table of S/N ratios (larger-is-better) for PC-PC joint.....	85
Table 8.6 : Response table of S/N ratios (larger-is-better) for ABS-PC joint.....	86
Table 8.7 : Response table of means for ABS-ABS joint.	87
Table 8.8 : Response table of means for PC-PC joint.	89
Table 8.9 : Response table of means for ABS-PC joint.	90
Table 8.10 : ANOVA results for lap joint shear load of ABS-ABS joint.	94
Table 8.11 : ANOVA results for lap joint shear load of PC-PC joint.....	94
Table 8.12 : ANOVA results for lap joint shear load of ABS-PC joint.....	94
Table 8.13 : Fisher test values.....	96
Table 8.14 : Fisher test values for the FSSW parameters of ABS-ABS joint.....	96
Table 8.15 : Fisher test values for the FSSW parameters of PC-PC joint.	96
Table 8.16 : Fisher test values for the FSSW parameters of ABS-PC joint.....	96

Table 8.17 : Optimum process parameters and levels for FSSW of ABS-ABS joint.	99
Table 8.18 : Optimum process parameters and levels for FSSW of PC-PC joint...	101
Table 8.19 : Optimum process parameters and levels for FSSW of ABS-PC joint.	102
Table 8.20 : Initial welding parameters and levels of ABS-ABS joint.	106
Table 8.21 : Initial welding parameters and levels of PC-PC joint.	107
Table 8.22 : Initial welding parameters and levels of ABS-PC joint.	108
Table 8.23 : Comparison of the results for ABS-ABS joint.....	111
Table 8.24 : Comparison of the results for PC-PC joint.	112
Table 8.25 : Comparison of the results for ABS-PC joint.....	112
Table 8.26 : Nugget heights for ABS-ABS welded joints with the lowest, moderate, highest lap joint shear load.....	114
Table 8.27 : Nugget heights for PC-PC welded joints with the lowest, moderate, highest lap joint shear load.....	117
Table 8.28 : Nugget heights for ABS-PC welded joints with the lowest, moderate, highest lap joint shear load.....	119

LIST OF FIGURES

	<u>Page</u>
Figure 2.1 : The ethylene molecule [1].	3
Figure 2.2 : Linear polyethylene [2].	4
Figure 2.3 : Illustration of molecular structures: (a) linear, (b) branched, (c) crosslinked, (d) network [7].	5
Figure 2.4 : Common classification of polymers [9].	6
Figure 2.5 : Relationship between temperature and specific volume for an amorphous and a semicrystalline polymer [10].	7
Figure 2.6 : Monomer units of ABS [17].	11
Figure 2.7 : ABS terpolymer phases a) SAN b) Butadiene rubber [17].	11
Figure 2.8 : Specific properties of ABS (acrylonitrile, butadiene, and styrene).	12
Figure 2.9 : Structure of PC [19].	14
Figure 4.1 : A schematic drawing of FSW process [28].	23
Figure 4.2 : Illustration of FSSW process [32].	25
Figure 4.3 : A schematic of a plunge type FSSW (a) plunging (b) bonding (c) drawing out [28].	26
Figure 4.4 : Representation of the refill FSSW: (a) friction, (b) first and (c) second extrusion, (d) pull-out [34].	27
Figure 4.5 : The difference of tool path in a) Basic FSSW b) Swing FSSW [35].	28
Figure 4.6 : An illustration of Stitch FSSW [36].	28
Figure 4.7 : Pinless FSSW process: (a) plunging, (b) stirring, (c) drawing out [37].	29
Figure 4.8 : Cause and effect (Ishikawa) diagram for FSSW process	29
Figure 4.9 : Cross-section view of a typical FSSW sample [45].	32
Figure 4.10 : A micrograph view of a sectioned FSSW sample [46].	33
Figure 4.11 : A representation of material flow for FSSW process with the horizontal and vertical directions [47].	34
Figure 5.1 : The influence of dwell time on failure load [50].	38
Figure 5.2 : The influence of penetration depth on failure load [50].	38
Figure 5.3 : FSSW tool pin geometries and diameters (d) [52].	40
Figure 5.4 : Lap shear fracture loads of different pin profiles [52].	40
Figure 5.5 : Tool pin profiles used in FSSW: a) straight, b) tapered, and c) threaded cylindrical, d) triangular [53].	41
Figure 5.6 : Influence of pin geometries and rotational speed on lap shear fracture load [53].	41
Figure 5.7 : Failure types: a) the cross nugget, and (b) the pull nugget failure [55].	42
Figure 5.8 : FSSW tool profiles: (a) straight, (b) tapered, and (c) threaded cylindrical, and (d) square, (e) triangular and (f) hexagonal [56].	43
Figure 5.9 : Lap shear tensile loads of FSSW tool pins [56].	43
Figure 5.10 : Typical trend of plunging force torque [59].	44
Figure 5.11 : Cross sections of welded samples under varying welding conditions for (a) maximum strength and (b) minimum strength [59].	44

Figure 5.12 : An example of Built-up-edge [62].....	45
Figure 5.13 : Dimensions of triflute pin tool [63].....	46
Figure 5.14 : The views (a), (b) from the top (c), (d) of cross sections welded by triflute and cylindrical pin [63].	46
Figure 5.15 : A representation of the bonded area formation [63].....	47
Figure 5.16 : Fracture types: (a) shear, (b) pull lower, (c) upper nugget, (d) pull nugget with mixed shear fracture [63].	47
Figure 5.17 : Types of fractures: (a) cross nugget, (b) upper sheet and, (c) boundary [67].	48
Figure 6.1 : Classification of (a) modeling and (b) optimization techniques [71]....	51
Figure 6.2 : Taguchi Method Flow Chart [73].	55
Figure 7.1 : CNC milling machine	66
Figure 7.2 : Clamping apparatus	67
Figure 7.3 : The FSSW tool used in experimentations	67
Figure 7.4 : The dimensions (in mm) of the lap-shear tensile specimen for ABS-ABS, PC-PC, and ABS-PC joints.	71
Figure 7.5 : Welding positions of clamping apparatus, FSSW tool, and welding sheets for ABS-ABS joints.....	72
Figure 7.6 : Welding positions of clamping apparatus, FSSW tool, and welding sheets for PC-PC joints	73
Figure 7.7 : Welding positions of clamping apparatus, FSSW tool, and welding sheets for ABS-PC joints.....	73
Figure 7.8 : The stages of FSSW process	75
Figure 7.9 : A FSSW specimen of ABS-ABS joint	77
Figure 7.10 : A FSSW specimen of PC-PC joint.....	77
Figure 7.11 : A FSSW specimen of ABS-PC joint	77
Figure 7.12 : Illustration of lap shear test specimen	78
Figure 7.13 : Tensile test of a welded joint	79
Figure 7.14 : Tensile test result of a welded ABS-ABS joint	79
Figure 7.15 : Tensile test result of a welded PC-PC joint.....	80
Figure 7.16 : Tensile test result of a welded ABS-PC joint.....	80
Figure 8.1 : Tool rotational speed-lap joint shear load graph for S/N ratio of ABS-ABS joint.....	84
Figure 8.2 : Plunge depth-lap joint shear load graph for S/N ratio of ABS-ABS joint.	84
Figure 8.3 : Dwell time-lap joint shear load graph for S/N ratio of ABS-ABS joint.	84
Figure 8.4 : Tool rotational speed-lap joint shear load graph for S/N ratio of PC-PC joint.....	85
Figure 8.5 : Plunge depth-lap joint shear load graph for S/N ratio of PC-PC joint. .	85
Figure 8.6 : Dwell time-lap joint shear load graph for S/N ratio of PC-PC joint.	86
Figure 8.7 : Tool rotational speed-lap joint shear load graph for S/N ratio of ABS-PC joint.....	86
Figure 8.8 : Plunge depth-lap joint shear load graph for S/N ratio of ABS-PC joint.	87
Figure 8.9 : Dwell time-lap joint shear load graph for S/N ratio of ABS-PC joint. .	87
Figure 8.10 : Tool rotational speed-lap joint shear load graph	88
Figure 8.11 : Plunge depth-lap joint shear load graph	88
Figure 8.12 : Dwell time-lap joint shear load graph of main effects	88
Figure 8.13 : Tool rotational speed-lap joint shear load graph	89

Figure 8.14 : Plunge depth-lap joint shear load graph	89
Figure 8.15 : Dwell time-lap joint shear load graph	90
Figure 8.16 : Tool rotational speed-lap joint shear load graph	90
Figure 8.17 : Plunge depth-lap joint shear load graph	91
Figure 8.18 : Dwell time-lap joint shear load graph	91
Figure 8.19 : Normal probability and residual values graphs for weld strengths in ABS-ABS joints	92
Figure 8.20 : Normal probability and residual values graphs for weld strengths in PC-PC joints.....	92
Figure 8.21 : Normal probability and residual values graphs for weld strengths in ABS-PC joints.....	93
Figure 8.22 : Contribution rates of welding parameters for ABS-ABS joint.	97
Figure 8.23 : Contribution rates of welding parameters for PC-PC joint.	98
Figure 8.24 : Contribution rates of welding parameters for ABS-PC joint.	98
Figure 8.25 : Main effects plot of FSSW of ABS-ABS joint	99
Figure 8.26 : Main effects plot of FSSW of ABS-ABS joint (optimum plunge depth-lap joint shear load).....	100
Figure 8.27 : Main effects plot of FSSW of ABS-ABS joint	100
Figure 8.28 : Main effects plot of FSSW of PC-PC joint (optimum tool rotational speed-lap joint shear load).	101
Figure 8.29 : Main effects plot of FSSW of PC-PC joint (optimum plunge depth-lap joint shear load).....	101
Figure 8.30 : Main effects plot of FSSW of PC-PC joint (optimum dwell time-lap joint shear load).....	102
Figure 8.31 : Main effects plot of FSSW of ABS-PC joint	103
Figure 8.32 : Main effects plot of FSSW of ABS-PC joint (optimum plunge depth-lap joint shear load).....	103
Figure 8.33 : Main effects plot of FSSW of ABS-PC joint (optimum dwell time-lap joint shear load).....	104
Figure 8.34 : Initial tool rotational speed-lap joint shear load graph of S/N ratios for ABS-ABS joint.	106
Figure 8.35 : Initial plunge depth-lap joint shear load graph of S/N ratios	106
Figure 8.36 : Initial dwell time-lap joint shear load graph of S/N ratios	107
Figure 8.37 : Initial tool rotational speed-lap joint shear load graph of S/N ratios for PC-PC joint.	107
Figure 8.38 : Initial plunge depth-lap joint shear load graph of S/N ratios for PC-PC joint.	108
Figure 8.39 : Initial dwell time-lap joint shear load graph of S/N ratios for PC-PC joint.	108
Figure 8.40 : Initial tool rotational speed-lap joint shear load graph of S/N ratios for ABS-PC joint	109
Figure 8.41 : Initial plunge depth-lap joint shear load graph of S/N ratios for ABS- PC joint.	109
Figure 8.42 : Initial dwell time-lap joint shear load graph of S/N ratios for ABS-PC joint.	110
Figure 8.43 : The cross-sectional schematic view of the FSSW joint.	113
Figure 8.44 : The cross-sectional macrostructures of ABS-ABS welded specimens for a) worst parameters b) moderate parameters and c) optimum parameters.	114
Figure 8.45 : The cross-sectional macrostructures of PC-PC welded specimens for a) worst parameters b) moderate parameters and c) optimum parameters.....	116

Figure 8.46 : The cross-sectional macrostructures of ABS-PC welded specimens for a) worst parameters b) moderate parameters and c) optimum parameters.....	118
Figure 8.47 : Failure modes of ABS-ABS joints	123
Figure 8.48 : Failure modes of PC-PC joints	125
Figure 8.49 : Failure modes of ABS-PC joints	127

**OPTIMIZATION OF FRICTION STIR SPOT WELDING PARAMETERS
WITH EXPERIMENTAL DESIGN METHOD AND INVESTIGATION OF
THE EFFECTS OF PROCESS PARAMETERS ON THE LAP JOINT
STRENGTH AND WELD MORPHOLOGY OF SIMILAR AND DISSIMILAR
THERMOPLASTICS: ACRYLONITRILE BUTADIENE STYRENE AND
POLYCARBONATE**

ABSTRACT

Thermoplastics are widely used in engineering applications, especially in the automotive and aerospace industries due to their flexibility, high fracture toughness, stress/weight ratios, thermal insulation, and good fatigue resistance. In the present study, similar and dissimilar joints of acrylonitrile butadiene styrene (ABS) and polycarbonate (PC) materials were friction stir spot welded by using a specially designed clamping fixture. In addition, a filler sheet was used to reduce the keyhole volume on different configurations of ABS and PC joints and improve the lap joint shear load-carrying capacity by analyzing the influences of tool rotational speed, plunge depth and dwell time on the weld. According to the design of experiments, the welding parameters were arranged Taguchi L₉ orthogonal array to determine the optimum levels of welding parameters. The quality of the welded specimens was examined depending on lap joint shear tests and morphological analysis of macrostructures. Using the analysis of variance (ANOVA) and the signal to noise ratio (S/N), influences of each welding parameter on the lap joint shear load were evaluated.

The significant parameters and the optimum combination level of welding parameters was achieved according to the ANOVA and the S/N ratio graphs. 800 rpm of tool rotational speed, 11.5 mm of plunge depth, 40 seconds of dwell time for ABS-ABS joints, 2400 rpm of rotational speed, 10.5 mm of plunge depth, 40 seconds of dwell time for PC-PC and 800 rpm of tool rotational speed, 10.5 mm of plunge depth, 20 seconds of dwell time for ABS-PC joint were found as optimum welding parameters.

Also, the results showed that the lap joint shear load was improved by about 21%, 15% and 57% for ABS-ABS, PC-PC, and ABS-PC joints, respectively.

Macrostructure examination plays an important role to evaluate the influences of welding parameters on joint strength. Using water jet cutting technique, weld morphologies were investigated as morphological analysis and visual comparisons.

Finally, the failure modes of the samples were observed for the highest, moderate and lowest lap joint shear loads as well as morphological analysis for similar and dissimilar joints of PC and ABS sheets.

**DENEYSEL TASARIM YÖNTEMİ İLE SÜRTÜNME KARIŞTIRMA
NOKTA KAYNAK PARAMETRELERİNİN OPTİMİZASYONU VE PROSES
PARAMETRELERİNİN BENZER VE FARKLI TERMOPLASTİKLERİN
(AKRİLONİTRİL BÜTADİEN STİREN VE POLİKARBONAT)BİNDİRME
BAĞLANTI MUKAVEMETİNE VE KAYNAK MORFOLOJİSİNE
ETKİLERİNİN ARAŞTIRILMASI**

ÖZET

Termoplastik malzemeler, mühendislik uygulamalarında özellikle havacılık ve otomotiv endüstrisinde, ağırlık gerilme oranları, ısı yalıtımı, esneklik, iyi yorulma direnci ve yüksek kırılma tokluğu özellikleri nedeniyle yaygın bir şekilde kullanılmaktadır. Bu çalışmada, akrilonitril bütadien stiren (ABS) ve polikarbonat (PC) levhaların benzer ve farklı bağlantıları, özel tasarımlı bir bağlama aparatı kullanılarak sürtünme karıştırma nokta kaynağı methodu ile birleştirilmiştir. Ayrıca, takım dönme hızının, dalma derinliğinin ve karıştırma süresinin kaynak üzerindeki etkilerini analiz ederek farklı konfigürasyonlardaki ABS ve PC kaynak bağlantılarının delik hacmini azaltmak ve kaynağın bindirme bağlantılı kopma yükünün taşıma kapasitesini arttırmak için bir dolgu plakası kullanılmıştır. Kaynak parametreleri, optimum proses parametreleri seviyelerini belirlemek için Taguchi L₉ ortogonal deney tasarımına göre ayarlanmıştır. Kaynaklı numunelerin kalitesi, bindirmeli bağlantı kopma testleri ve makro yapıların morfolojik analizlerine bağlı olarak incelenmiştir. Varyans analizi ve sinyal - gürültü oranı kullanılarak, her bir kaynak parametresinin bindirmeli bağlantı kopma yükü üzerindeki etkileri değerlendirilmiştir.

Önemli parametreler ve proses parametrelerinin optimum kombinasyon seviyesi, varyans analizine ve sinyal - gürültü oranı grafiğine göre elde edilmiştir. Optimum kaynak parametreleri 1000 devir/dakika dönme hızı, 11.5 mm dalma derinliği, 40 saniye karıştırma süresi ABS-ABS bağlantıları için, 2400 devir/dakika dönme hızı, 10.5 mm dalma derinliği, 40 saniye karıştırma süresi PC-PC bağlantıları için, 800 devir/dakika dönme hızı, 10.5 mm dalma derinliği, 20 saniye karıştırma süresi ABS-PC bağlantıları için bulunmuştur.

Ayrıca, sonuçlar bindirme bağlantılı kopma yükünün, ABS-ABS, PC-PC ve ABS-PC bağlantı parçaları için sırasıyla yaklaşık yüzde 21, 15 ve 57 oranında arttığını göstermiştir.

Makroyapı incelemesi, kaynak parametrelerinin bağlantı dayanımı üzerindeki etkilerinin değerlendirilmesinde önemli bir rol oynamaktadır. Kaynak morfolojisi, su jeti kesim yöntemi kullanılarak morfolojik analiz ve görsel karşılaştırmalar olarak incelenmiştir.

Son olarak, numunelerin kırılma modları, PC ve ABS levhalarının benzer ve farklı kaynak bağlantıları için morfolojik analizlerin yanı sıra, en yüksek, orta ve en düşük bağlantı kopma yüklerinde gözlenmiştir.

1. INTRODUCTION

This study was carried out to provide optimization of three welding parameters of friction stir spot welding, which is one of the methods of joining polymers. The success of the Taguchi method was demonstrated and deficiencies seen in many statistical experimental design studies were discussed in a holistic manner.

In the experiments, acrylonitrile butadiene styrene and polycarbonate sheets were used as polymeric materials. It was aimed to evaluate the obtained information in practice in the increasingly widespread applications of FSSW.

Process parameters, which are important criteria in terms of production economy, are optimized. While the experimental design was arranged to optimize tool rotational speed, plunge depth and dwell time, pre-heating time and plunge rate were kept constant.

The main objectives related to the design of the experiment:

- Systematic examination of Taguchi parameter design method in friction stir spot welding,
- Defining optimum welding performance by a specific combination of parameters in FSSW,
- Achieving the results at a certain level of statistical confidence through statistical data analysis and statistical test applications of the system design stages of the Taguchi method.

The study objectives:

- Investigate the influence of each FSSW parameters (tool rotational speed, plunge depth, dwell time) on the welded joints,
- To evaluate the combination of welding parameters for the highest lap joint shear load during the tests,

- Express the contribution of each welding parameter as a percentage on the weld strength and to determine the sensitivity of the change in weld strength in terms of the sensitivity of parameter changes,
- To create main effects plots and tables for weld strength optimization.

2. POLYMERS

The term "polymer" is used for plastics and a Greek word involving "poly" and "meros", simply meaning "many parts". Hence, a polymer is composed of long molecular chains and created by the synthesis of smaller molecules. After they transform polymers, the smaller units can be stated as "monomers".

In chemistry, polymers are generally organic and include in covalent carbon atoms. The existence of natural polymers extends from the early times of the world to the present. Examples of natural polymers include cellulose, lignin and natural rubber. The chemical reaction in which polymers are formed by the combination of monomers is called as *polymerization*. In addition, different chemical mechanisms have an important place in polymerization [1].

The polymerization process can be explained as conversion of ethylene into polyethylene, which is one of the most widely, produced polymers in the world. Ethylene molecule or monomer in the saturated form is shown in Figure 2.1.

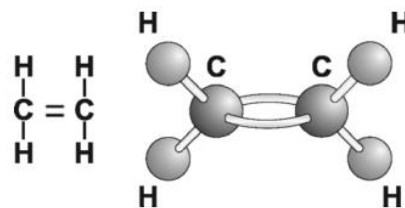


Figure 2.1 : The ethylene molecule [1].

Polymerizations can happen in different forms, but these type reactions consist of repetitive bonds of monomers. The monomers are held together by various heat combinations and the pressure of the catalyst, which allows them to bond by changing the chemical bonds. They generally form monomer chains, which are defined as polymers and are shown in a linear order. Figure 2.2 shows a linear polyethylene structure [2].

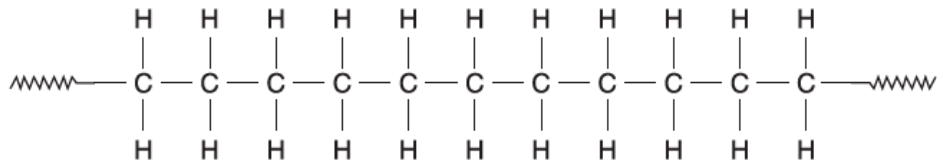


Figure 2.2 : Linear polyethylene [2].

Each individual chain may consist of several thousand to hundreds of thousand repeating mers or units in a polymer [3].

Before the 1920s, molecules having molecular weights were thought to be more than a few thousand. German chemist Staudinger tried to examine natural compounds (cellulose, rubber) and obtained a polymeric structure depending on the repetitive isoprene for rubber. He won the Nobel Prize in 1953 for his studies in the field of chemistry.

More precisely starting in 1930, polymer science saw its most significant developments with the first natural polymers were produced. Only a few years later, in 1933, ethylene was used in the high-pressure gas experiments conducted by Fawcett and Gibson in Australia, and they obtained a very small amount of waxy solids. Thus, polyethylene was discovered. Then, polyethylene was started to be used as one of the significant commodity polymers and several polymers have been found with different combinations of atoms. This provided building up various new methods of making polymers [4].

In the 1950s, it is also seen the advancement of polycarbonates as well as engineering thermoplastics polyimide, nylon, polysulfone, and phenoxy. They can compete with metals and many other materials due to their effective dimensional and thermal stability properties.

In recent years, a special polymer concept has been formed due to new polymerization methods, obtaining new and low cost monomers and structural properties of polymers. Polymers can now be produced from different elements of any quality in the final stage.

In the years ahead, the progress of polymers and polymer science will continue. The progress will be achieved through the development of new polymers as well as physical and chemical changes with all indications. In addition, development production methods will provide obtaining low priced productions. There are

environmental problems about recycling posed and the problems caused to critical conditions related to alloying of plastics in order to create a series of functional materials [5].

2.1 Classification of Polymers and Molecular Structures

The main feature distinguishing between polymers and other materials is that polymer samples consist of long molecules. The existence of these macromolecules significantly affects the properties of the polymeric material. For different polymer samples, there can be a considerable variation in the architecture of the individual molecules [6]. Advanced polymer synthesis methods allow important control over several molecular structures. For example, network, branched, linear, and crosslinked as depicted in Figure 2.3 [7].

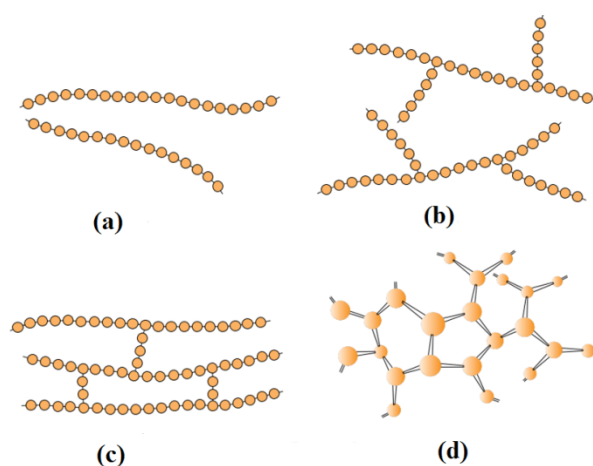


Figure 2.3 : Illustration of molecular structures: (a) linear, (b) branched, (c) crosslinked, (d) network [7].

There are extremely different polymers have been synthesized and more will be produced in the future [8].

All studies to classify polymers into different categories tend to be somewhat arbitrary. Classification is a useful method to display similar properties, which also has the advantage of reflecting the underlying molecular structure. One useful way and the most common classification is outlined in Figure 2.4 where they can be divided into 3 different classes; thermoplastics, thermosets, and rubbers. Furthermore, thermoplastic materials can be classified as crystalline or non-crystalline (amorphous) [6].

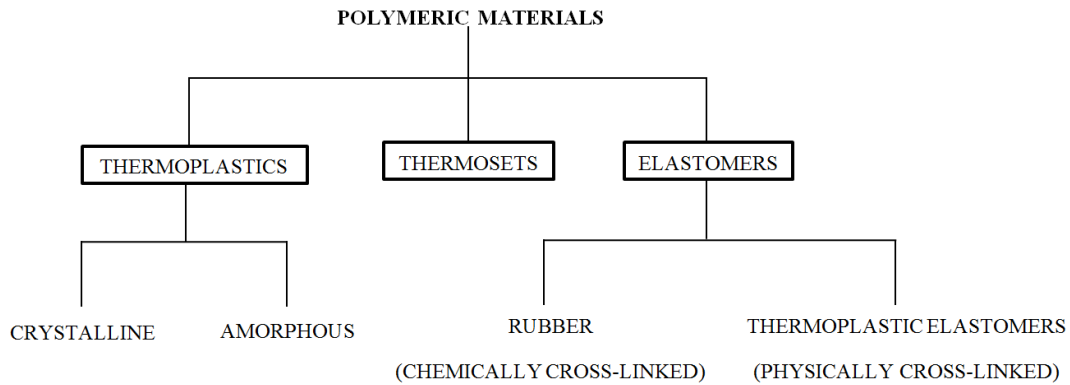


Figure 2.4 : Common classification of polymers [9].

Structurally, polymers are amorphous or semicrystalline. Due to the non-periodicity, amorphous materials do not have repeating unit cells in their structure as in crystalline. In amorphous material, the unit cell contains all atoms. It is difficult to understand the physical and chemical state of the amorphous materials in some special situations. Experimental and theoretical studies on amorphous materials are numerous, but most of the amorphous-state properties cannot be explained and the rest are open to discussion. This is a very difficult area due to the glass-liquid transition.

Glass transition is an important phenomenon to comprehend the effects of external conditions on physical changes for materials. There is great interest in food, medical, pharmaceutical, and polymer industries to detect and characterize this phenomenon. The point to be considered that the materials of relevance in these industries are similar issues on functionality and the glass transition phenomenon [1].

Materials having pure crystallines can be said to be well defined in terms of their melting temperature. Crystallin order is disappeared at the time of heating and the temperature at this point is the melting point. At some temperatures, the crystallinity of the polymers disappears. In amorphous and semicrystalline polymers, the relationship between specific volume and temperature is demonstrated in Figure 2.5. In case of cooling of polymer liquid, contraction is observed. this is caused by reduced thermal vibration and free field; because less field is sufficient for molecules in the loose state. Thermodynamic phase transformation occurs at the melting point (T_m) and the crystal structure is regular. A certain melting point is not defined in amorphous polymers. When the liquid crystalline phase is below the melting point, the polymer liquid proceeds contraction and thus falls to the glass transition

temperature (T_g). Liquid polymers become super-cooled liquids at temperatures below T_g as a result of their very high viscosity properties. Below T_g , the amorphous or glassy material is in a liquid state even if the viscosity is too high and can be separated from the crystalline phase.

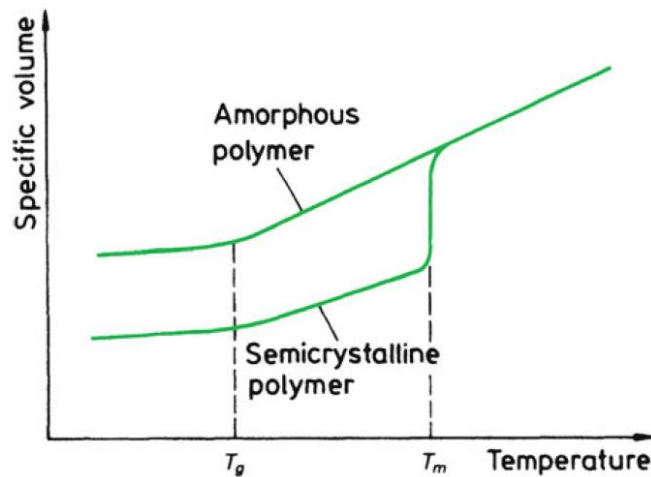


Figure 2.5 : Relationship between temperature and specific volume for an amorphous and a semicrystalline polymer [10].

The glass transition temperature (T_g) cannot be stated as a thermodynamic phase transformation. Many physical characteristics (heat capacity, expansion coefficient, viscosity, and elastic modulus) may change very quickly at T_g . Since T_g of polystyrene is about $100\text{ }^\circ\text{C}$, it is in a solid phase at room temperature. On the other hand, the reason why the rubber is flexible at room temperature is that its glass transition temperature is $-75\text{ }^\circ\text{C}$ [10].

2.2. Thermosets

Thermosetting polymers (more correctly called “thermosetting plastic materials”) are network polymers. While their initial state are in liquid or malleable phase, then they are transformed into a solid form. Many factors such as oxygen, heat, a reagent material, a catalyst, or UV light lead to a chemical reaction in the conversion process. An important point, conversion process of thermosets is irreversible without considering their initial state [11].

During their conversion, thermosets become harden continuously and softening is not observed upon heating. Adjacent molecular chains of network polymers have covalent cross-links. the chains, which is anchored by these bonds, withstand the

vibrational and rotational chain motions during the heat treatments are applied at the high temperatures. Therefore, softening is not carried out in the material throughout the heating process. When the material is heated to excessive temperatures, this results in severance of the cross-link bonds and degradation of the polymers. Thermosets are better than thermoplastics in terms of dimensional stability, stiffness and strength. Most of the crosslinked and network polymers are thermosetting such as epoxies, and phenolics [7].

Curing is defined as the conversion of a un-crosslinked thermosetting resin into a crosslinked network. For curing, the resin and an appropriate hardener is mixed and heated. However, the curing can occur even with little or without heat in some thermosetting systems (e.g., epoxies and polyesters). Since epoxies have better corrosion resistance, mechanical properties, and high-temperature properties than polyesters, they are often used instead of polyesters, but there are more difficulties of epoxies to handle because of higher viscosities. Vinyl esters are formed by reacting epoxies with an unsaturated acid such as acrylic acid or methacrylic acid. Thus, vinyl esters combine the advantages of epoxy resins with the lower viscosity and faster curing of unsaturated polyesters. Because vinyl esters involve a double bond at each end of the molecule, it is possible to cure vinyl esters in the same method as polyesters after being dissolved in styrene [12].

2.3. Thermoplastics

A nitrocellulose-based material was the first plastic and was obtained by Parkes in 1862 and Hyatt in 1866. The first known thermoplastic (a modified natural polymer) as known celluloid was formed by the addition of nitrocellulose to camphor and was used for movie film by 1900.

In the last decade, requirements for the polymer industry have been increasing day by day due to the rapid development and introduction of new and improved products. Plastics are the leader in the growth of engineering materials and followed by fibers and elastomers [13].

Nowadays, thermoplastics have gradually been replacing metals in the automotive and aerospace industries. Thus the cost for the industries has been significantly reduced. Weight reduction, flexibility, and thermal insulation properties are as

important as the reduction in production cost. Polymers also allowed new design opportunities. Due to the strict emission laws, polymeric materials have become more widely used than metals in the automotive industry [14].

Relatively weak Van der Waals force provides that very long chain-like molecules of a thermoplastic material are held together. When the material is subjected to heat, softening and flexibility are observed with the weakening of the forces between molecules. Thus, a viscous melting occurs at high temperatures.

It is observed solidification again when the material is allowed to cool. Softening by heat and solidifying on cooling for this cycle is possible to repeat more or less indefinitely and are highly favorable to these materials based on processing techniques. On the other hand, there are some disadvantages to thermoplastics, which have the problem of heat sensitivity. Thermoplastics are likened to wax because they can soften again upon heating and become solid after cooling.

Examples of thermoplastics include polymethyl methacrylate, polystyrene, polyethylene, polycarbonate, and polypropylene.

Thermoplastic materials can be examined in two basic classes. One of them is crystalline (ordered) and the other one is amorphous structure. In a molded plastic, molecular chains have complex physical properties and it is impossible for these plastics to be fully crystalline. There are also highly crystallizable plastics (nylon and polyethylene). However, it is probably more accurate to describe them as semi-crystalline. Some of the amorphous plastics are acrylic and polystyrene. Thermal history of the crystallizable plastics and hence the processing conditions used to obtain the molded product have a very important place for the presence of crystallization. Therefore, molding is very important mechanically for the crystallinity of thermoplastics.

During crystallization, molecules are packed closer and therefore plastics reach higher density. As described below (Table 2.1), amorphous and crystalline plastics have unique properties [15].

Table 2.1 : Properties of crystalline and amorphous structures [15].

Crystalline	Amorphous
Sharp melting point (most of the secondary bonds being broken down at the same time by the regular closed packed structure)	Broad softening range (the weak secondary bonds are broken down by thermal agitation of the molecules. The rate of creating throughout formless structure depends on producing broad temperature range for softening.)
High shrinkage (as the material changes the state from an amorphous state to a solid, the structure of the polymers form a closely packed, highly aligned structure and this results in a significant volume change due to the effect of high shrinkage.)	Low shrinkage (processing of all thermoplastics are performed in the amorphous state. During the solidification process, the random arrangement of molecules leads to little volume change and hence low shrinkage.)
High chemical resistance (the chemical attack on the material is prevented by the tightly packed structure.)	Low chemical resistance (chemicals can penetrate deep into the material and destroy many of the secondary bonds by means of the more random structure.)
Good fatigue and wear resistance (good fatigue and wear properties depend on a uniform structure of the material.)	Abrasion resistance and poor fatigue (random structure does not contribute much to these features.)
Acetal (POM) Polypropylene (PP) Polyamide (PA) Polyethylene (PE) Polyester (PEW, PBTF)	Polystyrene (PS) Polyvinyl Chloride (PVC) Acrylic (PMMA) Polycarbonate (PC)

2.4 ABS

ABS is the third member of a group of high impact composite materials after high impact polystyrene (HIPS) and PVC/nitrile rubber blends and depends on a thermoplastic matrix and a particulate rubber [16].

The discovery of ABS dates back to the 1940s. Although acrylonitrile-styrene copolymers had disadvantages, they were in use since the 1940s, but these copolymers caused the incorporation of the third monomer butadiene rubber. The properties imparted to the plastic by butadiene were higher strength and impact resistance. In the last years of the Second World War, high molecular mass butadiene - acrylonitrile copolymers and styrene-acrylonitrile copolymers were used to obtain polymeric bullet - proof sheets. The copolymer systems exhibit great impact resistance due to their thermoplastic flow properties at low levels. Examples of the first products of ABS are sheets, profiles, and pipes. It was the milestone for ABS that injection molding and graft polymerization techniques were developed. In 1950, ABS was used in various fields such as textiles, toys, fashion, and home appliances. In the early 1960s, it was decided to switch from cellulose acetate to ABS due to the

stability, toughness, and colorfast properties of ABS were better than cellulose acetate. In 1970, ABS was completely used instead of cellulose acetate in both Europe and North America. In 1990, additive manufacturing techniques were introduced and especially fused deposition modeling caused increasing use of ABS plastics for 3D printers in 1993.

Consequently, researches and developments in ABS systems aim to obtain new products and continue to offer promise for the future.

ABS consists of three monomers. These are acrylonitrile, butadiene, and styrene, and ABS is a thermoplastic of systematic polymerization of these monomers as shown in Figure 2.6. Two phases in the ABS terpolymer: a continuous phase of styrene-acrylonitrile (SAN) and a dispersed phase of polybutadiene as shown in Figure 2.7 a, b. It is possible to use ABS commercially since it has impact strength from medium to high levels, surface gloss and high heat distortion properties from low to high levels [17].

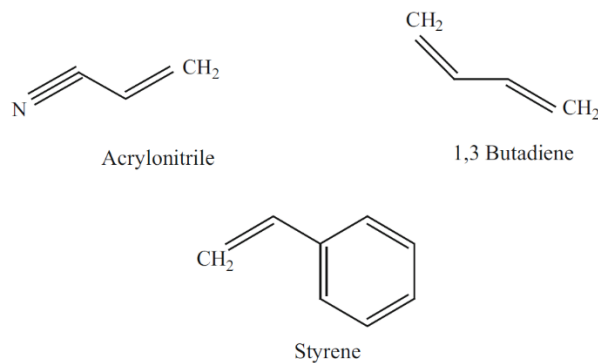


Figure 2.6 : Monomer units of ABS [17].

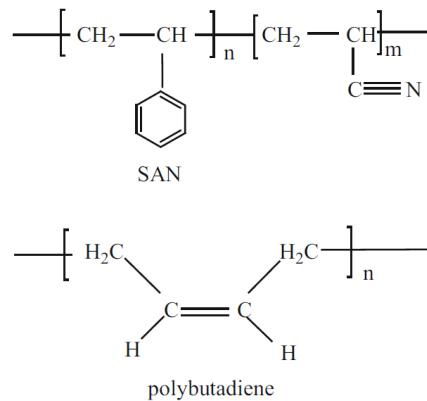


Figure 2.7 : ABS terpolymer phases a) SAN b) Butadiene rubber [17].

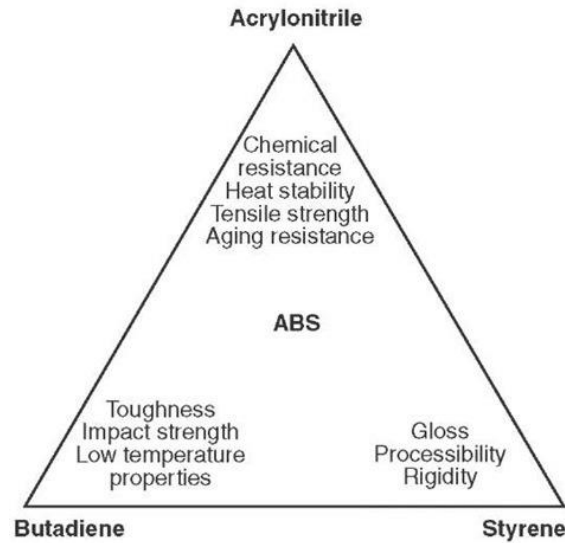


Figure 2.8 : Specific properties of ABS (acrylonitrile, butadiene, and styrene).

Some properties of ABS are adequate rigidity, good thermal stability, high toughness (even in cold conditions) and high resistance to chemical attack and environmental stress cracking. There are also other important properties such as durability, cheapness, and low coefficient of thermal expansion. The triangle in Figure 2.8 shows contributions to the final product of the properties and characteristics of ABS for each constituent acrylonitrile, butadiene, and styrene. ABS parts can be produced in very good surface quality due to the ease of molding of ABS, which does not show dimensional changes. Therefore, ABS has such a great combination that no other thermoplastics can possess. In addition, molecular and morphological factors are taken into consideration to decide the properties of ABS. Other critical factors are the type of rubber, the particle size of the rubber, the additive content, the matrix composition, and molecular mass. Besides all these, controlling the rubber particle size, distribution, and microstructure can be used to optimize the impact strength of ABS. The way to achieve greater toughness is to increase the content of butadiene rubber and the molecular weight of the uninoculated SAN phase. Surface gloss values can reach up to 95 percent, which may vary according to specific grade and mold or polishing roll surface. ABS and PC alloys (ABS-PC) can be used to obtain high toughness and balance thermal properties. Also, different products can be produced depending on user requests [17].

ABS has become the largest selling engineering thermoplastic because of its superior and balanced properties. ABS is like a “bridge” between commodity plastics and other high-performance engineering thermoplastics.

The highest rate of consumption of ABS is in major appliances; extruded/thermoformed door and tank liners take the first place in this field. The use of transparent ABS grades are preferred in refrigerator crisper trays. Examples of other applications in the appliance market are power tools, injection-molded housings for kitchen appliances, vacuums weepers, hairdryers, and sewing machines.

The second-largest market for ABS was transportation. General applications developed in this field are consoles, automotive instrument panels, doorpost covers, and other interior trim parts. It is possible to use ABS in automobile parts such as body panels, vacuum-formed seats, and radiator grilles. ABS plating grades play an important role in ABS sales and some of the applications are light bezels, mirror housings, knobs, decorative trim, and grilles.

In addition, miscellaneous applications of ABS are toy cars, boats, color photographic processor, miniature greenhouse or paddling pool, all plastic skis, pallets, parts for all plastic pumps, sandpit and crash helmets [16].

2.5 PC

At the end of the 1890s, the first polycarbonates were discovered by the reaction of hydroquinone and phosgene in pyridine. Some of the properties of the hydroquinone are crystalline, brittle and infusible.

The first aromatic polycarbonates were discovered and stimulated after the developments of aromatic polyesters such as polyethylene terephthalate. There was a period of about 50 years between first data about polycarbonates and the real discovery of useful thermoplastic aromatic polycarbonates. Polycarbonate chemistry was reexamined after the first aromatic polycarbonates of resorcinol and hydroquinone and it was discovered that the polycarbonates of bisphenol A (BPA) by the companies conducted independent investigations. This invented polycarbonate has unusual properties such as toughness, thermal stability, and transparency. Commercial production of polycarbonates started in Germany in 1958 and then in United States in 1960.

Since that time, extensive investigations have been carried out by several manufacturers to develop new products, blends, and processes for manufacturing of polycarbonates [18].

Polycarbonates belonging to the class of polymers are unusual and very useful. The majority of polycarbonate materials are based on bisphenol and characterized by the ---OCO--- heterochain unit. It is possible to make either from phosgene and bisphenol A (4,4'-dihydroxydiphenyl-2,2'-propane) or by ester exchange between bisphenol A and diphenyl carbonate as shown in Figure 2.8. However, more recently, “heat resistant” grades were launched possibly blended with BPA.

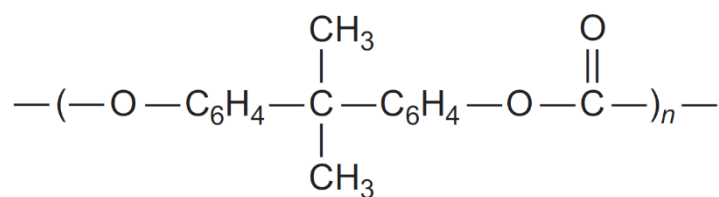


Figure 2.9 : Structure of PC [19].

In addition to having properties similar to acrylics such as amorphous and highly transparent thermoplastics, polycarbonates have excellent impact resistance, higher costs and lower resistance to UV and weather.

The reasons for preference of polycarbonates are their transparency, rigidity, impact and fatigue resistance, good creep behavior, insulating properties, dimensional stability, low moisture uptake, broad range of service temperatures (-100 °C up to +135 °C), food contact, and sterilization possibilities for appropriate grades. Thus, application areas of polycarbonates are transparent technical parts, optics, protection devices and esthetic.

Polycarbonates may have drawbacks in some cases due to their sensitivities to light and hydrolysis, requiring efficient protection for outdoor exposure; fire behavior, environmental stress cracking and attacks by chemicals such as bases, oils, chlorinated solvents, and ketones. The cost, which is determined by the performances, is higher than that of acrylic and the commodities. Polycarbonates based on BPA have currently disadvantages and lead to problems for ecology [19].

The processing methods of polycarbonates are conventional injection molding and extrusion. The applications where it is generally used are business machine housings,

machinery housings, automobile tail-light lenses, telephone parts, and unbreakable glass applications [20].

The total PC consumption may differ from country to country. For example, application areas of polycarbonates can be divided into in Europe as follow:

- Glazing and sheets - 32% (aircraft, roofs of verandas, sight glasses, boats)
- Electric electronic - 22% (optical media, computer, coil bobbins, connectors)
- CDs - 18%
- Automotive and transport - 9% (automotive lighting, exterior parts, bumpers)
- Appliances and consumer goods - 6% (electrical chargers, battery boxes, mobile phones)
- Medical and health care - 3% (lenses, instrument covers, handles, medical tubing)
- Bottles and packaging - 3% (baby bottles, water dispensers, water bottles)
- Leisure and safety - 3% (face shields, safety helmets)
- Miscellaneous - 4% (traffic lights, garden equipment, furniture, sporting goods) [19]

3. JOINING OF POLYMERS

The ideal design for polymer engineering is to produce one piece without any assembly process. On the other hand, the polymeric parts must be joined to each other or the metallic parts due to the mechanical limitations and other considerations. When several measures are taken and the established procedures are followed, the joining process becomes an efficient production method.

The most important step in the production of polymers and polymeric composite components is joining. Therefore, joinings are necessary always when part integration cannot be achieved due to complexity and high costs, different materials are used in the same component, disassembly, and repair of damage is required.

For a production cycle, joining is usually the final stage. Application of any polymer or composite material can be influenced by the effectiveness of the joining operation. Different joining techniques are applied to polymers. A classification of joining of polymer methods is illustrated in Table 3.1. In plastics and composites, joining techniques can be divided into three major categories: mechanical fastening, adhesive and solvent bonding, and welding [9].

Mechanical joining includes the fasteners, such as screws and it can use integrated design elements such as snap-fit or press-fit joints. In adhesive bonding, an adhesive is placed between the parts in order to bond the parts and transmit the load through the joint. In the welding process, polymer is heated and softened at the interface to provide polymer intermolecular diffusion and chain entanglements across the interface to obtain the weld strength during cooling and resolidification of the melt. Mechanical joining and adhesive bonding may be preferred for joining plastics with other materials, such as wood or steel.

Welding is limited to joining of same plastics or dissimilar but compatible plastics. Each method can be used in different applications. It is possible to classify plastics into two major groups, thermosets, and thermoplastics. Polymer molecules of

thermosets include primary chemical bonds, which form a three-dimensional structure. Since it is not observed softening or melting on heating for thermosets, they cannot be welded. Therefore, only adhesive bonding and fastening is appropriate as joining technique for thermosets. In thermoplastics, chemical bonds held together long polymer molecules or chains.

After heating, the polymer chains are free to form flow and diffusion as a result of weakening and breakage of the secondary bonds. Therefore, thermoplastics can be welded. Also, mechanical fastening and adhesion can be used to join thermoplastics [21].

Table 3.1 : Classification of plastic joining methods [21].

Mechanical Joining	Adhesive Bonding	Welding
Screws Snap Fit Press Fit Bracket Bolt Rivet Staple	Cross Linking Solvent Hot Melt	Thermal Mechanical Electromagnetic

3.1. Adhesives

Nowadays, new products are obtained by combining special new materials on the basis of their combination and properties. Polymers, ceramics, metals, rubber, cork, and combinations of any of these materials can be joined by adhesives. Adhesive bonding can be used in high technology industries such as aerospace, electronics, aeronautics, and automotive and in traditional industries such as packaging, construction, and sports. Adhesives have more advantageous properties than other joining methods and continue to be a good alternative for engineering applications. Low structural weight, lower manufacturing cost, and improved damage tolerance are some of these advantages. However, important problems of adhesive joinings such as reliability and large-scale applicability by the industries need to be eliminated. Before these problems, the joint strength under bad conditions and the durability are the most important issues. In terms of safety, it is necessary to use mechanical fasteners as a safety precaution for adhesively bonded structures. The result of such applications leads to heavier and more costly components. Therefore,

reliable and predictive methods can be developed in order to use materials and adhesives more efficiently [22].

In summary, adhesives have very strong advantages: bonding nearly any plastic by using correct adhesive, suitable for thermoset materials as well as thermoplastic materials, ease of use, very short curing times, little operator training and joint efficiencies up to 90%.

However, there are serious drawbacks of adhesives: releasing toxic fumes during use and cure, protective apparatus to use, surface preparation to provide a safety joining, depending on worker skill, difference in behavior between the cured adhesive and the base material [23].

3.2 Mechanical Fastening

Fastening is defined as mechanical connection of distinct parts by using a foreign body. The most common examples of fasteners are rivets, staples, screws, bolts, brackets, snap-fits, and clamps. Mechanical fastening can either be permanently closed or consist of joints that can be reopenable. Although they are simple processes, they need remarkable labor and often external parts. In addition, because of the high-stress concentrations around the fasteners, these connections often do not perform excellent performance [23].

Snap fits, screws, spring clips, and metal inserts are used for operable joints. Hot staking and rivets are used to provide permanent joints. In plastics, snap fits are used to provide a versatile fastening mechanism, which is ideal for ease of molding in complex geometries. A snap-fit can lock on into a recess due to consisting of a snap-on lug. A plastic spring is used to keep in place the lug and the spring is the plastic cantilevered arm for attaching the lug to the body. In order to increase the number of opening and closing of this type of connection, it can be designed based on the fatigue of the plastic spring. Snap-fit joints are preferred for rapid assembly applications but they are not used for load-bearing applications. Recently, there are analyses to increase their load-carrying capacity and life by improving the design of snap fits [24].

3.3 Welding

In the joining of polymeric materials, the fundamental processes of mechanical fastening or integral mechanical attachment, adhesive bonding, and welding or "thermal bonding" can all be used but brazing, soldering, and weld-brazing are not used. adhesive bonding is provided by using thermal spraying in some situations and by applying thermoplastic adhesives to polymeric substrates. Weld-bonding is an application process, at least for thermoplastics. However, weld bonding has not been used commercially and may offer few if any distinct advantages. From past to present, if polymeric materials have been used to create semi-structural and structural parts, they have most likely been thermosetting polymers, with or without reinforcement such as epoxy and epoxy glass used in different applications. The ways to join these polymers are mechanical fastening and adhesives. Some properties of thermoplastic have increased interest due to easier processing, recyclability and better impact resistance than thermosetting polymers. Although fasteners and adhesives are the methods for joining of thermoplastics, they require an alternative joining technique since these polymers have reversibly softening property upon the heating and hardening upon cooling processes that is namely "welding" or "thermal bonding". Generally, heating methods are used to define the classification of welding processes. In the welding of plastics, there are many methods: spin, ultrasonic, hot plate, vibration, laser/infrared are the most common (Table 3.2) [25].

Table 3.2 : Classification of plastic welding methods [25].

Thermal Welding	Mechanical (Friction) Welding	Electromagnetic Welding
Laser Hot Gas Hot Plate Extrusion Infrared	Spin Linear Ultrasonic Vibration Friction Stir Friction Stir Spot	Resistance Induction Microwave Dielectric

In welding of polymers, softening and fusion occur by heating at the interface. Molecular forces in thermoplastics, thermosets, and elastomers determine the weldability of plastics. The thermosets form irreversible cross-linking reactions since they are reactive during processing and curing. There are only two methods of bonding thermosets and elastomers: mechanical fastening and adhesive bonding. When sufficient heat is supplied to activate the mold and welding samples, the thermoplastics are recycled. The fusion welding is more sensitive to surface

contamination and different materials. The purpose of the fusion welding or the use of solvents is to provide the joining of soluble polymers. According to previous studies, the most common welding technique for thermoplastics is fusion welding. Diffusion may occur when the glass transition temperature in amorphous polymers and the melting temperature in crystalline polymers are exceeded. There are various methods to weld thermoplastics. Mechanical motion generate thermal energy, at the joint. While convection, radiation and conduction processes are examples of external sources, molecular friction is an example of internal source [26].

4. FRICTION STIR WELDING AND FRICTION STIR SPOT WELDING

4.1 Friction Stir Welding

Friction stir welding (FSW) can be stated as one of the upgraded conventional friction welding process. In 1991, FSW was invented and developed by The Welding Institute (TWI). During the past two decades, FSW is one of the most important and latest welding techniques for joining metals. At first, although FSW of aluminum alloys attracted much attention as the solid-state joining process, it has now extended to both thermoplastics and harder metals.

In the FSW technique, after a tool with a shoulder and a profiled pin is rotated, it slowly penetrates two rigidly fixed materials along the line of welding. A tool with cylindrical pin and a schematic representation of FSW are illustrated in Figure 4.1. When the load is applied, the tool shoulder is in firm contact with the top surface of the workpiece. The heat is needed to soften the material and obtained by friction and plastic deformation. The frictional heat is provided between the FSSW tool and the workpieces. The tool shoulder heats up more than the pin surface. Rotation of the tool pin results in the deformation or stirring, also leading to the generation of additional heat [27].

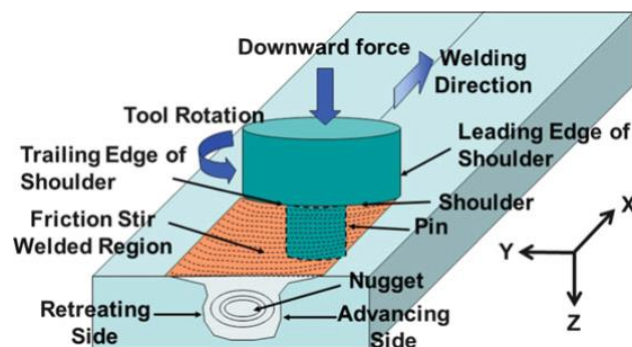


Figure 4.1 : A schematic drawing of FSW process [28].

The advantages of FSW are low temperature, low operation time, no preparation and machine/tool consumable costs, high joint quality and plastic deformation. This process can easily overcome the drawbacks compared to other welding techniques [29].

However, the FSW process only allows the production of linear welds and is not commercially suitable to join polymers.

As the production of plastics has increased, there has been a need to develop new joining methods to develop production and provide more consistent and integrity welds. Hot gas, butt welding, and extrusion are the current methods to weld thick thermoplastic materials, chemical storage containers, and tanks. The skill of the operator is effective in hot gas and extrusion welding for quality welding. In manufacturing large thermoplastic structures, vessels and high-quality welding, automatic FSW can replace these manual techniques. Although the FSW process for thermoplastics is not widely used commercially, it has an important position in the welding of plastics [30].

4.2 Friction Stir Spot Welding

FSSW was proposed by Mazda Corporation in Japan based on linear friction stir welding (FSW) in 1993 and was successfully used for the rear door and hood of the sports car Mazda RX-8. There are some technical deficiencies of the conventional resistive spot welding process for magnesium and aluminum alloys such as electrode wear, weld porosity, production efficiency in low levels and high energy consumption. So, the automotive industry is looking for different new joining methods. Some of them are rivets, adhesives, and toggle locks. The FSSW is a way of solution in terms of operation cost, weld quality and strength [31].

As stated above, FSSW is a point welding as well as a technique derived from FSW. In the FSSW process, a non-consumable tool makes a rotational movement and plunged into the workpieces for joining. After this step, the tool plunged into the chosen plunge depth and the feed stops. The tool continues to rotate in this position for a while called the dwell time or hold time. In the final step, the rotating tool is retracted. Basically, the tool penetration depth and dwell time are effective in determining the weld geometry, mechanical properties, material plasticization, and

heat generation of friction stir spot welding process. FSSW operation is illustrated in Figure 4.2.

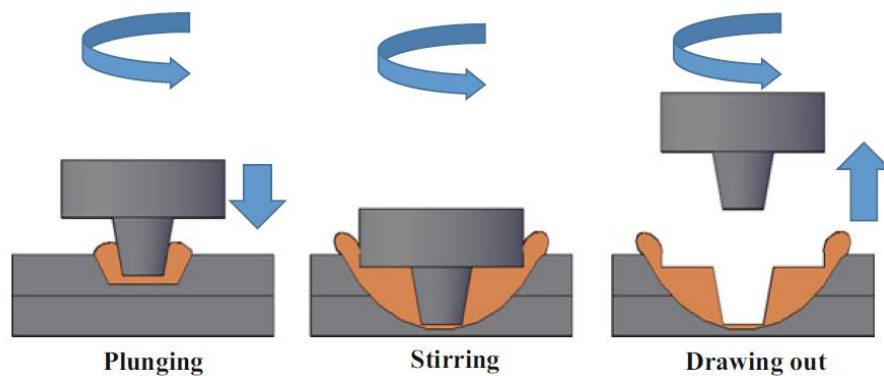


Figure 4.2 : Illustration of FSSW process [32].

In previous studies, it was stated that the heat of deformation and friction is mostly generated by the tool shoulder. In addition, material flow is provided by the tool pin. FSSW parameters include dwell time, plunge depth as well as the rotational speed and tool geometry. These parameters are important to determine the weld strength and surface quality of welded specimens [32].

4.2.1 Types of Friction Stir Spot Welding Process

In recent years, there have been some developments in FSSW. This welding method is classified into five categories:

1. Plunge type FSSW
2. The Refill FSSW
3. Swing FSSW
4. Stitch FSSW
5. Pinless FSSW

4.2.1.1 Plunge type FSSW

In current industries, plunge type FSSW is the most widely used. The first step of plunge type FSSW starts by rotating the tool with a protruded pin. Then, the tool is plunged into the materials from the top surface and reaches a predetermined depth. After a certain dwell time, the tool is retracted from the welded specimen and a keyhole is left. The friction heat occurs between the tool and the workpiece and softening begins. In circumferential and axial directions, the rotating pin leads to the

material flow. A solid bond region is formed by The pressure of tool shoulder and mixing of the plasticized material. Plunge type FSSW is illustrated in Figure 4.3 [33].

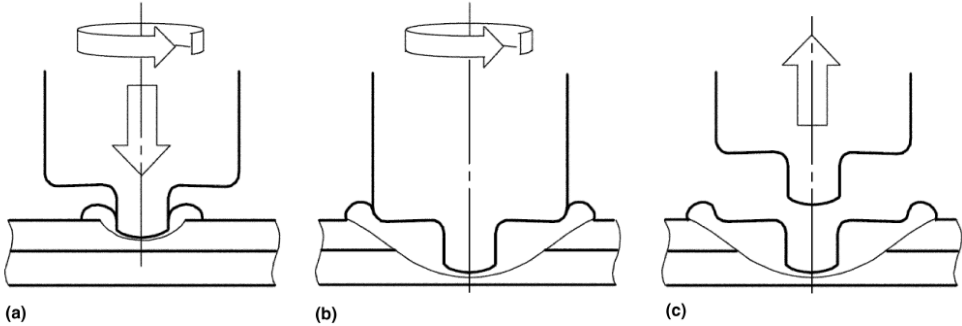


Figure 4.3 : A schematic of a plunge type FSSW (a) plunging (b) bonding (c) drawing out [28].

4.2.1.2 Refill FSSW

The refill FSSW was firstly developed in Germany. The refill FSSW includes four steps as shown in Figure 4.4 and the tool of the refill FSSW consists of three elements: sleeve, pin, and clamp. During the process, the clamp that restrict material flow holds the plates firmly. Although the rotational motion of the pin and sleeve in the same direction, it is also possible to provide axial rotation. The sleeve and pin, which move opposite to one another, form an area for the plasticized material. When reaching the predetermined penetration depth, the movement of the sleeve and pin are in the reverse direction, apply force to the displaced material to refill the keyhole completely. At the final step, the tool is retracted from the material. The process provides a flat surface and minimum material loss. Application areas of this process are limited. Because it is complicated, expensive and waiting times are long. Joint strength is improved by removing the keyhole [34].

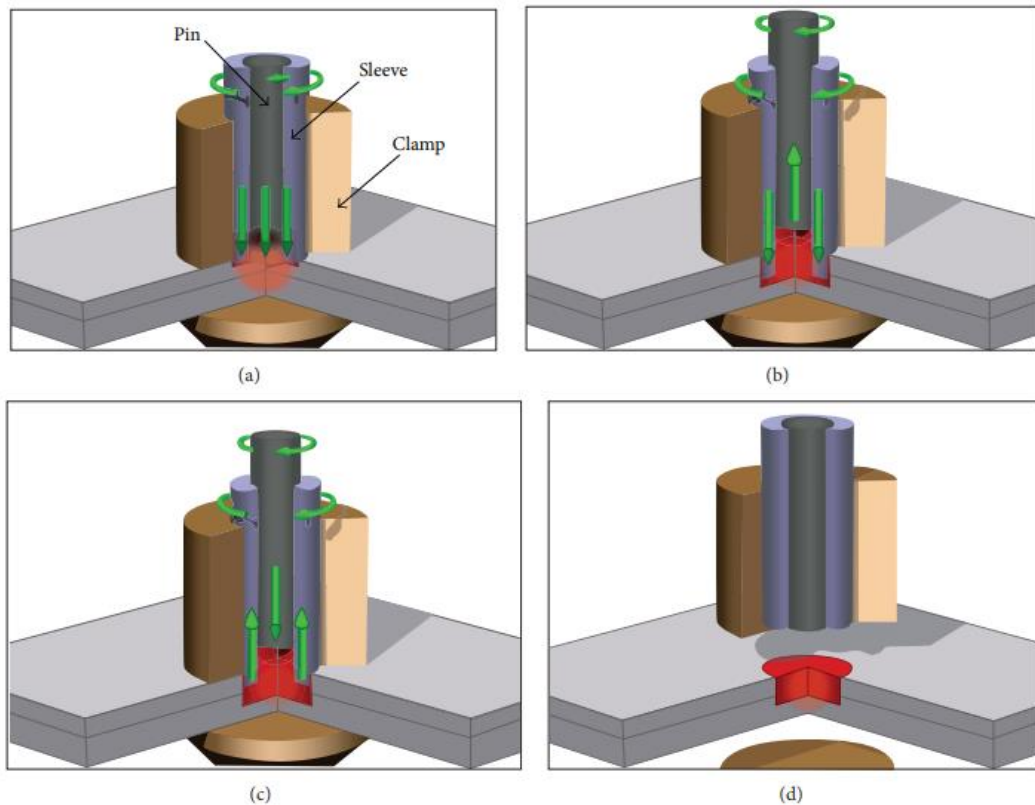


Figure 4.4 : Representation of the refill FSSW: (a) friction, (b) first extrusion (c) second extrusion, (d) pull-out [34].

4.2.1.3 Swing FSSW

Swing FSSW is another version improved by The Welding Institute (TWI). Basic FSSW and Swing FSSW are similar processes. A tool is forced into the sheets with the plunging movement for joining but during the dwelling phase, the tool moves in a linear direction with a small tilt angle and a large radius. There are three sub-paths (from 1 to 3) as depicted in Figure X, the tool moves in this predetermined path. While path 1 is the starting of the stirring, path 3 is the ending of stirring and path 2 represents one complete circular way. The tool makes a small tilt angle and is tilted during stirring. Finally, the rotating tool is retreated similar to Basic FSSW. In addition, Swing FSSW provides better joint strength and larger joint area than basic FSSW. The difference in tool travel path between basic FSSW and swing FSSW is depicted in Figure 4.5 [35].

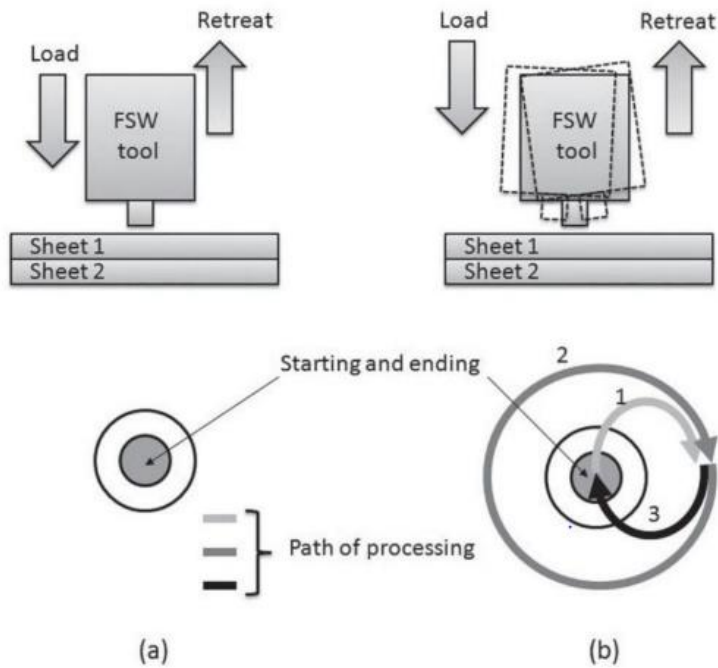


Figure 4.5 : The difference of tool path in a) Basic FSSW b) Swing FSSW [35].

4.2.1.4 Stitch FSSW

Stitch FSSW is one of the variations of FSSW as illustrated in Figure 4.6. In the stitch FSSW, the tool plunges into the materials and traverses linearly in a short distance before retracting. The aim of this method is to obtain joints with larger joining area for higher weld strength [32].

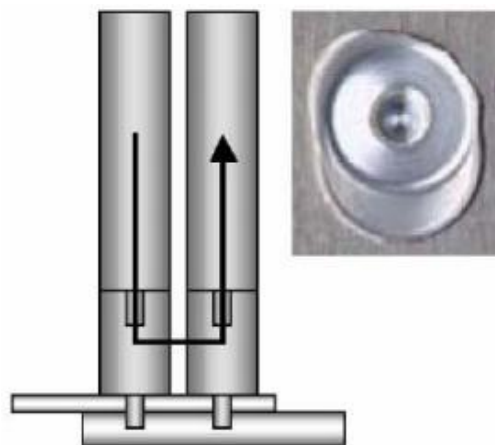


Figure 4.6 : An illustration of Stitch FSSW [36].

4.2.1.5 Pinless FSSW

Pinless FSSW process was invented by Tazokai. In 2009, a scroll groove tool without a probe has been proposed for this process. The advantages of the pinless tool are its simpler process and better appearance. Pinless FSSW is schematically

illustrated in Figure 4.7. (It is obtained high strengths due to leaving no impression or keyhole). As a result of recent studies, it is stated that high strength welded joints can be achieved with short dwell time in this method [34].

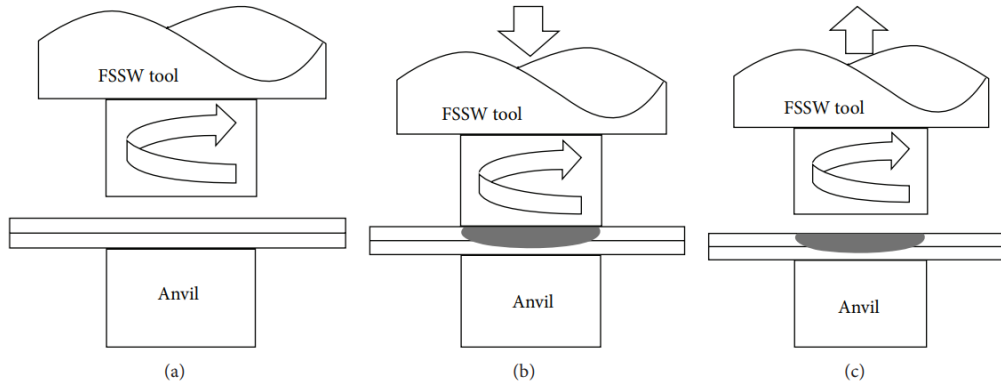


Figure 4.7 : Pinless FSSW process: (a) plunging, (b) stirring, (c) drawing out [37].

4.2.2 Process Parameters

In the literature, there are different process and material variables that influence the material flow and heat input for FSSW techniques as well as welding quality of thermoplastics in FSSW.

FSSW welding parameters (rotational speed, plunge depth and dwell time) that may affect the quality of welded joints are arranged as illustrated in Figure 4.8 by using Ishikawa diagram called cause and effect diagram. Rotation speed, plunge depth and dwell time as FSSW process parameters have a significant influence on the joint quality [38].

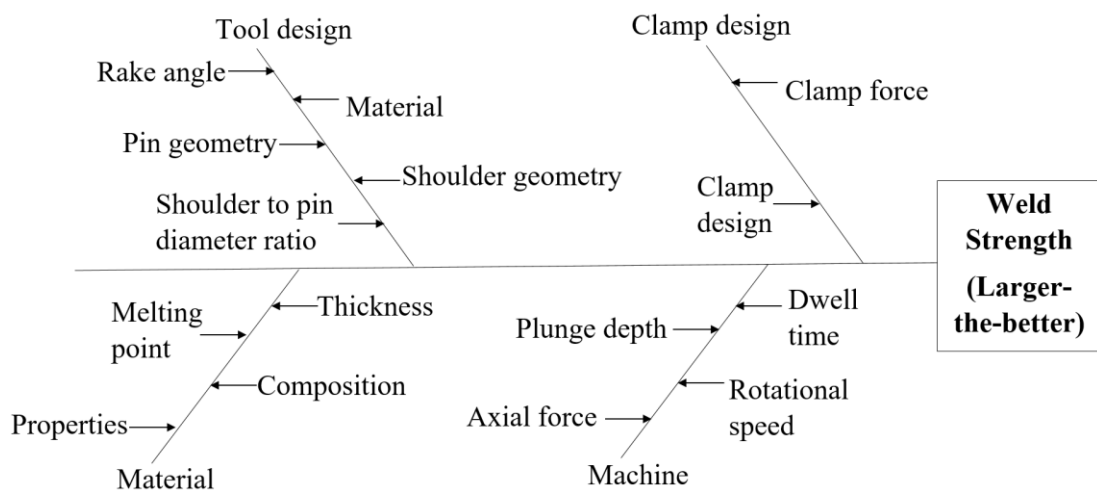


Figure 4.8 : Cause and effect (Ishikawa) diagram for FSSW process

It is recommended to perform the FSW of steels at low speed so that the material properties do not change. For example, FSW of low carbon steel should be welded lower than 500 rpm. While these are considered for linear FSW, they are not suitable recommendations for FSSW. There are very few studies on the rotational speed in FSSW. In terms of mechanical properties of welded specimens, joints with low rotational speeds are higher than joints with high rotational speeds. There is no comprehensive literature and the influences of rotational speed on the microstructure are not clearly understood [39].

The dwell time can be stated as the time interval, which the pin stays by rotating at its bottom position before retracting. The most effective process parameter for joint strength is the dwell time and followed by the rotational speed [40]. As expected, longer dwell time generate more heat because the tool spends more time in the weld area for generating heat. In the literature about FSSW, there are very few studies examining the effect of dwell time on steel. In the first studies, an improvement in shear strength was observed with increase in dwell time. Larger dwell times result in a larger bonded area in the joints.

In the literature, the plunge rate has not taken into consideration broadly. When the tool plunge into the materials, the heat increases between the tool and materials. As the plunge rate increases, the heating rate increases and the microstructure is more rapidly influenced in the starting of the FSSW cycle. However, the disadvantage of fast plunge speed is the wear of the tool due to the less softening of the material after the plunging. There is a great influence of plunge rate on the joint strength.

It is possible to define the plunge depth as the contact condition that exists between the welding sheets and tool shoulder during the FSSW operation. When the plunge depth is increased, a huge amount of material will be displaced with the effect of the tool shoulder. At very shallow plunge depths, the forging force will not be sufficient and a proper weld joint will not occur. Observation of several different kinds of flaws and defects depend on the poor selection of plunge depth [41].

4.2.3 Tool design for Friction Stir Spot Welding

A tool shoulder and a pin are the parts of FSSW tool. In the surface areas, the tool shoulder produces a large amount of deformational and frictional heat. The shoulder also applies forging pressure to the welding area. In thick materials, the majority of

the heat is produced by the pin. Furthermore, the pin provides the transport of the material. Various tool designs will change their influences on the joint properties of welded specimens [32].

It was investigated influences of different shoulder designs (concave and flat) on mechanical properties of joints and founded that fatigue life and shear strength of welded joints made using concave shoulder had higher than flat shoulder [42]. In addition, three different tool designs were investigated: a tool with a smooth pin and shoulder, with threaded pin and shoulder, and with only smooth pin. According to the results, very small energy of FSSW was used to create a stir zone and the threaded pin had a negligible effect on the energy produced through FSSW [43]. In another study, it was utilized three different tools with varying pin lengths to analyze influences on static strength. It was explained that as the pin length increase tensile shear strength increased when keeping the penetration depth of shoulder constant [44].

4.2.4 Mechanical properties, microstructure, and macrostructure of Friction

Stir Spot Welds

In FSSW, mechanical properties determine the quality of FSSW joints like the other joining techniques. Static and endurance strength of joints are analyzed with several mechanical tests. In the industry, some of these tests are commonly used and there is a standard for the tests. However, some of the tests are used in a particular industry. Cross tension, coach peel, and lap shear tests are some of the static strength tests. The direction of application of the load in the welding zone is variable, consequently leading to different stress concentration in the weld area. Automotive and aerospace industry generally uses the endurance tests in the case of cyclic fluctuations in the applied load.

Microstructure is examined to obtain important information about the metallurgy of the joint. Visual geometric information such as actual weld depth, hook formation, and nugget/stir zone can be achieved from cross-sectional figures. Grain size, texture and hardness profile are the other properties, which have been analyzed [33].

There are several microstructural regions and these require a proper nomenclature. The five characteristics of the FSSW include these regions: Stir Zone (SZ), Parent

Material (PM), Thermomechanically Affected Zone (TMAZ), Heat Affected Zone (HAZ), and Hook as illustrated in Figure 4.9.

Parent Material (PM) is the material away from the area where the weld is applied but there is still the possibility of exposure to the thermal cycling from process. Heat does not change the microstructure and mechanical properties.

Heat Affected Zone (HAZ) is an area close to the weld-center and subjected to a thermal cycle, which affects the microstructure as well as the mechanical property during welding. Also, it was not observed plastic deformation in this zone.

Thermomechanically Affected Zone (TMAZ) is the region where the material undergoes plastic deformation by the welding tool. Even if there is no recrystallization in this region, high plastic tension can be achieved for some materials. It is clear that there is a boundary between TMAZ and the recrystallized area.

Stir Zone (SZ) is the completely recrystallized region and the nearest area of the tool pin. In the stir zone, the grains are approximately equiaxed but the grains are smaller in the parent material.

The Hook is a characteristic feature of FSSW and a geometrical defect caused by the interface of the welding materials [45].

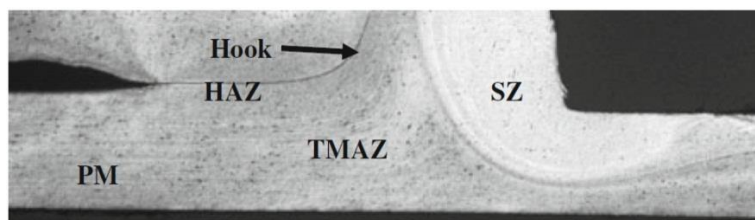


Figure 4.9 : Cross-section view of a typical FSSW sample [45].

It was examined macrostructure of FSSW for aluminum 6061-T6 lap-shear samples. In the weld, a keyhole was observed. The upper sheet thickness of the workpieces under the shoulder indentation decreased during the squeezing motion of the tool and the upper sheet expanded. Bending was observed along the shoulder indentation under the boundaries of the neighboring material. Furthermore, the squeezed out material is accumulated outside of the shoulder indentation. As stated before, three apparent regions of FSSW samples are shown in Figure 4.10 [46].

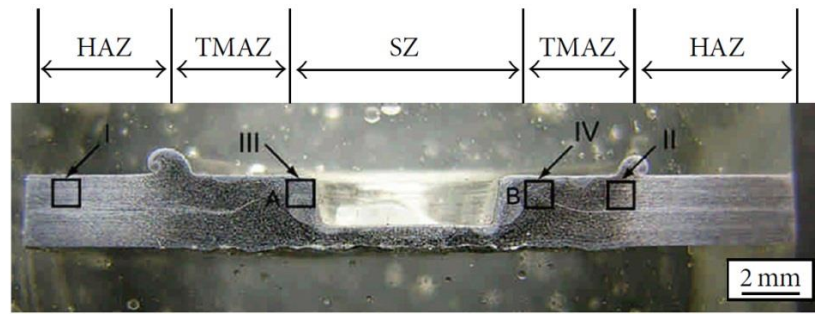


Figure 4.10 : A micrograph view of a sectioned FSSW sample [46].

4.2.5 Material flow

In the FSSW process, material flow can be observed by analyzing the flow pattern and distribution of the different materials. During FSSW, plasticized materials can be transported horizontally and vertically as illustrated in Figure 4.11. In the welding used a tool with threaded pin, the material under the shoulder is firstly moves along the pin root. Then, rotating threaded tool spirals downwards the material due to the dragging force. The material reaching the end of the pin is moved by a force both upwardly and outwardly and then moves again along a helical rotation path towards the pin. In all movements, the transport of the material is repeated several times at greater distances around the tool in order to form a stirring area. It has been observed that the upper and lower materials are joined at the root of the pin before the mixed materials move downwardly from the threads in the pin. The flow of material moving vertically and the formation of a mixed region around the pin is limited by only a smooth cylindrical pin. The term called "interlock" occurs between overlapped metal workpieces. As a result, it is recommended that threaded pin tool can be used to increase the stirring zone in the FSSW process [47].

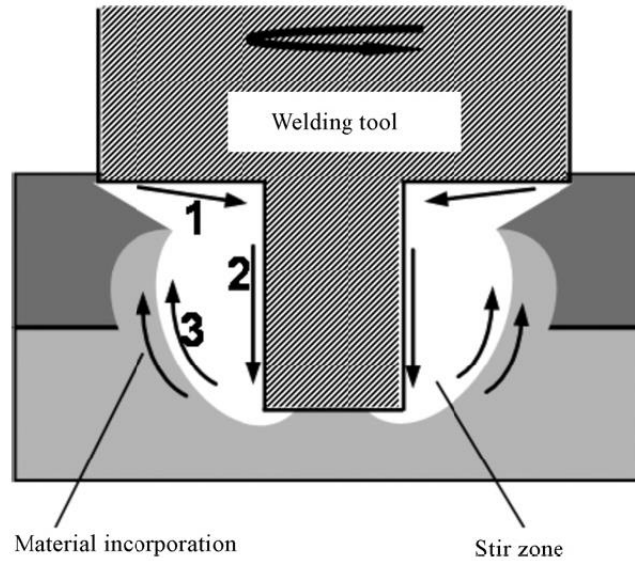


Figure 4.11 : A representation of material flow for FSSW process with the horizontal and vertical directions [47].

4.2.6 Advantages and disadvantages of FSSW

Similar to FSW, friction stir spot welding process has many advantages compared to other welding methods. Some of these are listed in Table 4.1. From the top model cars to the newest desktop computers, manufacturers benefit from FSW / FSSW processes in more areas. Despite these advantages, large process forces are required during FSSW process. Due to these forces in the FSSW process, large rigid robots must be used for welding.

Table 4.1 : Advantages of FSSW process [48].

Metalurgical benefits	Environmental benefits	Energy benefits
Solid-phase process Good dimensional stability and repeatability No loss of alloying elements Excellent mechanical properties in the joint area Fine recrystallized microstructure Low distortion Absence of solidification cracking	No shielding gas required Eliminate grinding wastes Minimal surface cleaning required Consumable material saving such as wire and rags No harmful emissions Environmental friendly	Improved materials use allow reduction in weight Short cycle times Decreased fuel consumption in lightweight aircraft, automotive and ship applications

Some problems of FSSW are as follows:

1. After the welding process, a keyhole formation in the welding area
2. Contact in a very small region
3. Difficulty in cleaning the oxide and impurities at the welding interface
4. Poor intermixed materials

There are other situations that make the development of FSSW difficult such as the high-speed, high-volume, and cost-conscious requirements of auto-body assembly lines [49].

4.2.7 Areas of applications

Applications in many different sectors and a variety of industries such as power generation, automotive, robotics, aerospace, nuclear and petrochemical have caused the growing of FSSW and FSW methods for similar and dissimilar materials. Thus, it is clear that the two welding methods are used in many industrial applications. Therefore, the investigation of optimization may allow the use in new areas to avoid the deficiencies of conventional welding methods due to they are solid-state welding technique [31].

5. FRICTION STIR SPOT WELDING OF POLYMERS

There are very few studies on the incorporation of polymers with FSSW, and published studies generally involve specific polymers. These investigations can be listed as follows:

- Polypropylene (PP) [50-54]
- High Density Polyethylene (HDPE) [55-57]
- Polycarbonate (PC) [58-62]
- Acrylonitrile butadiene styrene (ABS) [63-65]
- Polymethyl methacrylate (PMMA) / Acrylonitrile butadiene styrene (ABS) [66]

These studies can be divided into two categories according to the type of thermoplastic materials used in the FSSW process.

- Semi-crystalline thermoplastics (PP, HDPE) [50-57]
- Amorphous thermoplastics (ABS, PC, PMMA) [58-66]

The main parameters affecting the weld strengths are: rotation speed, dwell time, plunge depth and tool geometry. It was investigated the influences of dwell time and tool penetration depth on the weld strength for polypropylene sheets of 5 mm thickness. The experiment was performed at predetermined values for dwell time and tool penetration depth parameters. In the experimental results, the tensile failure load increased up to a certain point (80 s) with the increase in dwell time but then the load decreased slightly (Figure 5.1). Also, maximum tensile failure load was obtained at nearly 8 mm penetration depth. Excessive penetration depth led to decreasing of the weld thickness and tensile failure load (Figure 5.2) [50].

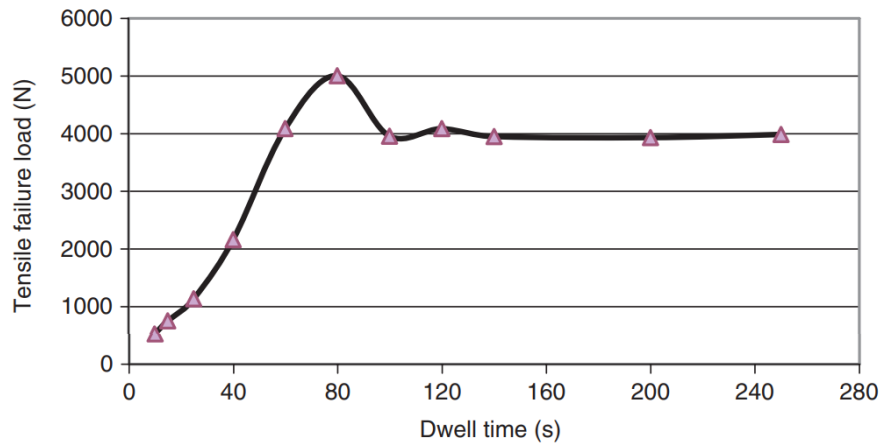


Figure 5.1 : The influence of dwell time on failure load [50].

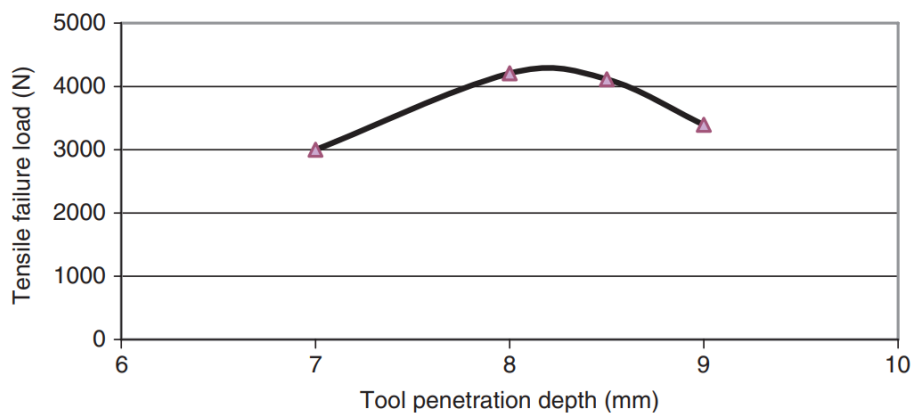


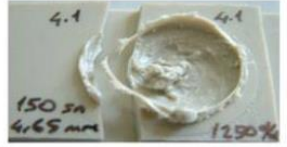

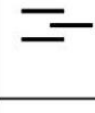



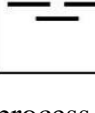





Figure 5.2 : The influence of penetration depth on failure load [50].

As stated in the joining of thermoplastics, there are three different methods: welding, fastening, and adhesive bonding. Two components could be joined rapidly by fasteners, however, a tight joint may not be achieved and localized stresses may cause them to move away from the thermoplastic. Unlike fastening, adhesive bonding can be preferred due to its permanent connection property and does not allow large stress concentrations. It was investigated that the joining of thermoplastics by FSSW, adhesive bonding, and hybrid joining as FSSW–adhesive bonding on different overlap configurations of PP sheets of 3 mm thickness. While maximum tensile forces were obtained in the welded specimens, minimum tensile forces were obtained in the adhered specimens. Furthermore, the highest tensile force was obtained in the type 2 design, while the lowest tensile force was obtained in the type 1 design. The failures were divided into three categories: occurred around the pin (mode 1), around the shoulder (mode 2) and at the edge of the welding area (mode 3) (Table 5.1). In type 1 and 2 as shown in the Table 5.1, failure modes 2 and 3 were observed. However, type 3 had a different failure mode of broken samples for

FSSW and weld bonded joints. The failure occurred in the base material. The failure was observed along the adhered line for adhesive-bonded specimens. Mode 1 indicated a weak joint and was not seen in the FSSW and weld bonded specimens [51].

Table 5.1 : Samples for different joint designs after tensile test [51].

Different Joint Designs		Adhesive Bonded	Friction Stir Spot Welded	Weld Bonded
type1				
type2				
type3				

The process parameters (plunge depth, dwell time, plunge rate, delay time, and rotational speed) and tool geometry of FSSW (pin length, pin profile, shoulder and pin diameter, shoulder concavity and pin angle) should be chosen optimally. In the literature, there are very few studies examining the influences of FSSW tool geometry on thermoplastic sheets. It was used four different pin profiles (tapered, threaded, and straight cylindrical, and square) and varying tool dimensions (shoulder diameter, pin length, shoulder angle, and pin angle) to investigate the tool geometry influences on FSSW of 4 mm thick polypropylene sheets (Figure 5.3). The highest fracture load was obtained with a tapered tool (Figure 5.4). The joint strength decreased along with an increase in the pitch length for the threaded pin. Therefore, weld quality and joint strength were significantly affected by the pitch length of threaded pins [52].

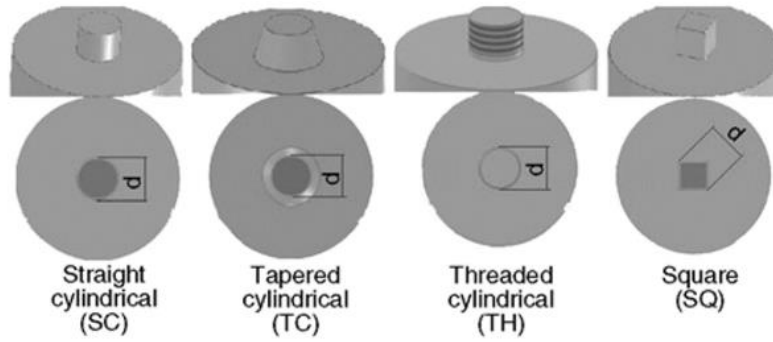


Figure 5.3 : FSSW tool pin geometries and diameters (d) [52].

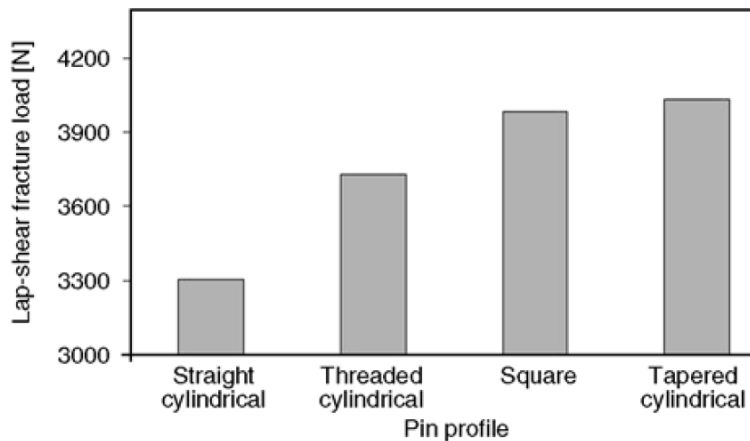


Figure 5.4 : Lap shear fracture loads of different pin profiles [52].

Another study to understand the effect of the FSSW parameters and tool pin profiles on weld strength was performed on 4 mm thick PP sheets. It was observed three different fracture modes: the cross-nugget, the mixed nugget and the nugget pull-out failure during the lap-shear tensile test. In the experiment, four different tool pin geometries were used (tapered cylindrical, triangular, straight cylindrical and threaded cylindrical) illustrated in Figure 5.5. In the study, while the range of rotation speed was between 360 r/min and 1400 r/min, the plunge depth was 5.7 mm, the dwell time was 120 s and 0.26 mm/s was the value of plunge rate. The influences of the pin geometry and the rotational speed on the joint strength were illustrated in Figure 5.6. When the rotational speed increased to 900 r/min, it was observed that the joint strength decreased due to the generation of the heat in the stir zone. As seen in Figure 5.6, when the tapered cylindrical pin was used, the maximum lap shear fracture load was obtained. Then, all FSSW operations were performed by the tapered cylindrical pin. Also, the fracture modes and macrostructures were observed (Table 5.2) [53].

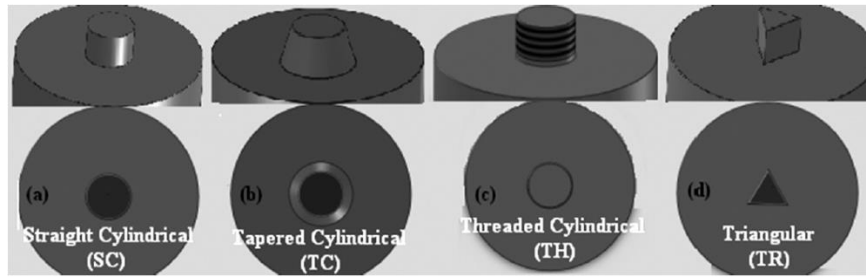


Figure 5.5 : Tool pin profiles used in FSSW: a) straight, b) tapered, and c) threaded cylindrical, d) triangular [53].

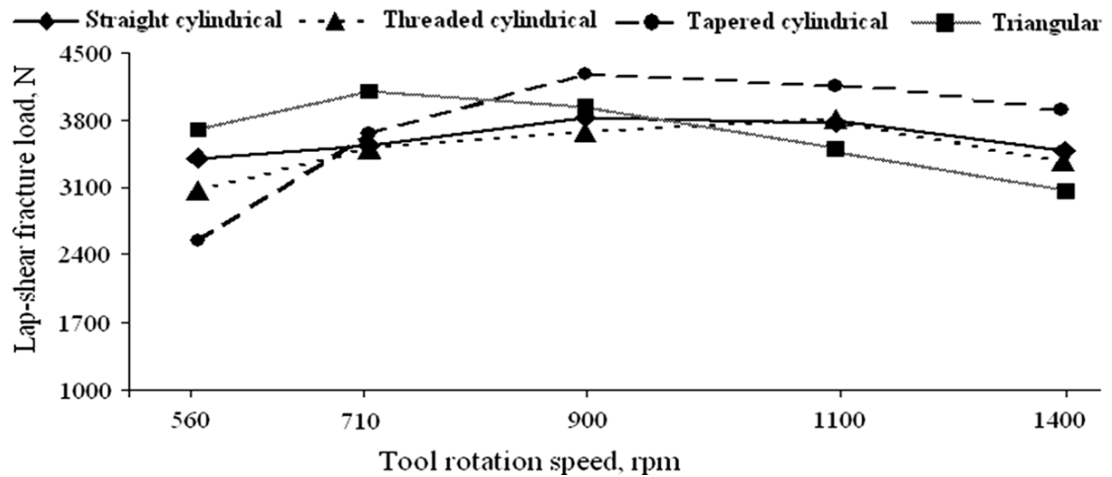


Figure 5.6 : Influence of pin geometries and rotational speed on lap shear fracture load [53].

Table 5.2 : Influence of tapered cylindrical pin on fractures [53].

Tool rotation speed (r/min)	Fracture mode	Macrostructure	Quality of weld-metal consolidation	Probable reason for the formation
360			very poor	Insufficient flow of the joining materials due to low heat
560			poor	Although there was insufficient heat, a weld was formed
710			better than in the previous case	Heat input is sufficient for a good-quality weld
900			very good	Heat input is sufficient for a good-quality weld
1120			good	Heat input is sufficient for a good-quality weld
1400			worse than in the previous case	Poor weld quality occurred due to excessive heat

There are not many studies about for FSSW of polymers applications using Taguchi approach. It was used the Taguchi method for finding optimum process parameters and the contribution of individual process parameters of FSSW of HDPE sheets with a thickness of 4 mm. Three levels of welding parameters (dwell time, plunge depth, and tool rotational speed) were selected and arranged according to the L₉ orthogonal array. As a result, the most effective factor was dwell time and followed by rotation speed. 60 s for dwell time, 6.2 mm for plunge depth, and 700 rpm for rotational speed were the optimum welding parameters. Furthermore, two failure morphologies were observed during tensile tests (Figure 5.7). The cross nugget and the pull nugget failure had a weakest and highest joint strength, respectively [55].

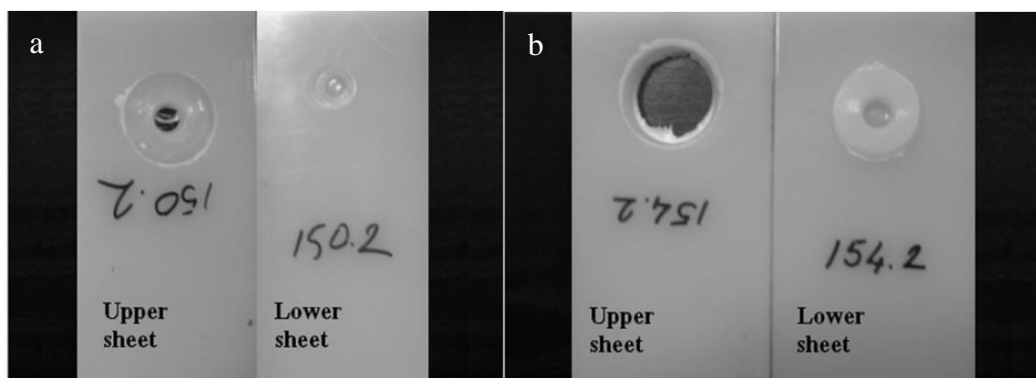


Figure 5.7 : Failure types: a) the cross nugget, and (b) the pull nugget failure [55].

One of the few studies about effects of FSSW tool geometries on polymers in literature has been examined for polyethylene. It was investigated the influences of FSSW tool properties and process parameters on weld strength in FSSW of polyethylene sheets in 4 mm thickness. In this study, threaded cylindrical, tapered cylindrical, straight cylindrical, triangular, square, and hexagonal (Figure 5.8) with varying shoulder geometries, concavity angle, pin angle, and pin length were selected as process parameters. It was observed that the nugget thickness and joint strength were affected significantly by the tool pin geometries. In addition, macrostructure and joint strength of the weld depend on optimum process parameters. While maximum tensile load was achieved with the tapered cylindrical pin, the minimum tensile load was obtained by the straight cylindrical pin profile (Figure 5.9) [56].

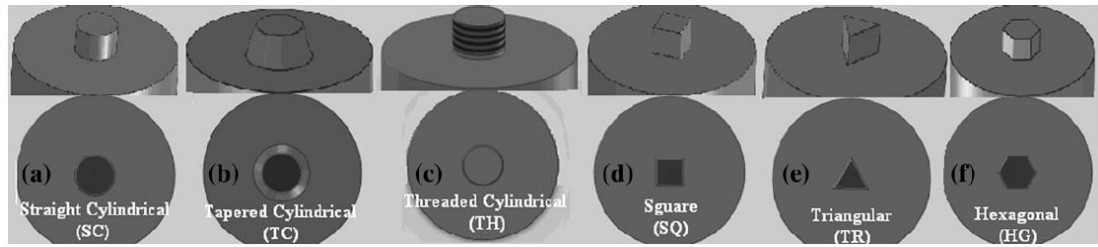


Figure 5.8 : FSSW tool profiles: (a) straight, (b) tapered, and (c) threaded cylindrical, and (d) square, (e) triangular and (f) hexagonal [56].

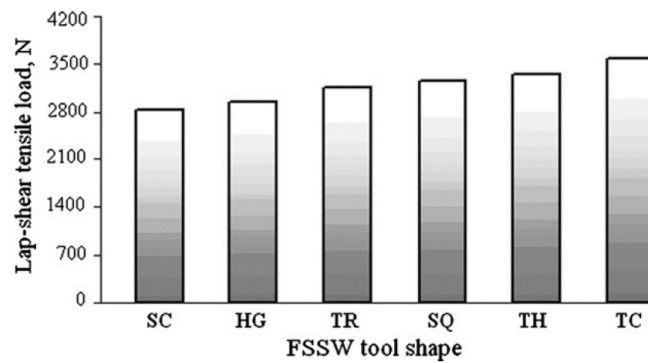


Figure 5.9 : Lap shear tensile loads of FSSW tool pins [56].

While the above-mentioned studies are about the FSSW of semi-crystalline thermoplastics (PE, PP), there are very few studies in the literature for amorphous thermoplastics (ABS, PC, PMMA). There are some investigations in FSSW of PC sheets in 3 mm thickness. In one of the studies, FSSW was applied to polycarbonate sheets for optimizing the process conditions and full factorial design was used in the experiments. FSSW parameters were chosen as rotational speed, plunge rate, waiting time, dwell time, and pre-heating time. It was found that the maximum plunging force (Point A, F_{max}) is obtained immediately after the surface contact with the upper sheet. The force begins to decrease and then the force remains constant until the tool shoulder reaches the surface of the upper sheet (Point D). This force can be called a steady-state force (F_{ss}). In addition, the point at which the pin contacts the surface of the lower workpiece is considered to determine this force (Point B). The stages of plunging forces are shown in Figure 5.10 [59].

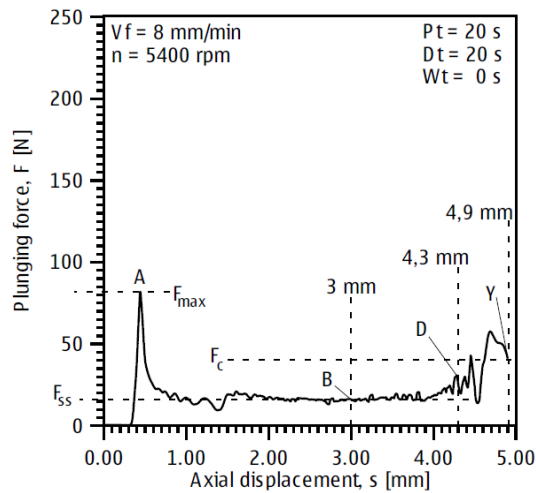


Figure 5.10 : Typical trend of plunging force torque [59].

While the lowest strength was obtained with plunge rate at high levels and preheating time, tool rotation speed, dwell time, and waiting time in low levels, the maximum strength was obtained with high levels of waiting time, dwell time, preheating time and plunge rate and tool rotation speed at low levels. The cross-sections of welded samples under varying conditions for maximum and minimum strength were shown in Figure 5.11 [59].

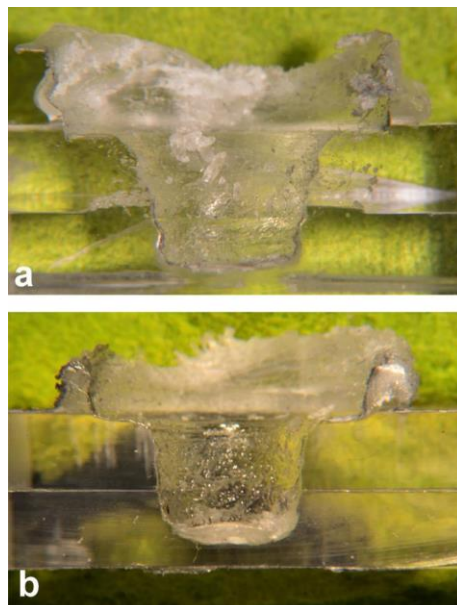


Figure 5.11 : Cross sections of welded samples under varying welding conditions for (a) maximum strength and (b) minimum strength [59].

In another study, FSSW of 3 mm thick PC sheets was investigated to find the most effective parameters. Experiments were arranged depending on two full factorial

designs. After that, a 3^3 optimization plan was conducted by the most relevant welding parameters for three levels. Polycarbonates tend to shrink more than other plastics. During cooling, internal cavities may increase depending on the shrinkage of polycarbonate. Tearing of the inner material leads to porosity. In low levels of waiting, dwell and pre-heating times caused the existence of Built Up Edge on the surface of the pin and shoulder as shown in Figure 5.12. This phenomenon affects the pin geometry. During the process, the plastic material is attached to the tool and the inner diameter of the welded sample decrease. Therefore, the Built Up Edge is an undesirable situation. In the chip zone, this formation produces higher temperatures and does not occur at higher preheating, dwell, and waiting times. While the tool rotational speed had the lowest effect on weld strength, the dominant effective parameter was the dwell time for FSSW of polycarbonate sheets. The influence of preheating time is negligible on joint strength. The dwell time, plunge rate and waiting time has an important influence on the joint strength [62].

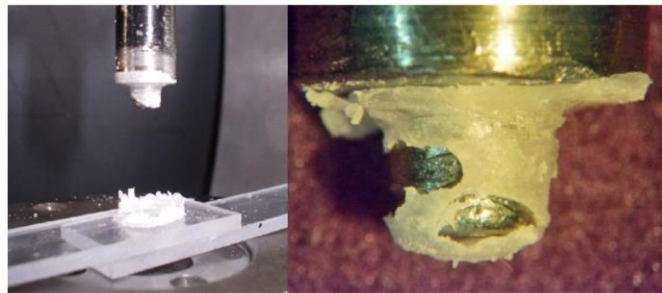


Figure 5.12 : An example of Built-up-Edge [62].

The common problem of FSSW is the characteristic keyhole forming in the weld zone. It plays an important role in mechanical tests. Researchers develop new welding tools to solve this problem. It was used a triflute pin tool to decrease the keyhole volume without using extra equipment (Figure 5.13). In addition, a simple clamping plate was utilized to assist fixing and perform the FSSW of ABS sheets in 4 mm thickness [63].

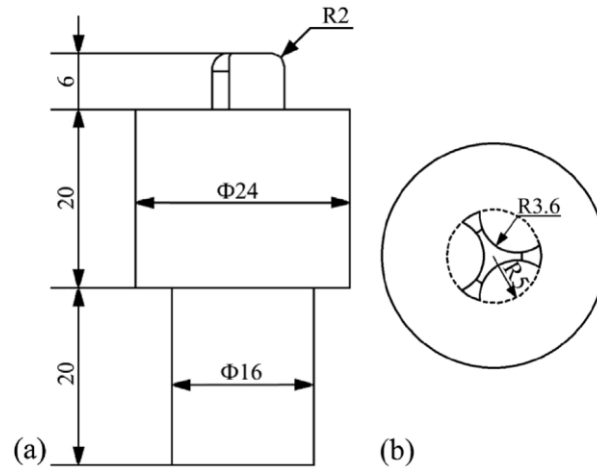


Figure 5.13 : Dimensions of triflute pin tool [63].

The cross-sections of the samples welded by triflute pin tool and cylindrical pin tool were shown in Figure 5.14. The triflute pin caused the formation of three columns and the keyhole volume decreased compared to the cylindrical pin. The ring was formed by a cylindrical pin tool and this ring was larger than that produced triflute pin tool due to the substitution of more material. Therefore, the triflute pin was more advantageous than the cylindrical pin [63].

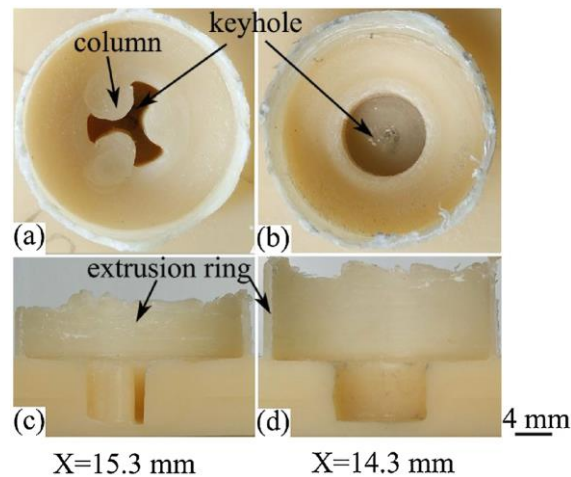


Figure 5.14 : The views (a), (b) from the top (c), (d) of cross sections welded by triflute and cylindrical pin [63].

The simple material flow of the FSSW process of ABS sheets was illustrated schematically in Figure 5.15. Centrifugal and the extrusion force leads to vertical material and dragging of the material flow in the stir zone (SZ). Then, it was observed the formation of nugget due to mixing of the lower and upper sheet material. TMAZ was the close region to the nugget because the material was less

softened in the region depend on the conducted heat from the stir zone. As depicted in Figure 5.15b and 5.15c, plastic deformation and bonding occur in the lapped surfaces, respectively.

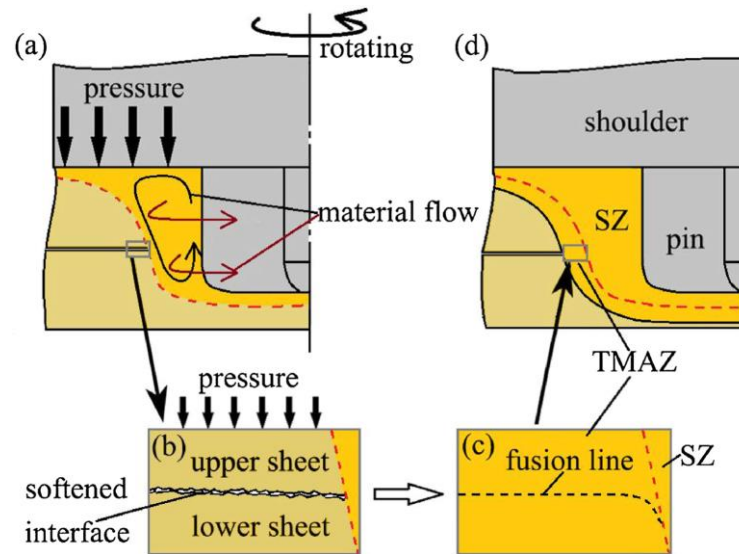


Figure 5.15 : A representation of the bonded area formation [63].

During the lap shear tests, four fracture types were observed: shear, pull lower and upper nugget and pull nugget with mixed shear fracture (Figure 5.16).

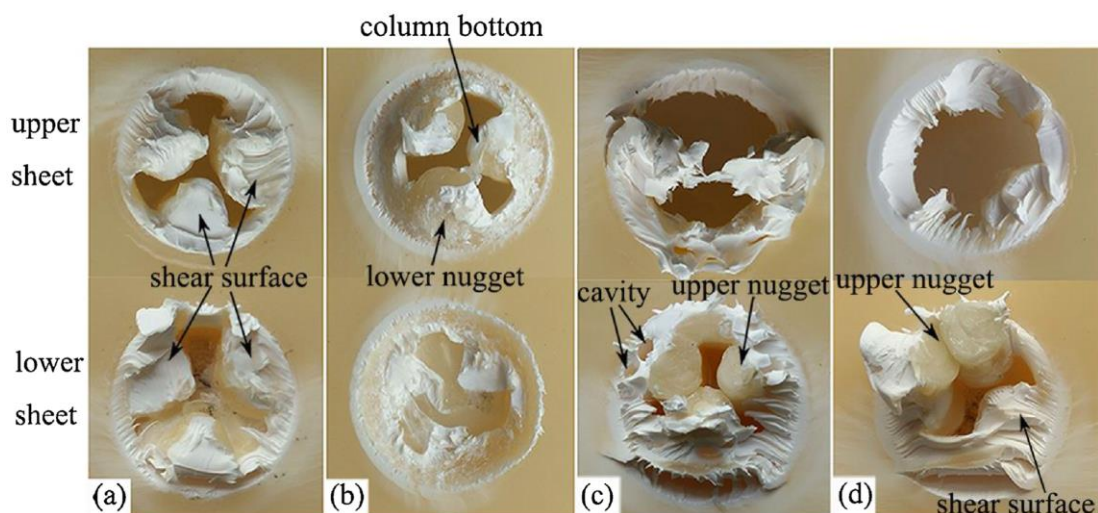


Figure 5.16 : Fracture types: (a) shear, (b) pull lower, (c) upper nugget, (d) pull nugget with mixed shear fracture [63].

In previous studies, the effect of process parameters (tool rotation speed, plunge depth, and dwell time) was investigated. In the other study on FSSW for 6 mm thick ABS workpieces, it was observed that tool geometry and process parameters influenced the mechanical performance and weld morphology. According to the

results, an increase in the rotational speed and decrease in the plunge rate led to a decrease in the joint shear strength. In addition, it was found that the proper extension of dwell time had a negligible influence on the weld strength in the moderate tool rotation speed but had a positive effect on the fracture load. High values of fracture loads were obtained with the flat pin tool when compared with other pin geometries (cylindrical, triflute, triangular) [65].

In the literature, there are very few studies about FSSW of two dissimilar thermoplastics. FSSW of ABS and PMMA sheets with 5 mm thickness was investigated to find influences of process parameters on joint strength [66]. There is a requirement to apply a suitable technology for joining of dissimilar plastics. During the joining process, both materials must have chemical compatibility and the melting temperatures of these materials should be close to each other [67]. In the study, 3³ full factorial method was used to arrange process parameters (rotational speed, dwell time, and plunge rate). According to the results, when the rotational speed increased, weld strength first increased but then decreased. The highest weld strength was achieved at the 800 rpm for the tool rotational speed parameter. While the increase in the plunge rate values resulted in low weld strength. Weld strength increased from 10 to 30 seconds with increasing the dwell time time [66].

Three fracture types were observed during the lap shear tests (Figure 5.18). In the cross nugget failure, high joint strength was not obtained because of the thin nugget and small bonded area. However, the upper sheet failure had a high strength. The fracture is called as boundary failure had a very low joint strength due to generating low frictional heat.

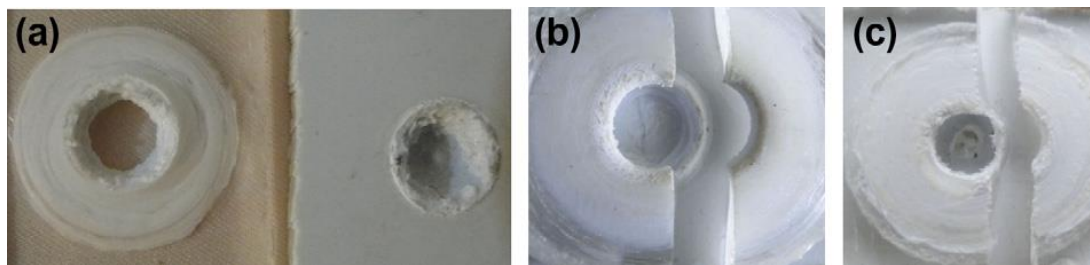


Figure 5.17 : Types of fractures: (a) cross nugget, (b) upper sheet and, (c) boundary [66].

6. OPTIMIZATION AND DESIGN OF EXPERIMENT

6.1 Modeling and Optimization Techniques

Optimization is used in many applications especially for engineering and industrial fields. Fundamentally, optimization is a process used to find the optimal solutions for a particular problem [68]. In other words, optimization is the science of obtaining the best results exposed to variable resource limitations. The production functions (planning, maintenance, design, operation, quality control) need to be optimized. Nowadays, the importance of optimization has been recognized by academic institutions and institute professionals to improve performance [69].

The existence of optimization techniques goes back to the periods of Newton, Lagrange, and Cauchy. Furthermore, differential analysis techniques for optimization were developed with the contributions of Newton and Leibnitz in calculus. In the mid-twentieth century, complex optimization processes were implemented by high-speed computers. Thus, the development of new methods for optimization stimulated. Subsequently, there have been spectacular improvements in optimization techniques and new well-defined areas in optimization theory have been revealed [70].

The reason for optimization in many engineering and industrial applications is to keep energy consumption and cost at minimum levels and to keep performance and efficiency at maximum levels. Resources, money and time are always limited in real terms. Therefore, optimization is very important in practice due to achieving maximum profit, performance, efficiency, and output. The calculation stages of the optimization problem are considered the main problem in engineering and industry since determining objective functions takes the most time in optimization [68].

There are many conventional optimization methods to solve different production optimization problems. It is not possible to say that all techniques are robust. Each technique can be applied to a particular optimization problem. Conventional

optimization methods are often used for unimodal and simple objective process applications. When they are preferred in multimodal applications, most of the methods cannot be used or high yields cannot be achieved. Therefore, better methods are needed to solve discrete, complex, multimodal and discontinuous problems [69].

Many mathematical models, such as neural computing (NC), genetic algorithm (GA), response surface method (RSM), statistical regression techniques or artificial neural networks (ANN), design of experiments (DOE) and Taguchi method, have been developed to determine the relationship between welding performance and welding parameters to select the appropriate welding parameters.

Recently, meta-heuristic search-based techniques used by researchers are based on tabu search (TS), simulated annealing (SA), and genetic algorithm (GA) techniques.

Parameter optimization techniques developed by researchers can be divided into as conventional and nonconventional methods. Different input-output and in-process parameter relationship modeling and optimization techniques in a general classification are shown in Figure 6.1 a,b [71].

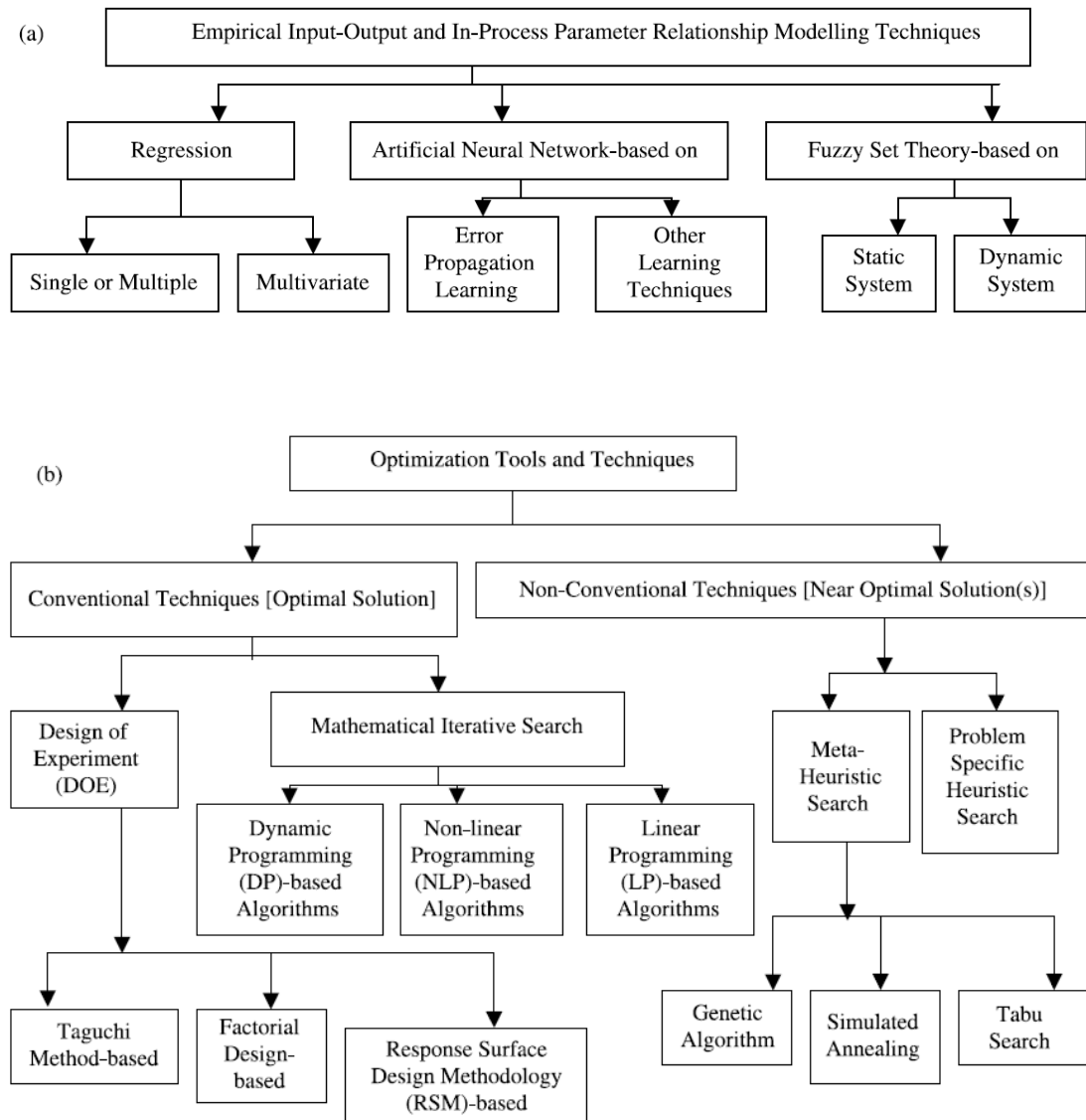


Figure 6.1 : Classification of (a) modeling and (b) optimization techniques [71].

6.2 Design of Experiment

Design of experiments (DOE) is the technique of identifying and examining all possibilities of an experiment consisting of multiple factors. This method is also known as factorial design. First, design of experiments was used in agricultural experiments in the late 1920s and is still in use.

Although factorial designs of experiments are broadly used, their drawbacks are:

1. The high number of variables makes the experiment unpractical in terms of cost and time.
2. Different results may be obtained in two designs of the same experiments.

3. Interpreting results with multiple factors has difficulty because of the lack of design and analysis guidelines.

Dr. Taguchi introduced a new method because of the drawbacks. Fractional factorial designs were simplified and standardized to obtain consistent results.

Experimental designs were developed in discipline and structurally. Thus, a standard and easy design methodology was obtained. Similar results would be obtained from the same experiments of different designs. The deficiencies of factorial and fractional experiments were eliminated [72].

6.3 The Taguchi Approach

To make design of experiment easier and more widespread in the industry, Taguchi considered the following application techniques:

1. *Definition of quality* – According to Taguchi, quality is the consistency of performance depending on engineering. Consistency is the primary feature, it is independent of the application and the method of measurement of the results is not important. Consistency increases as performance approaches the target. A two-step optimization approach to improve quality:

- a. Determine factor-level combination that decreases performance variability.
- b. Arrange the process parameter levels so that performance and target are close to each other.

2. *Standardized DOE* – A set of tables, defined as orthogonal arrays (OAs), is used in the design of the experiments. They can be stated as the smallest fractional factorials for the most widespread experiment designs.

3. *Robust design strategy* – To prevent products and processes from being affected by uncontrollable factors, noise factors should be developed. Thus, the effects of a greater number of noise factors are examined and small experiments are easily carried out. A performance close to the target and a decreasing variation around the mean is achieved.

4. *Loss function* – The development of monetary units can be easily measured by the mathematical formula of the loss function. It is an easy way to determine the expected improvement in cost savings in DOE results.

5. *Signal-to-noise (S/N) analysis* – Signal to noise ratios are an easy way to analyze multi-sample test results and simplify DOE results. The logarithmic transformation of S/N results provides the prediction of improvement in performance depend on the analysis.

The Taguchi method was developed as a way to treat noise factors and decrease the variation and scatter around the target. Noise factors affect the reaction of the process and are economically out of control. For example, weather conditions and wear are the primary sources of variations. The result is a “robust” design with a high S/N ratio that is least affected by noise.

Taguchi's methods comprise of three different methods. They are defined below:

1. System design
2. Parameter design
3. Tolerance design

In the system design, process levels of design factors are determined and identified. There are designing and testing systems, which depend on nominal parameters and selected parts. Generally, the system design includes innovation and knowledge of feasible technology.

Unlike system design, factor levels that provide the best performance for the products are determined by the parameter design. The reason for selecting the optimum condition is that the noise factors cause minimum variations in system performance.

Tolerance design adjusts the results of parameter design and tightens the tolerance of effective parameters for the product. Thus, higher costs will arise such as better materials, newer types of equipment and higher expenditures for inspections [72].

6.4 Background and Overview

Due to the poor and completely improper of the Japanese telephone system, an electrical communication laboratory was established with Dr. Taguchi to improve the system. When engineering tests and experiments were carried out, time and money were affected negatively. So, new ways were developed to optimize the test process and to improve quality.

Dr. Taguchi proposed the method called as Taguchi methods. The most important benefit of experimental design is not mathematically but philosophically. In addition, the Taguchi method is unique and powerful compared to traditional applications. The approaches of Dr. Taguchi mainly may be identified as follows:

1. Quality design should be into the production and not investigated into it.
2. The quality increases as the target deviation is minimized. Environmental factors should be considered in the design of products.
3. Measurement of the cost quality is a function of standard deviation and the losses should be determined throughout the system [72].

6.5 Methodology

The following steps are used in Taguchi methodology and also summarized in Figure 6.2:

1. Define the parameters and quality characteristics.
2. Specify the number of levels of process parameters and determine the interaction between the parameters.
3. Choose the suitable orthogonal array, and then set the parameters to array.
4. Perform the experiments in the orthogonal array layout.
5. Analyze the results obtained from the experiment by Analysis of Variance.
6. Determine the optimum levels of process parameters.

The main objectives of the parameter design are:

- a. Finding the optimum parameters of a process/product
- b. Evaluation of the contribution of each parameter on quality
- c. Estimation of quality properties depend on the optimum processing

The main tools used in the Taguchi method are:

- a. S/N (Signal to Noise) ratio to measure the quality
- b. Orthogonal arrays for simultaneous examination of multiple process parameters [73].

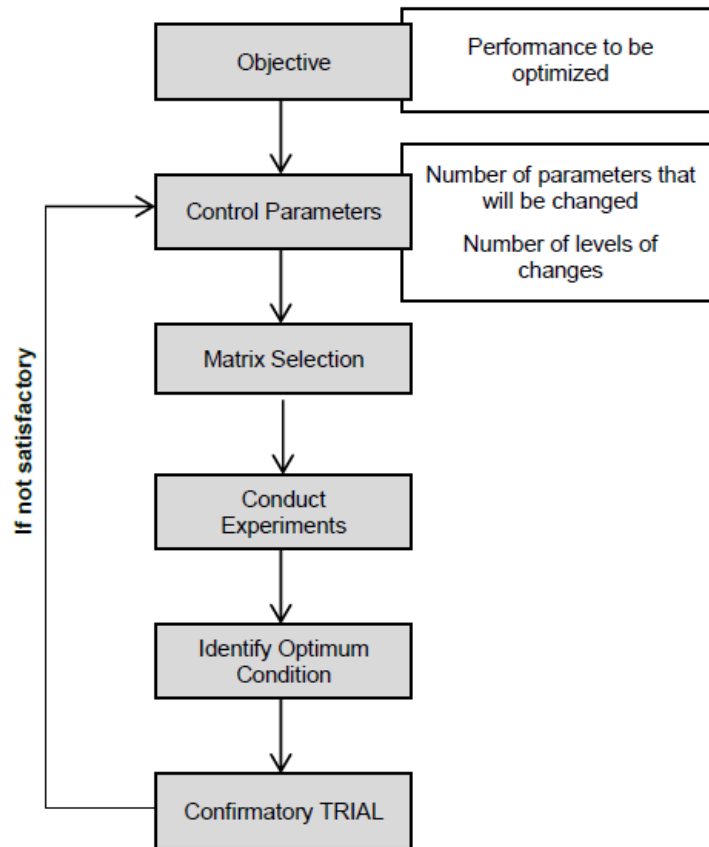


Figure 6.2 : Taguchi method flow chart [73].

6.5.1 Defining the problem

Clarification of the problem or the objective of the investigation to be carried out is the first step of the application of the Taguchi Method. This can be expressed as evaluating what parameters to be optimized. For example, temperature, cost, weight, roughness, flow rate, thickness, and so on. The decision of the object is required for quality characteristics depend on the selected object of the study. The preparations before the experiment may vary according to the problem studied. To sum up, the first step of the process plan involves the choice of the object for the study, the definition of the problem, identification of the areas of concern [74].

6.5.2 Selection of parameters and number of levels

There are some particular operating parameters for the process. The next step is to determine the noise factors, experiment condition, quality characteristics and define the parameters that have influences on the process after definition of the problem. Control parameter values can be controlled and changed. When the number of parameter levels increases, the number of experiments increases. However, reducing

the number of levels may result in a non-conclusive test. Optimization of settings that minimize controllable and uncontrollable noise variables is provided by robust parameter designs [74].

6.5.3 Selection of appropriate orthogonal array

After this step, the Orthogonal Array (OA) is selected for the parameter design showing the conditions and number of each experiment. The number of parameters and the variation levels for each parameter has a significant effect in OA selection [74].

Each process consists of a combination of parameter or parameters having a value. The best results will be obtained when each parameter works at the optimum level. In OA, performance effects can be examined simultaneously with all parameters varying at the same time [75]. OAs are balanced because all factors of the experiment occur in an equal number of times for each level. A Taguchi OA is represented as $L_n(m^k)$. Here “L” refers to Latin square, “n” refers to the number of experiments, “m” refers to the levels of the performed experiment and “k” refers to the number of selected factors or parameters, in other words, the number of columns of experimental layout. There is a “rule of thumb”. The degrees of freedom of the experiment should always be equal or greater than the degrees of freedom required to investigate the influences of interactions. Degree of freedom can be expressed the number of fair and independent comparisons [76].

In the selection of orthogonal sequences, the degree of freedom of each parameter and the total degree of freedom, which is the sum of degrees of freedom, are calculated. The total degree of freedom is preferred whichever orthogonal array fits. In the calculation of the total degree of freedom, whether there is an interaction between factors should be considered. The degree of freedom of a factor is 1 minus the number of levels (Lakshminarayanan and Balasubramanian, 2008).

$$f_A = k_A - 1 \quad (6.1)$$

f_A : Degree of freedom of factor A

k_A : Number of levels of factor A

If there is an interaction, the degree of freedom is equal to the product of the degrees of freedom of factors.

$$f_{(AxB)} = f_A \cdot f_B \quad (6.2)$$

$f_{(AxB)}$: Degree of freedom of factor (AxB)

f_A : Degree of freedom of factor A

f_B : Degree of freedom of factor B

Thus the minimum degree of freedom of experiment is equal to the sum of degrees of freedom of factors or interactions. The total degree of freedom of the experiment plan is equal to 1 minus the number of experiments in the selected orthogonal sequence.

$$f_T = N - 1 \quad (6.3)$$

f_T : The total degree of freedom of experiment plan

N : Number of experiments

For example, when it is desired to analyze the effects of 2 levels of 7 factors and there is no interaction, the following calculations are performed.

$$f_A = 2 - 1 = 1$$

$$f_B = 2 - 1 = 1$$

$$f_C = 2 - 1 = 1$$

$$f_D = 2 - 1 = 1$$

$$f_E = 2 - 1 = 1$$

$$f_F = 2 - 1 = 1$$

$$f_G = 2 - 1 = 1$$

$$f_T = N - 1$$

Since $N = 8$, the ideal orthogonal array L_8 should be chosen.

According to the number of factors, it is decided to use 2 or 3 level orthogonal array. If the experiment involves factors different levels, the orthogonal array should be rearranged according to the dominant level. The orthogonal sequence is selected according to Table 6.1 for 2-level factors and Table 6.2 for 3-level factors. In the

tables, the “*” sign indicates repetitive experiments, while “X” indicates situations where design is not possible.

Table 6.1 : Selection of two-level orthogonal arrays [76].

OA	Number of factors (2-level)														
	1	2	3	4	5	6	7	8	9	10	11	12	13	14	15
L ₄	4	4	1	X	X	X	X	X	X	X	X	X	X	X	X
L ₈	4*	4*	4	2	1	1	1	X	X	X	X	X	X	X	X
L ₁₆	4*	4*	4*	4	3	2	2	2	2	1	1	1	1	1	1
L ₃₂	4*	4*	4*	4*	4	3	2	2	2	2	2	2	2	2	2
L ₆₄	4*	4*	4*	4*	4*	4	3	2	2	2	2	2	2	2	2
L ₁₂₈	4*	4*	4*	4*	4*	4*	4	3	2	2	2	2	2	2	2
L ₂₅₆	4*	4*	4*	4*	4*	4*	4*	4	3	2	2	2	2	2	2

Table 6.2 : Selection of three-level orthogonal arrays [76].

OA	Number of factors (3-level)							
	1	2	3	4	5	6	7	8
L ₉	4*	4*	1	1	X	X	X	X
L ₁₈	1	1	1	1	1	1	1	1
L ₂₇	4	4	4	2	1	1	1	1

Another example of an orthogonal array is illustrated in Table 6.3. The representation of the levels of process parameter is indicated by the numbers 1, 2 and 3, not by signs (+ or -). Each orthogonal layout is identified by a code. Depending on the number of parameters and levels, it is allowed to select the appropriate orthogonal array from Table 6.4. The number of rows means the number of experiments to be conducted [77].

Code : L_n (m^k)

- n: number of lines
- m: number of parameter levels
- k: number of parameters

Table 6.3 : Orthogonal arrays (three-level, L_9) [72].

CONDITION \ COLUMN	$L_9(3^4)$			
	1	2	3	4
1	1	1	1	1
2	1	2	2	2
3	1	3	3	3
4	2	1	2	3
5	2	2	3	1
6	2	3	1	2
7	3	1	3	2
8	3	2	1	3
9	3	3	2	1

Table 6.4 : Orthogonal test arrays [78].

	Orthogonal array	Number of lines	Max. number of parameters	Max. number of columns for the respective levels			
				2-lv.	3-lv.	4-lv.	5-lv.
2-level arrays	L_4	4	3	3	-	-	-
	L_8	8	7	7	-	-	-
	L_{12}	12	11	11	-	-	-
	L_{16}	16	15	15	-	-	-
	L_{32}	32	31	31	-	-	-
	L_{64}	64	63	63	-	-	-
3-level arrays	L_9	9	4	-	4	-	-
	L_{27}	27	13	-	13	-	-
	L_{81}	81	40	-	40	-	-
Multilevel arrays	L_{16}	16	5	-	-	5	-
	L_{25}	25	6	-	-	-	6
	L_{64}	64	21	-	-	21	-
Mixed 2- and 3-level arrays	L_{18}	18	8	1	7	-	-
	L_{32}	32	10	1	-	9	-
	L_{36}	36	23	11	12	-	-
	L_{36}	36	16	3	13	-	-
	L_{50}	50	12	1	-	-	11
	L_{54}	54	26	1	25	-	-

6.5.4 Performing the experimental run

This step can also be called the implementation and conduction of the research. The experiments are performed depending on the Taguchi orthogonal array and then the results and performance characteristics of the trials in each sequence are obtained. During trials, there may be an inconsistency. Therefore, the trials should be closely monitored. Here, it is possible to conduct only one trial for the combination of each parameter or more repetitions according to the number of noise parameters [72].

6.5.5 Statistical analysis and S/N ratio calculations

In an engineering design problem, objective function plays an important role. When this is not done, the experiments may be inefficient and optimum levels may give wrong results. Determining the significance of the settings and the accuracy of the S/N ratio is not an easy task for a problem [79].

S/N ratio approach is used to evaluate the quality characteristics deviating from desired value in the Taguchi method.

In the optimum parameter examination, S / N ratio is used to convert the evaluation of test results to a value. The S/N ratio is shown in dB units and can be formulated as:

$$S/N = -10 \log(MSD) \quad (6.4)$$

MSD means the mean-square deviation of the output characteristic.

It is possible to classify the S / N ratio characteristics in three different categories: the smaller the- better, the nominal- the-better and the larger- the better.

For smaller- the-better:

$$S/N = 10 \log \left(\frac{1}{n} \sum_{i=1}^n \frac{1}{y_i^2} \right) \quad (6.5)$$

For nominal- the-better:

$$S/N = 10 \log \left(\frac{\bar{y}}{s_y^2} \right) \quad (6.6)$$

For larger- the-better:

$$S/N = 10 \log \left(\frac{1}{n} \sum_{i=1}^n y_i^2 \right) \quad (6.7)$$

where “ y_i ” is the results of experiments, and “ n ” is the number of repetitions and “ m ” is the target value of result [80].

Analysis of variance, which is a statistical tool, is used to evaluate the experimental results. Analysis of variance enables finding the effect of each parameter variation in the quality of the piece.

Instead of the full factorial experiment, the Taguchi method is faster, less expensive and partial factorial experiment. Orthogonal arrays (OAs) are the basis of Taguchi’s design for the partial factorial. There should be an analysis of confidence for the qualifying results in the analysis of partial experiment. Fortunately, a statistical method called analysis of variance (ANOVA) provides a measure of confidence. Data are not directly analyzed by this technique, but variance can be determined. Confidence is calculated from the variance [81].

Sum of Squares: The total variation of the two factors A and B and the interaction between these factors is written as follows:

$$SS_T = SS_A + SS_B + SS_{(A \times B)} + SS_e \quad (6.8)$$

SS_T : Sum of squares

SS_A : Sum of squares of factor A

SS_B : Sum of squares of factor B

$SS_{(A \times B)}$: Sum of squares of A and B factor interactions

SS_e : Sum of squares of columns left blank in orthogonal array (error sum of squares)

$$SS_T = \left[\sum_{j=1}^N y_j^2 \right] - \frac{T^2}{N} \quad (6.9)$$

N : Number of trials

T : Sum of all observations

y_j : number of the j th observation

$$SS_A = \frac{(A_1 - A_2)^2}{N} \quad (6.10)$$

A_1 : Sum of observed results when factor A is at level 1

A_2 : Sum of observed results when factor A is at level 2

Variance: The variance of a factor is the ratio of the sum of squares of a factor to that degree of freedom of that factor.

$$V_A = \frac{SS_A}{f_A} \quad (6.11)$$

V_A : Variance of factor A

Degree of freedom: The rank of quadratic form is called as degree of freedom and can be calculated as follows:

And degree of freedom is calculated for the error variance as below:

$$f_e = f_T - f_A - f_B \quad (6.12)$$

f_e : degree of freedom for error variance

f_T : total degree of freedom of the experimental plan

f_A : degree of freedom for factor A

f_B : degree of freedom for factor A

Statistically, Fisher's test called F test is a tool to find out which design parameters have an important influence on the quality property. F-test provides checking the null hypothesis that there is no deviation on the mean values of each factor level [82].

When performing the standard F test, it is estimated that the errors are independent and normally distributed with equal deviations. If F test assumptions are not applied, severity calculations may not reflect accurate results. However, it is stated that the standard F test can be used even if it does not provide some assumptions since it is insensitive to deviations from the assumptions. The F value does not indicate the magnitude of the factorial effect statistically but its existence [83].

There are intermediate levels commonly used for the F test and it is tabled for significance levels of 1%, 5%, and 10%. If F test statistic exceeds the critical F value the null hypothesis is rejected. For example, if it is used a 5% level of significance, there would be a probability of $\alpha=0.05$ for each test, that is, each test would have a 95% probability of correctly not rejecting the null hypothesis.

$$F_A = \frac{V_A}{V_e} \quad (6.13)$$

F_A : F value of factor A

The net totals of the squares are calculated before finding the percentage of contribution that expresses the power of the factors to reduce variation.

$$SS'_A = SS_A - (V_e)(f_A) \quad (6.14)$$

SS'_A : Net sum of factor A squared

$$P_A = \frac{SS'_A}{SS_T} \times 100 \quad (6.15)$$

P_A : Contribution percentage of factor A

6.5.6 Confirmation test

Finally, after having obtained the optimal parameters, the experiment result and the predicted result are verified in the confirmation test. If the optimum combination of parameters and levels coincidentally match with one of the experiments in the orthogonal array (OA), then the confirmatory much with one of the experiments in the OA, thus the confirmation test is not required [83].

6.6 Advantages and Disadvantages of Taguchi Method

Orthogonal array design is a very simple technique for evaluating outputs and forms the basis of the Taguchi method. In some cases, although the studies have been criticized as insufficient and inefficient by some researchers, the simplicity of the Taguchi method has led to widespread use in the manufacturing industries [83].

The main purpose of the Taguchi method is to increase the quality with less influencing the cost. Optimal settings are provided with the Taguchi method to improve quality and are insensitive to the variation of noise factors. Simply, the Taguchi method is user-friendly compared to conventional processes that are complex in design and difficult to use.

One of the advantages of the Taguchi method is that it can emphasize a mean performance value closer to the target within certain limits. Furthermore, the implementation of the Taguchi experimental design is explicit and easy in many engineering applications. For these reasons, the Taguchi method is a powerful as well as simple tool. Also, the Taguchi method can quickly narrow the scope for research or use data to define problems in the production process.

However, due to negative thoughts on modeling and data analysis, important concepts of Taguchi method were overshadowed. The most important drawback of the Taguchi method is that it gives close results and does not exactly show the most effective parameter on the performance characteristic. Furthermore, since all combinations of factors cannot be tested, this technique should not be used to investigate interactions between all variables. In the Taguchi method, it is difficult to evaluate the relationships between parameters and it has been criticized for this reason.

Another drawback of the Taguchi method is its offline characteristic. Therefore, it is not applicable for dynamic and variable processes. The Taguchi method does not improve quality at low levels, but it deals with the designing stage of quality. Therefore, the method is applied most influentially as one of the first steps in process development [84].

7. EXPERIMENTS

7.1 Materials and Method

7.1.1 Acrylonitrile butadiene styrene (ABS) and Polycarbonate (PC)

In the experiment, ABS and PC sheet materials are used. Both of the materials are in the crystalline structure and amorphous polymers. ABS and PC sheets having 4 mm thickness, 25.4 mm width and 100 mm length have been manufactured from granules with plastic injection molding.

The common problem of the FSSW process is the forming of characteristic keyhole in the joints and this problem has an important effect on mechanical test results. For this purpose, a polycarbonate or acrylonitrile butadiene styrene filler sheets were used to improve weld strength by reducing the size of the keyhole in the study.

In all similar and dissimilar joints of ABS and PC, filler sheets of 48 mm length, 4 mm thickness, 25.4 mm width were cut from the workpieces produced for the FSSW process. While ABS filler sheets are used for ABS-ABS joints, PC filler sheets are used for PC-PC and ABS-PC joints.

The main properties of ABS and PC material were listed in Table 7.1 and Table 7.2, respectively.

Table 7.1 : The main properties of ABS.

Material	Density (g/cm ³)	Melting Temperature (°C)	Tensile Strength (MPa)	Hardness Rockwell
ABS	1.04	210-240	38	110

Table 7.2 : The main properties of PC.

Material	Density (g/cm ³)	Melting Temperature (°C)	Tensile Strength (MPa)	Hardness Rockwell
PC	1.20	288-316	60	126

7.1.2 Experimental setup for Friction Stir Spot Welding

A Computer Numerical Control (CNC) milling machine was used for friction stir spot welding (FSSW) operations. It was decided to use CNC for the experiments because of the facility of working more precisely in terms of parameters such as time, speed and depth, and performing the tests without operator errors.

Also, a clamping apparatus having a central through-hole was used to fix the lapped polymer sheets. This clamping apparatus is suitable for welding of similar and dissimilar materials. After the fixing of the clamping apparatus on the table of the CNC milling machine, the sheets are placed in the slots and fastened from both right and left sides of the clamping apparatus. CNC machine and clamping apparatus are shown in Figure 7.1 and Figure 7.2, respectively.



Figure 7.1 : CNC milling machine.



Figure 7.2 : Clamping apparatus.

7.1.3 Friction Stir Spot Welding Tool

The tool with a shoulder and threaded cylindrical is used in this investigation. The pin was designed with thread for increasing the frictional heat and stirring ability [85]. In the present study, the threaded cylindrical tool pin made up of H13 hot work steel with a shoulder diameter of 20 mm, a pin diameter of M5 thread screw and a pin length of 5 mm was used (Figure 7.3).

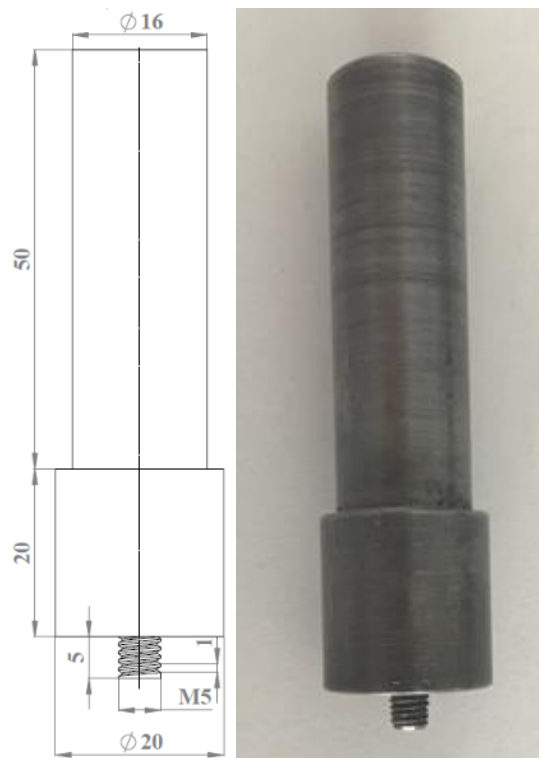


Figure 7.3 : The FSSW tool used in experimentations.

7.2 Preliminary research and evaluation of experiments

In the first step of the experimental design, some trial experiments can be performed to find approximate ranges of variables. If the tests of factor levels result in acceptable weld quality for these ranges, they are selected as process parameter levels at the beginning of the experiment design depending on investigations in the literature and according to the experiment design method.

In the FSSW of polymers, there are some important factors affecting the tensile strength and tool rotational speed, plunge depth and dwell time can be considered among these factors. Therefore, based on preliminary research/evaluation experiments, tool rotational speed, plunge depth and dwell time were selected as process parameters to observe the effects on weld strength in the study.

As a result of trials for this study and studies in the literature, it was not necessary to select preheat time and plunge rate as variable factors. The pre-heating time and plunge rate were kept constant as 20 s and 8 mm/min, respectively.

7.3 Determination of FSSW Parameters and Levels for Taguchi Method

In the study, FSSW of similar and dissimilar thermoplastics (ABS-ABS, PC-PC, and ABS-PC) were performed by using a specially designed clamping fixture. In addition, a filler sheet was used to reduce the keyhole volume on different configurations of ABS and PC joints and improve the lap joint shear load-carrying capacity of the weld by analyzing the influences of the process parameters. The factors and their levels were arranged Taguchi L₉ orthogonal array to determine the optimum levels of process parameters.

For FSSW of ABS-ABS, PC-PC and ABS-PC sheets, the factors, and levels of the process are determined to set the experimental design matrix to be used in the Taguchi method and determine the optimum levels (Table 7.3, Table 7.4, Table 7.5).

Table 7.3 : Welding parameters and their levels for ABS-ABS joints.

Symbol	Welding Parameter	Unit	Level 1	Level 2	Level 3
A	Tool Rotational Speed	rpm	1000	2000	3000
B	Plunge Depth	mm	10.5	11	11.5
C	Dwell Time	s	20	30	40

Table 7.4 : Welding parameters and their levels for PC-PC joints.

Symbol	Welding Parameter	Unit	Level 1	Level 2	Level 3
A	Tool Rotational Speed	rpm	800	1600	2400
B	Plunge Depth	mm	10.5	11	11.5
C	Dwell Time	s	20	30	40

Table 7.5 : Welding parameters and their levels for ABS-PC joints.

Symbol	Welding Parameter	Unit	Level 1	Level 2	Level 3
A	Tool Rotational Speed	rpm	800	1600	2400
B	Plunge Depth	mm	10.5	11	11.5
C	Dwell Time	s	20	30	40

7.4 Selection of Taguchi Orthogonal Array

L_9 orthogonal array consisting of nine rows and four columns was applied for this investigation. In the FSSW experiments of ABS-ABS, PC-PC and ABS-PC sheets, the experimental layouts of rotational speed, plunge depth and dwell time parameters are illustrated in Table 7.6. The last column is empty for experimental errors after each welding parameter is placed in a column. Therefore, orthogonality is not affected by this situation. Thus, it is sufficient to perform only 9 experiments for FSSW of two similar (ABS-ABS, PC-PC) and one dissimilar (ABS-PC) thermoplastics. In the FSSW process, a total of 27 pairs of sheets were used for each configuration. (ABS-ABS, PC-PC, and ABS-PC).

Table 7.6 : L_9 orthogonal array of welding parameters and levels for each joint.

Experiment No.	Welding Parameters		
	A	B	C
	Tool Rotational Speed	Plunge Depth	Dwell Time
#	(rpm)	(mm)	(s)
1	1	1	1
2	1	2	2
3	1	3	3
4	2	1	2
5	2	2	3
6	2	3	1
7	3	1	3
8	3	2	1
9	3	3	2

7.5 Experimental Design Matrix

The experiments were performed according to the principles of the design of the experiments in order to determine the influence of the welding parameters. Since three levels and three factors were considered, L₉ OA was used in this study. For a larger number of factors, higher and mixed levels, a number of other orthogonal arrays are applicable [86]. In the study for ABS-ABS, PC-PC and ABS-PC joints, the three parameters (rotational speed, plunge depth and dwell time) are taken into consideration and the values with their symbols and levels are listed in Table 7.7, Table 7.8 and Table 7.9.

Table 7.7 : L₉ orthogonal array for process parameters and their levels of ABS-ABS joints.

Experiment No.	Welding Parameters		
	A	B	C
	Tool Rotational Speed	Plunge Depth	Dwell Time
#	(rpm)	(mm)	(s)
1	1000	10.5	20
2	1000	11	30
3	1000	11.5	40
4	2000	10.5	30
5	2000	11	40
6	2000	11.5	20
7	3000	10.5	40
8	3000	11	20
9	3000	11.5	30

Table 7.8 : L₉ orthogonal array for process parameters and their levels for ABS-PC joints.

Experiment No.	Welding Parameters		
	A	B	C
	Tool Rotational Speed	Plunge Depth	Dwell Time
#	(rpm)	(mm)	(s)
1	800	10.5	20
2	800	11	30
3	800	11.5	40
4	1600	10.5	30
5	1600	11	40
6	1600	11.5	20
7	2400	10.5	40
8	2400	11	20
9	2400	11.5	30

Table 7.9 : L₉ orthogonal array for process parameters and their levels for ABS-PC joints.

Experiment No.	Welding Parameters		
	A	B	C
	Tool Rotational Speed	Plunge Depth	Dwell Time
#	(rpm)	(mm)	(s)
1	800	10.5	20
2	800	11	30
3	800	11.5	40
4	1600	10.5	30
5	1600	11	40
6	1600	11.5	20
7	2400	10.5	40
8	2400	11	20
9	2400	11.5	30

7.6 Process Preparations

7.6.1 Manufacturing of sheets for FSSW

For the FSSW process, sheets of 4 mm thickness, 25.4 mm width and 100 mm length were manufactured from ABS and PC granules by plastic injection under appropriate conditions. Also, a filler sheet with a length of 48 mm, a width of 25.4 mm and a thickness of 4 mm was put on above the upper sheet to reduce the keyhole volume of the welded sheets. Filler sheets were used in all FSSW processes of similar and dissimilar joints of ABS and PC materials. Figure 7.4 shows the ABS and PC sheets with filler sheets in lap position and their dimensions.

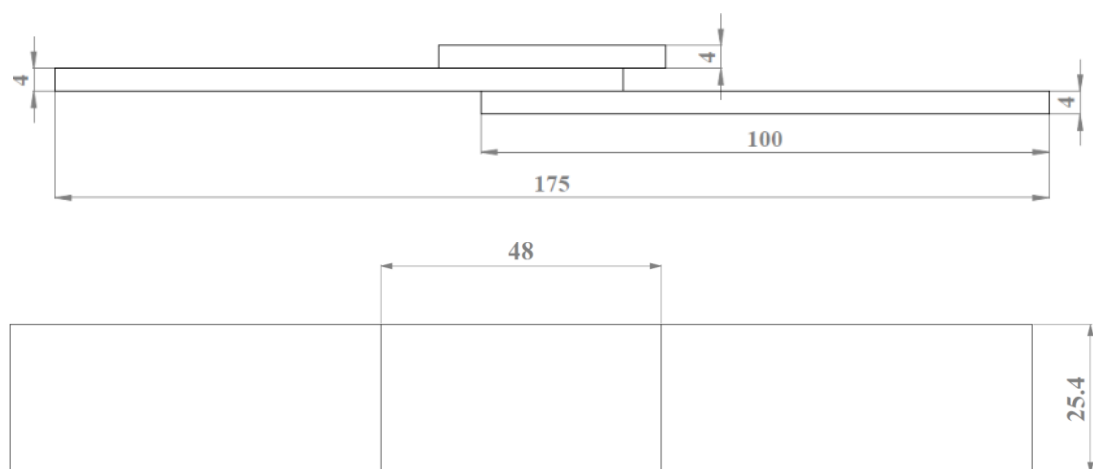


Figure 7.4 : The dimensions (in mm) of the lap-shear tensile specimen for ABS-ABS, PC-PC, and ABS-PC joints.

7.6.2 Fixing of the clamping apparatus

Firstly, before starting the FSSW process the clamping apparatus must be properly positioned on the worktable of CNC milling machine and fixed.

7.6.3 Setting of the FSSW tool

After fixing the clamping apparatus, the FSSW tool was fastened on the arbor of the CNC milling machine. The same FSSW tool was used in all experiments.

7.6.4 Fixing the work adaptor plates on the clamping apparatus

The prepared ABS-ABS, PC-PC and ABS-PC sheets were placed in the slots of clamping apparatus and fastened to produce FSSW joints. An important point is to ensure that the sheets remain stable during FSSW processes. Therefore, the sheets and filler sheets were properly fixed in each experiment. Welding positions of clamping apparatus, FSSW tool and welding sheets for each experiment are illustrated for ABS-ABS, PC-PC and ABS-PC joints in Figure 7.5-7.7, respectively.

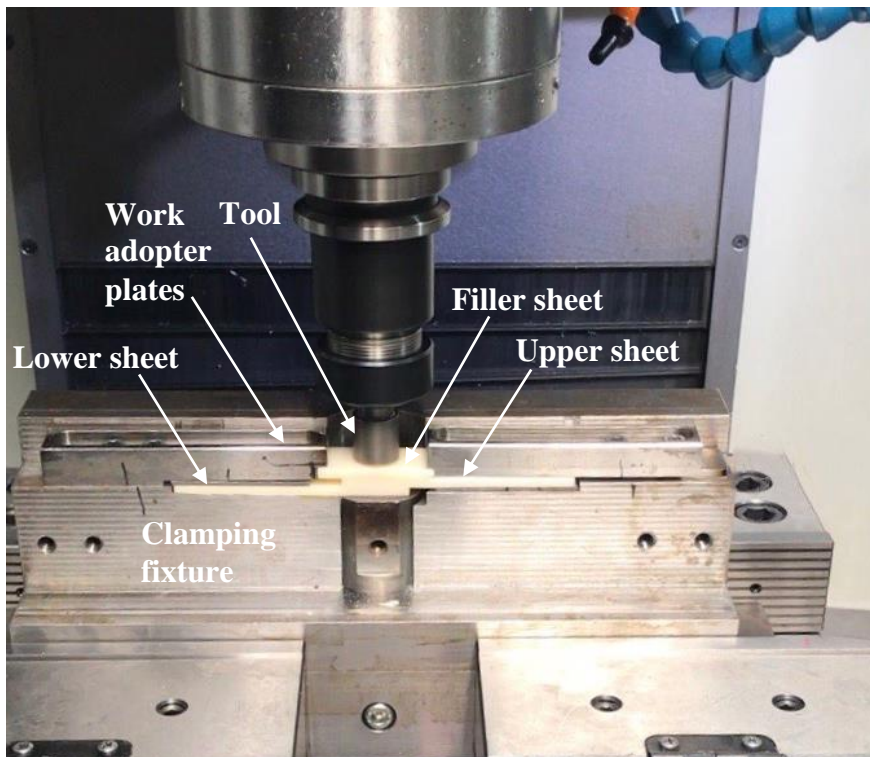


Figure 7.5 : Welding positions of clamping apparatus, FSSW tool, and welding sheets for ABS-ABS joints.

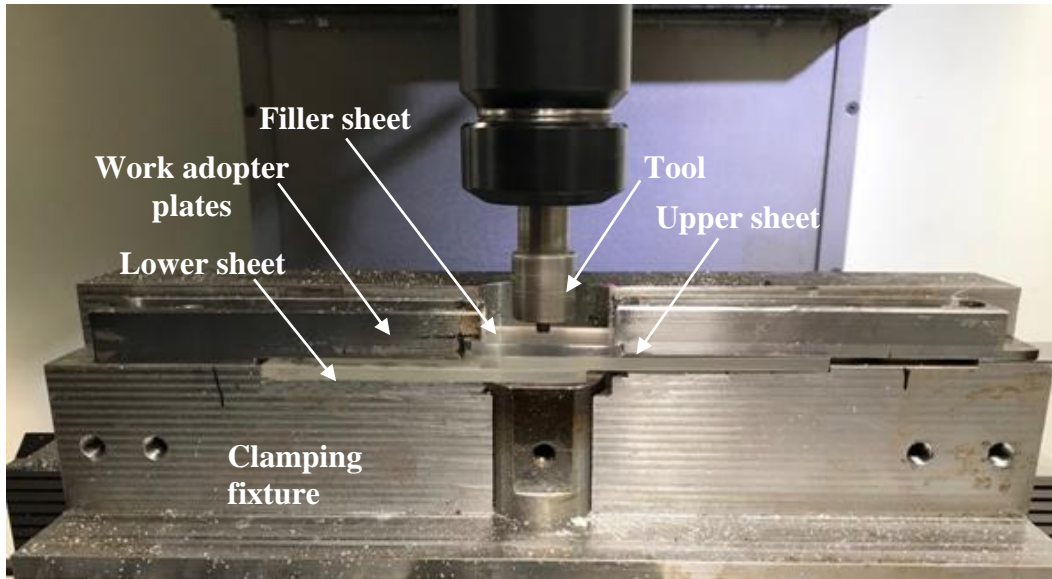


Figure 7.6 : Welding positions of clamping apparatus, FSSW tool, and welding sheets for PC-PC joints.

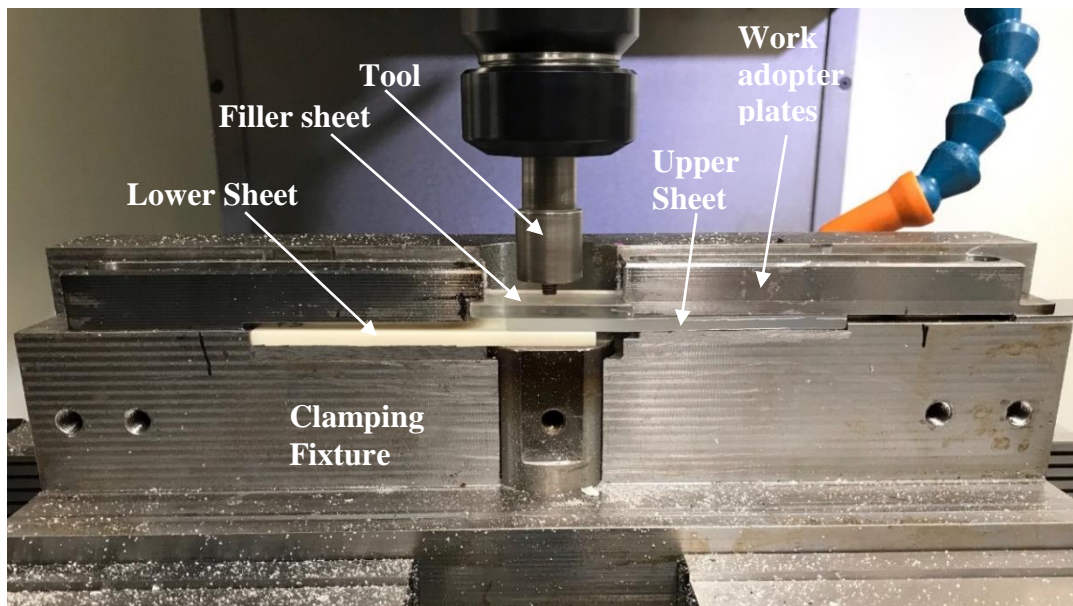


Figure 7.7 : Welding positions of clamping apparatus, FSSW tool, and welding sheets for ABS-PC joints.

7.6.5 Setting of the operating parameters

Welding parameters (rotational speed, plunge depth and dwell time) were carefully controlled during FSSW.

For FSSW of ABS-ABS joints, 3 different rotational speeds (1000, 2000, 3000 rpm) plunge depths (10.5, 11, 11.5) and dwell times (20, 30, 40 s) values are precisely set on the CNC.

For FSSW of PC-PC and ABS-PC joints, 3 different rotational speeds (800, 1600, 2400 rpm) plunge depths (10.5, 11, 11.5) and dwell times (20, 30, 40 s) values are precisely set on the CNC. Based on the studies in the literature and trial welds, it was decided that the tool rotational speed values of ABS-ABS joints should be different from the rotational speed of PC-PC and ABS-PC joints since sufficient welding quality could not be obtained.

All other factors (pre-heating time, plunge rate, and FSSW tool geometries) were kept constant throughout all experiments.

7.7 Manufacturing of Welded Joints

After all settings are completed, the production of welded joints can be started.

The FSSW process consists of 5 stages as schematically in Figure 7.8:

- Tool rotation
- Pre-heating
- Plunging
- Stirring
- Tool retraction

7.7.1 Tool Rotation

For all joints (ABS-ABS, PC-PC, and ABS-PC), the FSSW process begins with rotating of the tool with a predetermined high rotational speed. The welding tool is approached the sheets with a constant plunge rate of 8 mm/min.

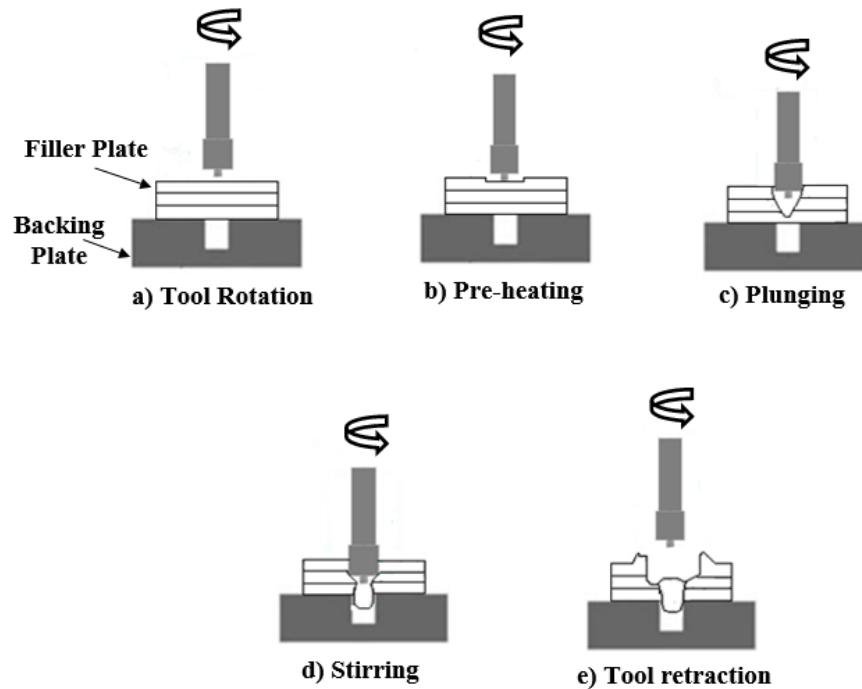


Figure 7.8 : The stages of FSSW process.

7.7.2 Pre-Heating

The tool continues to move vertically 0.2 mm to the filler sheet with a constant plunge rate. Then, the feed is stopped and the tool starts to apply pressure for a preheating time. As a result of previous works and trial experiments, pre-heating time was applied 20 seconds.

In the study, this preheating time was standardized for all joints. After sufficient preheating due to friction between the tool and sheets, the tool begins to move to the predetermined depth.

While 0.2 mm depth was sufficient for pre-heating in ABS-ABS joints, 5.2 mm depth was selected to provide required pre-heating for PC-PC and ABS-PC joints.

7.7.3 Plunging

After the pre-heating step, the operation continues by moving vertically against the sheets with a constant plunging speed. During this phase, polymer particles are ejected from the welding area due to the plunge movement of the tool. The tool continues to move by rotating until it reaches the specified depth.

7.7.4 Stirring

As soon as the tool reaches the predetermined depth, the vertical motion is stopped. Then, the stirring phase starts with the rotating tool and maintains for a prescribed dwell time. Plunging and stirring steps lead to produce frictional heat. During the stirring phase, the material surrounding and underlying around the tool is heated and softened as a result of the stirring of the tool [62]. Therefore, the temperature increases between the material and the tool. As the temperature increases, it causes the plastic flow of the welded zone. Applied force by tool shoulder causes the continuation of the plastic deformation until the dwelling period is complete.

7.7.5 Tool retraction

Upon reaching the predetermined dwell time, the rotating tool is immediately retracted from the sheets and the solid-state phase is formed between the materials.

When the welding is completed, a hole is formed in the welding zone due to the pin on the tool.

7.7.6 Cooling and cleaning of the FSSW tool

Due to the ability of the tool to cool rapidly in the air, the tool was not cooled. At the end of each experiment, the molten polymers surrounding the tool shoulder and pin affecting the process were cleaned with mechanical brush and compressed air.

7.7.7 Completion of experiments in the experimental design matrix

After the first test repetitions were completed, the second and third repetitions were performed for each experiment.

The FSSW experiments of ABS-ABS, PC-PC, and ABS-PC joints were repeated by changing the tool rotational speed, plunge depth and dwell time in order to observe the effect of process parameters.

Examples of successfully friction stir spot welded materials for ABS-ABS, PC-PC and ABS-PC are shown in Figure 7.9, Figure 7.10 and Figure 7.11, respectively.

Steps of FSSW experiments were completed and after a certain period (one week), the specimens became ready for the tensile tests.

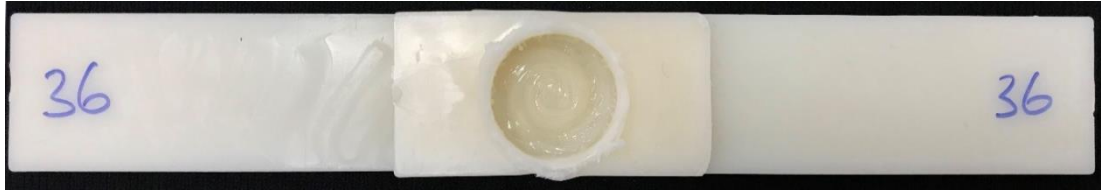


Figure 7.9 : A FSSW specimen of ABS-ABS joint

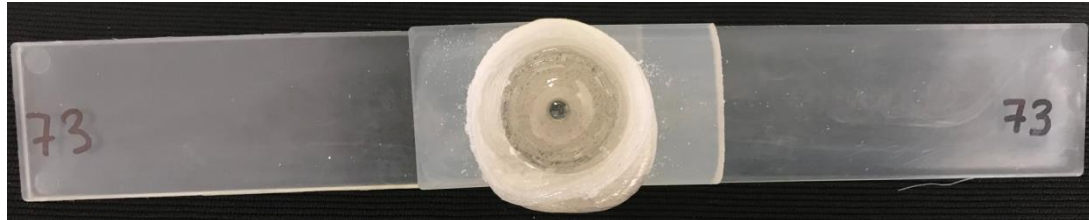


Figure 7.10 : A FSSW specimen of PC-PC joint

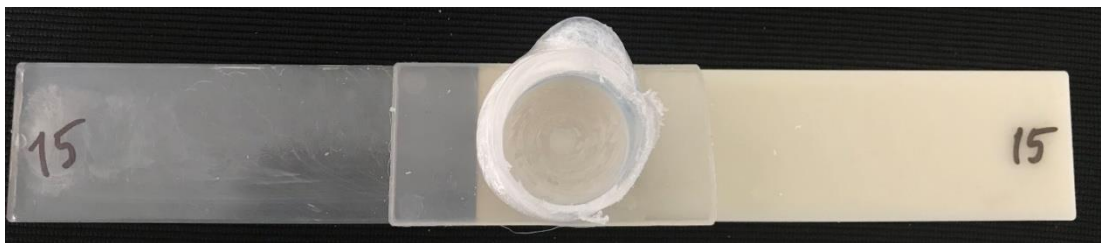


Figure 7.11 : A FSSW specimen of ABS-PC joint.

7.8 Characterization of Welded Joints - Lap Joint Shear Load Tests

7.8.1 Preparation of tensile test samples

Firstly, the photographs of specimens were recorded for examination of the weld morphology before and after the FSSW process.

A total of 4 samples were friction stir spot welded for each experiment in the study. 3 of the welded samples were used for the lap joint shear load tests and 1 of them was used for morphological analysis. Prepared lap joint shear load test specimen is shown in Figure 7.12. The support plates were added to the welded specimens to avoid bending during the tensile tests.

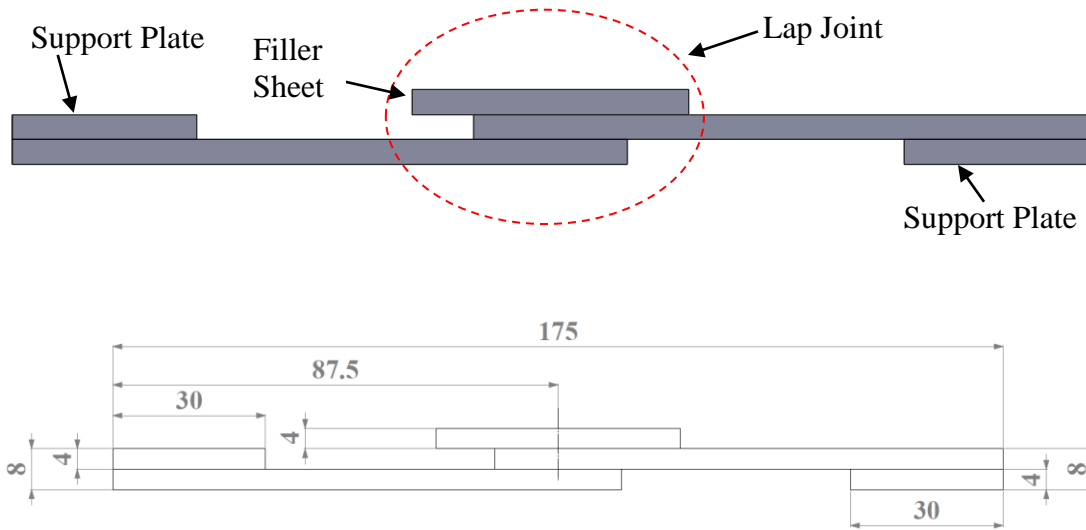


Figure 7.12 : Illustration of lap shear test specimen.

7.8.2 Marking of measuring points of tensile test samples

Lap joint shear tests were performed to investigate the mechanical properties of welded specimens (Figure 7.13). A sample tensile test results for three joints (ABS-ABS, PC-PC, and ABS-PC) joined with FSSW are shown in Figure 7.14, 7.15 and 7.16, respectively.

The specimens were tested in a SHIMADZU tensile testing machine with 100 kN of load cell by using a noncontact video extensometer with an initial gauge length $L_0 = 70$ mm at a constant crosshead speed of 5 mm/min.



Figure 7.13 : Tensile test of a welded joint.

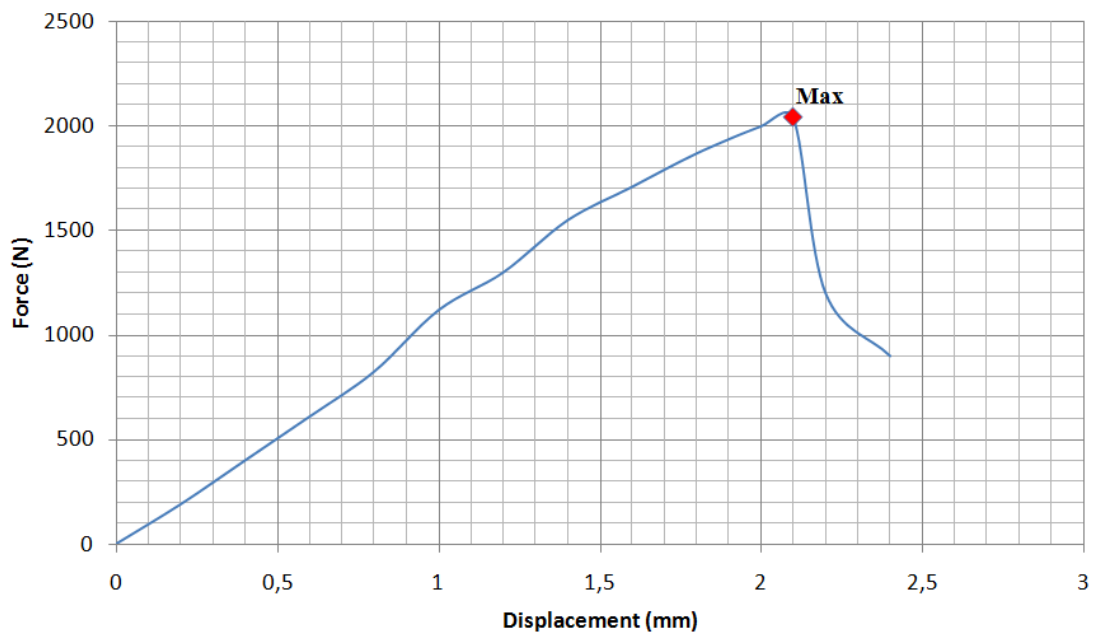


Figure 7.14 : Tensile test result of a welded ABS-ABS joint.

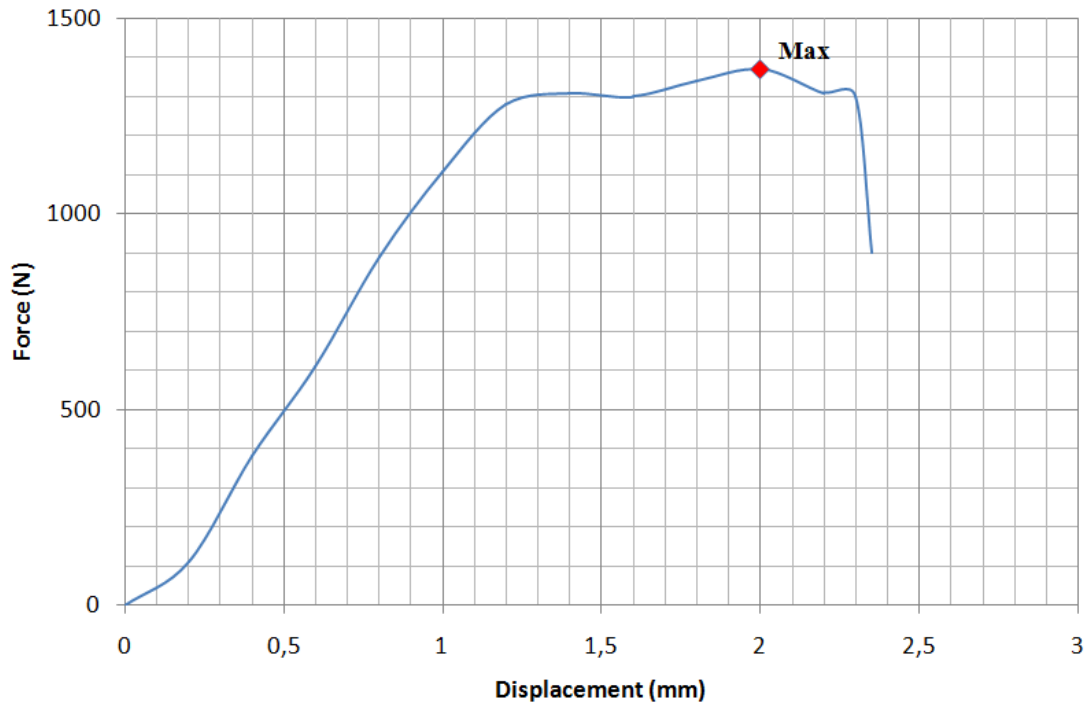


Figure 7.15 : Tensile test result of a welded PC-PC joint.

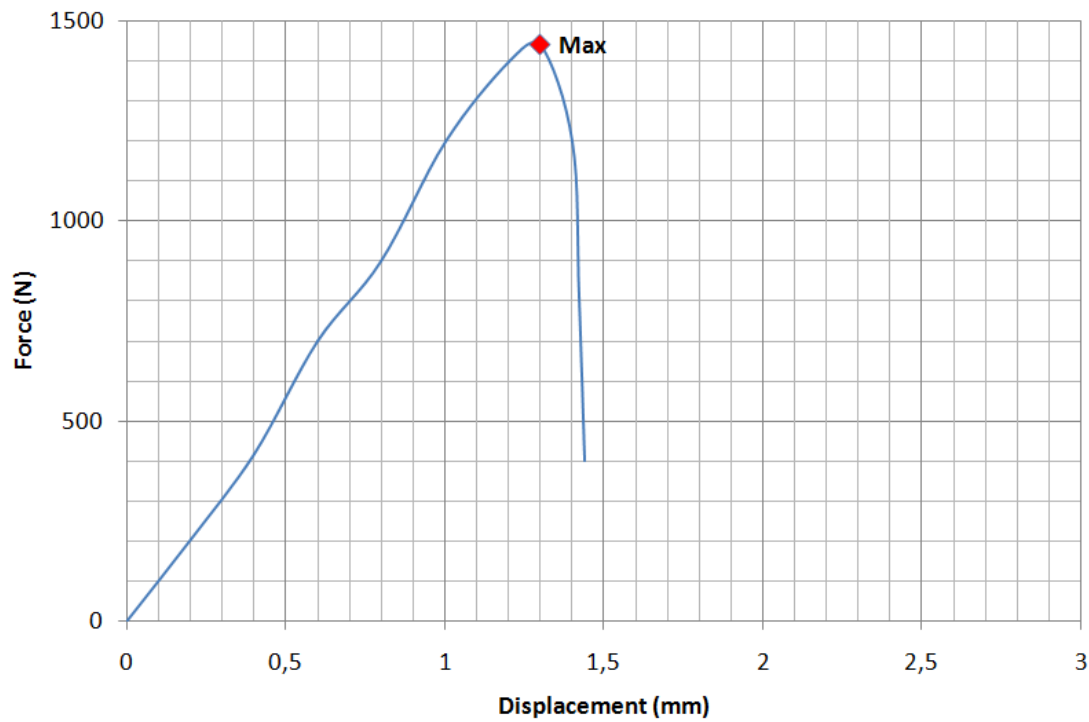


Figure 7.16 : Tensile test result of a welded ABS-PC joint.

8. RESULTS

8.1 Results of Taguchi Methods for Lap Joint Shear Load

For each weld configuration of thermoplastics, three specimens were used in tensile tests. Mean of three the lap joint shear loads obtained by the experiments designed with the Taguchi method are given for FSSW of ABS-ABS, PC-PC and ABS-PC joints in Table 8.1, Table 8.2 and Table 8.3, respectively.

Table 8.1 : Experimental results for lap joint shear load and calculated S/N ratios for ABS-ABS joints.

Experiment No.	Welding Parameters			Lap Joint Shear Load (N)	S/N Ratios (dB)
	A	B	C		
	Tool	Plunge Depth (mm)	Dwell Time (s)		
#	Rotational Speed (rpm)				
1	1000	10.5	20	1469	63.34
2	1000	11	30	1787	65.04
3	1000	11.5	40	2034	66.16
4	2000	10.5	30	1519	63.63
5	2000	11	40	1802	65.11
6	2000	11.5	20	1644	64.31
7	3000	10.5	40	1458	63.27
8	3000	11	20	1366	62.70
9	3000	11.5	30	1663	64.41

Table 8.2 : Experimental results for lap joint shear load and calculated S/N ratios for PC-PC joints.

Experiment No.	Welding Parameters			Lap Joint Shear Load	S/N Ratios
	A	B	C		
	Tool Rotational Speed	Plunge Depth	Dwell Time		
#	(rpm)	(mm)	(s)	(N)	(dB)
1	800	10.5	20	1293	62.23
2	800	11	30	844	58.52
3	800	11.5	40	1340	62.54
4	1600	10.5	30	1340	62.54
5	1600	11	40	1489	63.45
6	1600	11.5	20	1575	63.94
7	2400	10.5	40	1840	65.29
8	2400	11	20	1718	64.70
9	2400	11.5	30	1509	63.57

Table 8.3 : Experimental results for lap joint shear load and calculated S/N ratios for ABS-PC joints.

Experiment No.	Welding Parameters			Lap Joint Shear Load	S/N Ratios
	A	B	C		
	Tool Rotational Speed	Plunge Depth	Dwell Time		
#	(rpm)	(mm)	(s)	(N)	(dB)
1	800	10.5	20	1581	63.98
2	800	11	30	1094	60.78
3	800	11.5	40	1289	62.20
4	1600	10.5	30	950	59.55
5	1600	11	40	979	59.81
6	1600	11.5	20	964	59.68
7	2400	10.5	40	1174	61.39
8	2400	11	20	1049	60.41
9	2400	11.5	30	883	58.91

8.1.1 Signal-to-noise (S/N) ratio analysis

In the Taguchi experimental design, while the term "signal" refers to the desired value, the term "noise" refers to undesired value. The S/N ratio is the ratio of the mean to the squared deviation. The experiment is designed in order not to be affected by unmanageable factors. So, the signal to the noise ratio should be high.

The S/N ratio is used to determine performance characteristics deviating from the desired value in the Taguchi method [87].

The S/N ratio is calculated as follows:

$$S/N = -10 \log (\text{MSD}) \quad (8.1)$$

MSD is the mean square deviation for the output characteristics for the output.

Due to the highest lap joint shear load is desired, the mean squared deviation (MSD) for "the larger is better" is stated:

$$MSD = \frac{1}{n} \sum_{i=1}^n \frac{1}{y_i^2} \quad (8.2)$$

with y_i : value of output characteristic for the test and n : number of the i th test.

Last column of Table 8.1, Table 8.2 and Table 8.3 indicates S/N ratios determined by Equation (1) and (2). These values calculated using Minitab v.17.

8.1.2 Response tables of S/N ratios and main effects plots

It is not possible to clearly understand the influence of each process parameter on the lap joint shear load from Table 8.1, 8.2 and 8.3.

Since the orthogonal experiment design is used, each welding parameter can be divided into 3 levels. For example, the average S/N ratios for the tool rotation speeds at levels 1, 2 and 3 can be obtained by averaging the S/N ratios of experiments 1-3, 4-6 and 7-9, respectively.

In the results obtained from Minitab program, S/N ratios response tables (Table 8.4, 8.5, 8.6) and main effect plots (Figure 8.1-8.3, 8.4-8.6, 8.7-8.9) were determined according to tensile test results for ABS-ABS, PC-PC, and ABS-PC joints, respectively.

Table 8.4 : Response table of S/N ratios (larger-is-better) for ABS-ABS joint.

Symbol	Welding Parameters	S/N Ratios (dB)						Rank
		Level 1	Level 2	Level 3	Max.	Min.	Delta	
A	Rotational Speed	64.85	64.35	63.47	64.85	63.47	1.38	3
B	Plunge Depth	63.42	64.29	64.97	64.97	63.42	1.55	1
C	Dwell Time	63.46	64.36	64.85	64.85	63.46	1.40	2

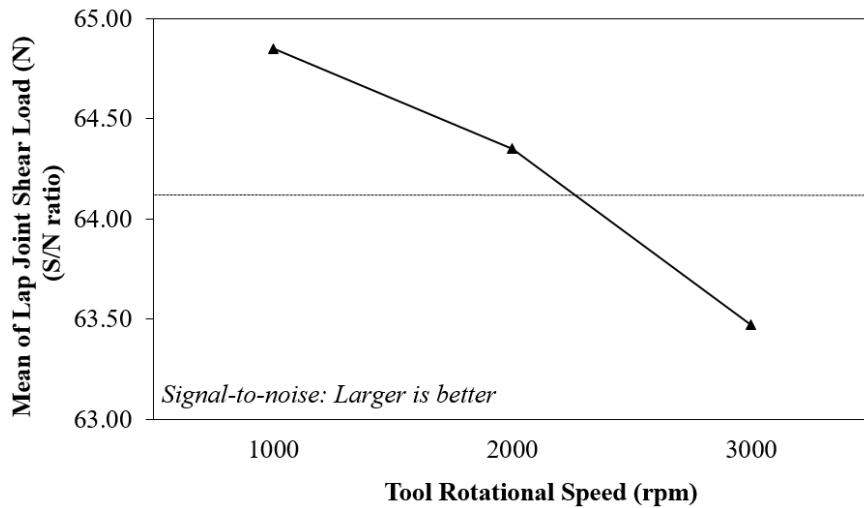


Figure 8.1 : Tool rotational speed-lap joint shear load graph for S/N ratio of ABS-ABS joint.

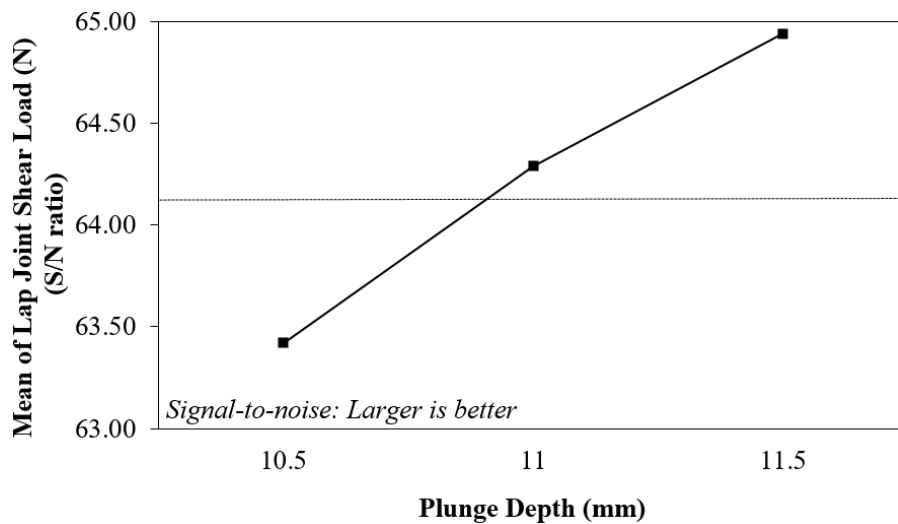


Figure 8.2 : Plunge depth-lap joint shear load graph for S/N ratio of ABS-ABS joint.

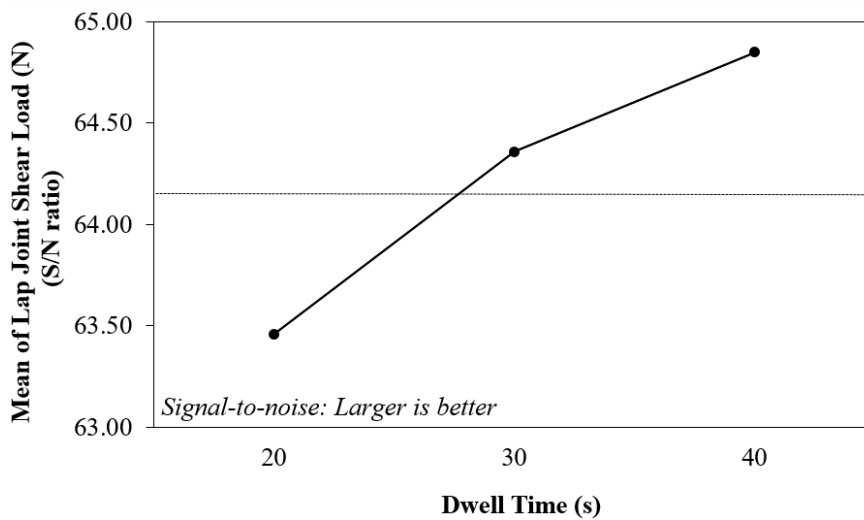


Figure 8.3 : Dwell time-lap joint shear load graph for S/N ratio of ABS-ABS joint.

Table 8.5 : Response table of S/N ratios (larger-is-better) for PC-PC joint.

Symbol	Welding Parameters	S/N Ratios (dB)						Rank
		Level 1	Level 2	Level 3	Max.	Min.	Delta	
A	Rotational Speed	61.10	63.32	64.52	64.52	61.10	3.42	1
B	Plunge Depth	63.36	62.23	63.35	63.36	62.23	1.13	3
C	Dwell Time	63.63	61.55	63.77	63.77	61.55	2.22	2

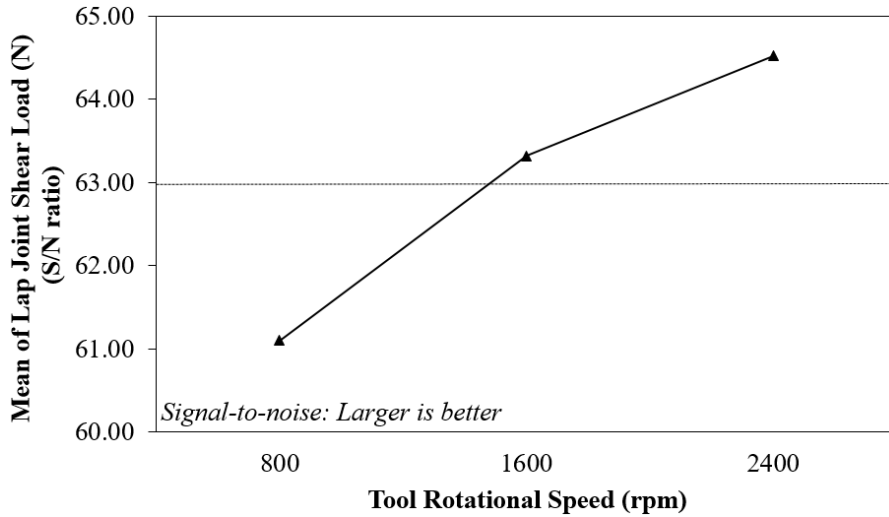


Figure 8.4 : Tool rotational speed-lap joint shear load graph for S/N ratio of PC-PC joint.

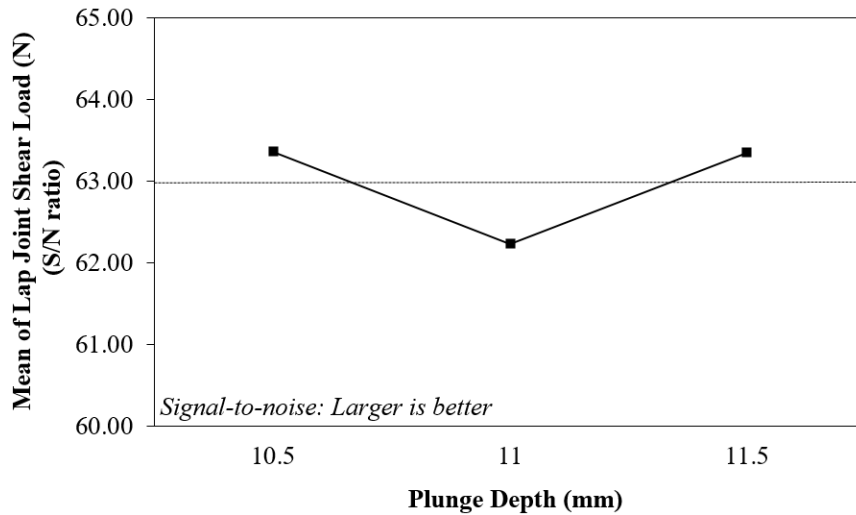


Figure 8.5 : Plunge depth-lap joint shear load graph for S/N ratio of PC-PC joint.

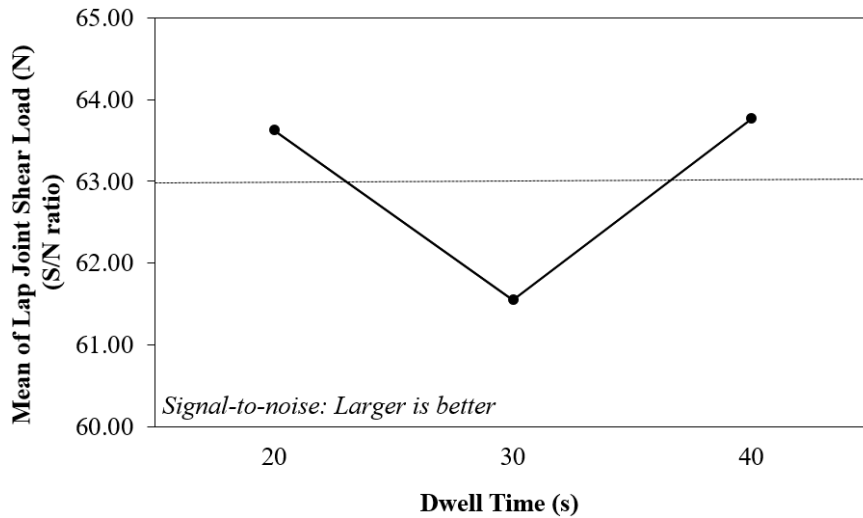


Figure 8.6 : Dwell time-lap joint shear load graph for S/N ratio of PC-PC joint.

Table 8.6 : Response table of S/N ratio (larger-is-better) for ABS-PC joint.

Symbol	Welding Parameters	S/N Ratios (dB)			Max.	Min.	Delta	Rank
		Level 1	Level 2	Level 3				
A	Rotational Speed	62.32	59.68	60.24	62.32	59.68	2.64	1
B	Plunge Depth	61.64	60.34	60.27	61.64	60.27	1.37	3
C	Dwell Time	61.36	59.75	61.14	61.36	59.75	1.61	2

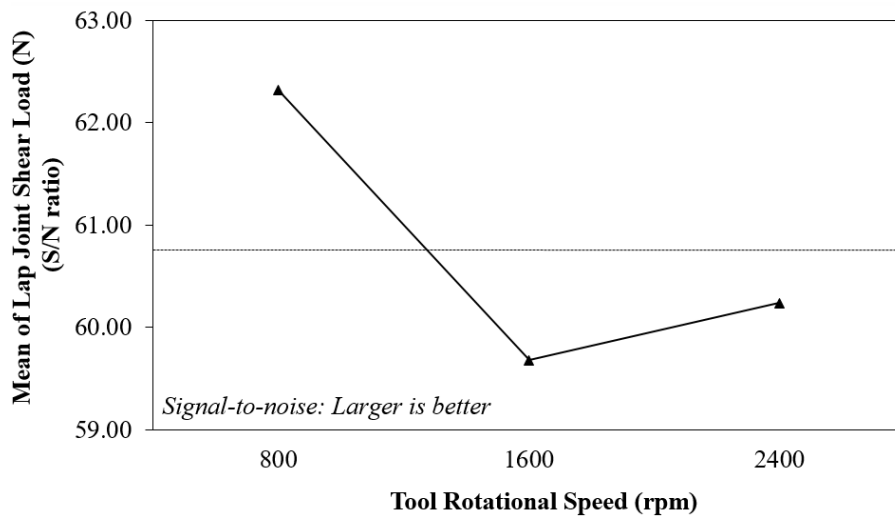


Figure 8.7 : Tool rotational speed-lap joint shear load graph for S/N ratio of ABS-PC joint.

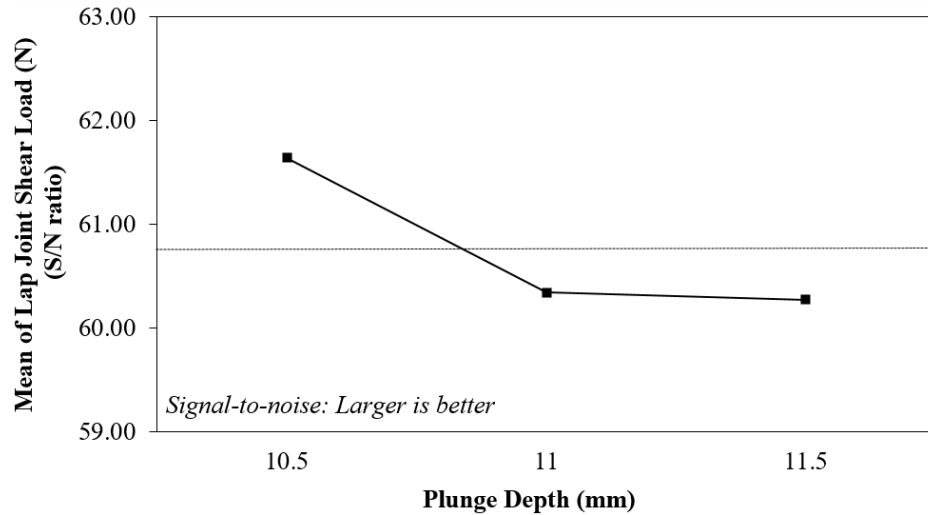


Figure 8.8 : Plunge depth-lap joint shear load graph for S/N ratio of ABS-PC joint.

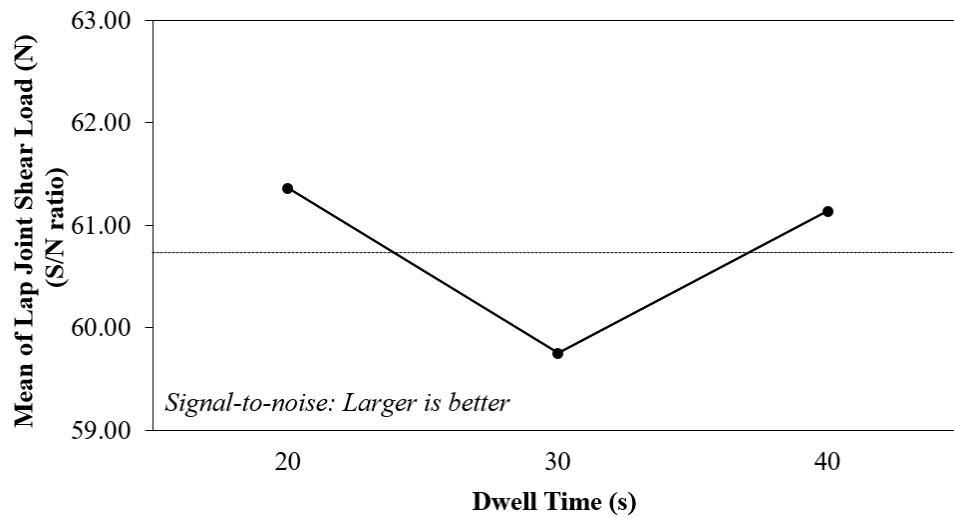


Figure 8.9 : Dwell time-lap joint shear load graph for S/N ratio of ABS-PC joint.

8.1.3 Response tables of means and main effect plots

Similar to the response tables and main effects plots for S/N ratios, the response tables (Table 8.7, 8.8 and 8.9) and main effects plots (Figure 8.10-8.12, 8.13-8.15 and 8.16-8.18) of means were created to show the effects of welding parameters on weld strength for ABS-ABS, PC-PC, and ABS-PC joints, respectively.

Table 8.7 : Response table of means for ABS-ABS joint.

Symbol	Welding Parameters	Means						
		Level 1	Level 2	Level 3	Max.	Min.	Delta	Rank
A	Rotational Speed	1763	1655	1496	1763	1496	267	3
B	Plunge Depth	1482	1652	1780	1780	1482	298	1
C	Dwell Time	1493	1656	1765	1765	1493	272	2

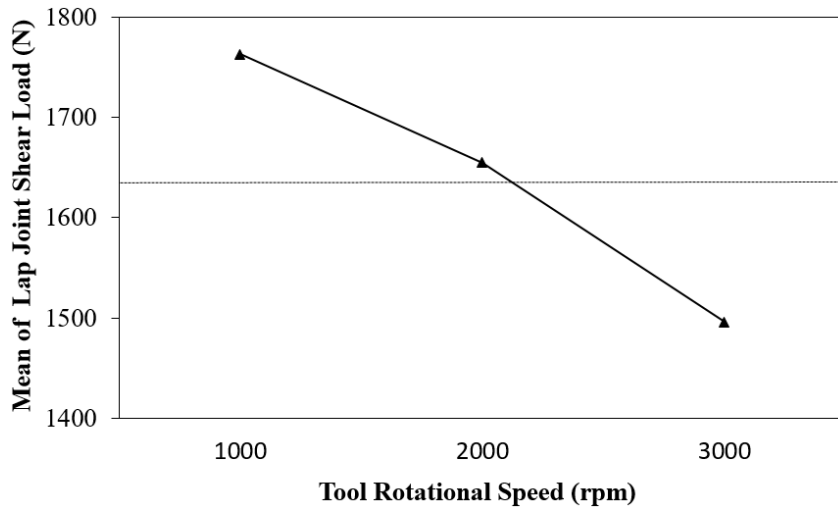


Figure 8.10 : Tool rotational speed-lap joint shear load graph of main effects for ABS-ABS joint.

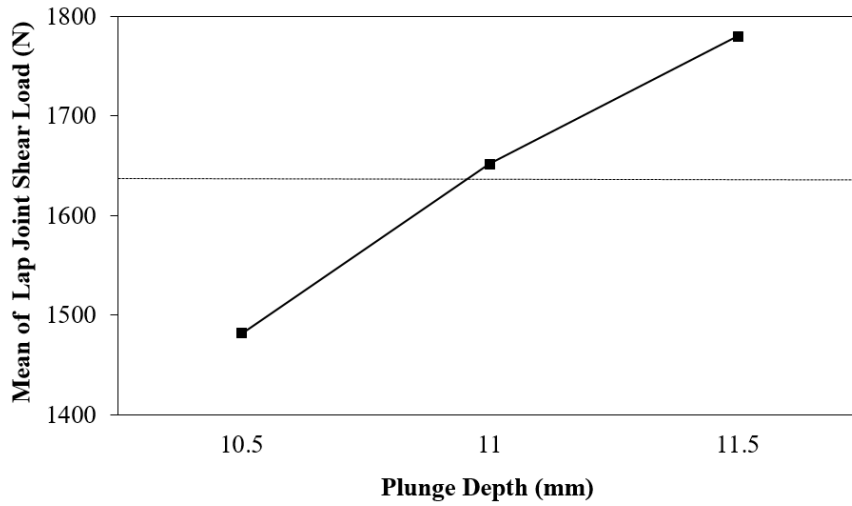


Figure 8.11 : Plunge depth-lap joint shear load graph of main effects for ABS-ABS joint.

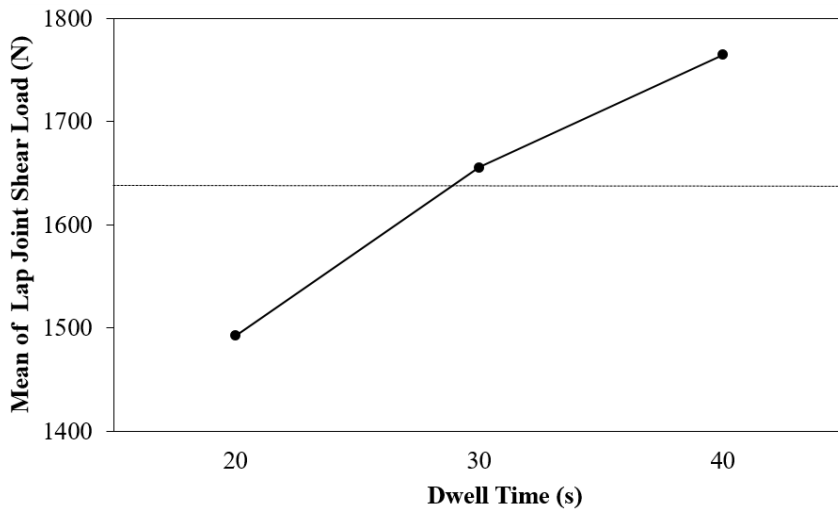


Figure 8.12 : Dwell time-lap joint shear load graph of main effects for ABS-ABS joint.

Table 8.8 : Response table of means for PC-PC joint.

Symbol	Welding Parameters	Means						
		Level 1	Level 2	Level 3	Max.	Min.	Delta	Rank
A	Rotational Speed	1159	1468	1689	1689	1159	530	1
B	Plunge Depth	1491	1350	1475	1491	1350	141	3
C	Dwell Time	1529	1231	1556	1556	1231	325	2

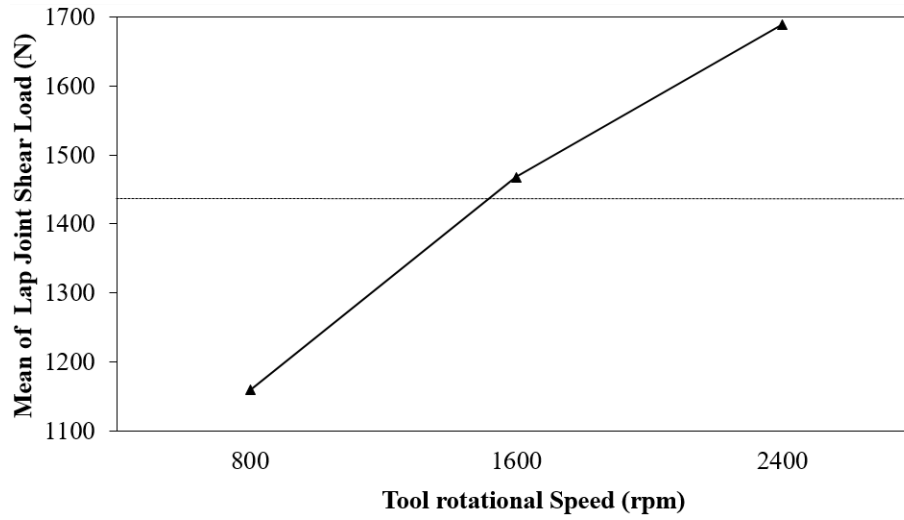


Figure 8.13 : Tool rotational speed-lap joint shear load graph of main effects for PC-PC joint.

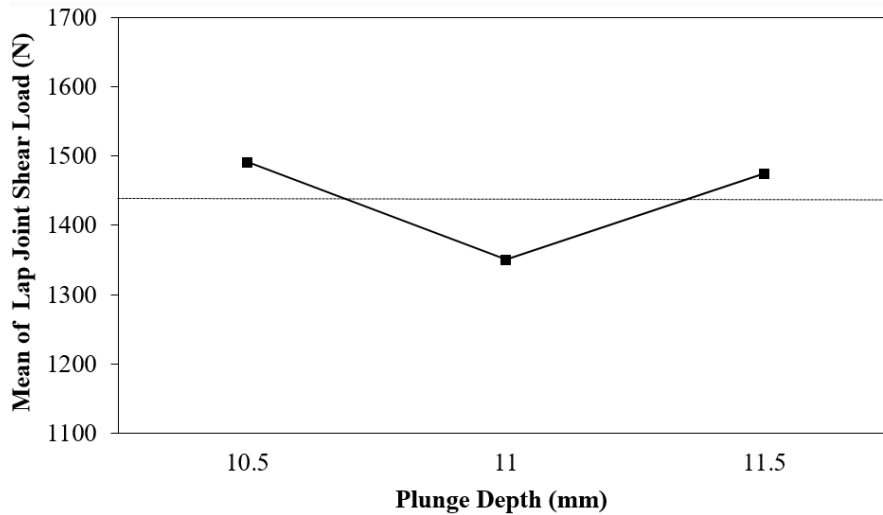


Figure 8.14 : Plunge depth-lap joint shear load graph of main effects for PC-PC joint.

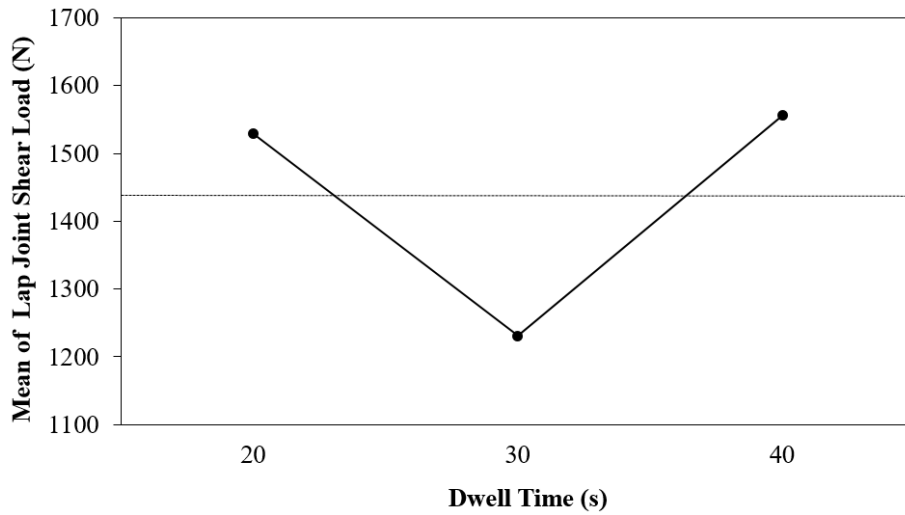


Figure 8.15 : Dwell time-lap joint shear load graph of main effects for PC-PC joint.

Table 8.9 : Response table of means for ABS-PC joint.

Symbol	Welding Parameters	Means						
		Level 1	Level 2	Level 3	Max.	Min.	Delta	Rank
A	Rotational Speed	1321	964	1035	1321	964	357	1
B	Plunge Depth	1235	1041	1045	1235	1041	194	3
C	Dwell Time	1198	976	1147	1198	976	222	2

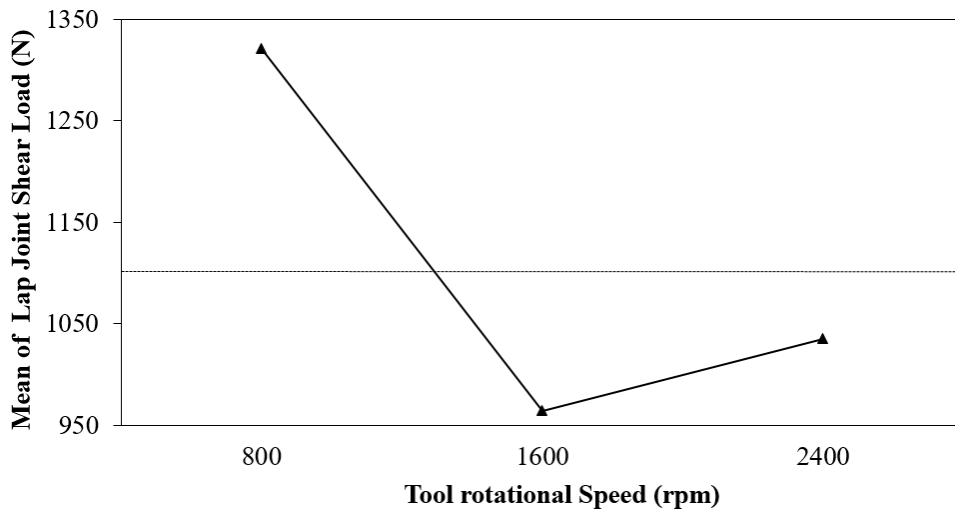


Figure 8.16 : Tool rotational speed-lap joint shear load graph of main effects for ABS-PC joint.

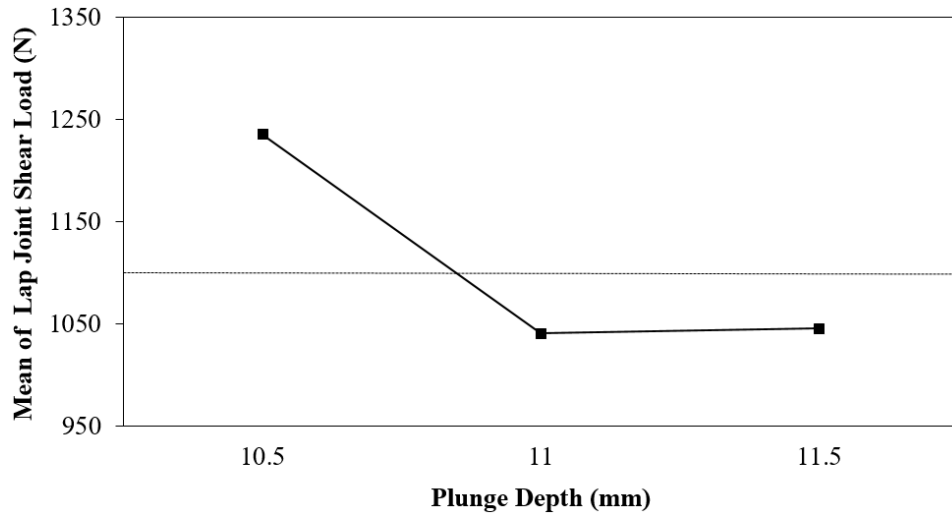


Figure 8.17 : Plunge depth-lap joint shear load graph of main effects for ABS-PC joint.

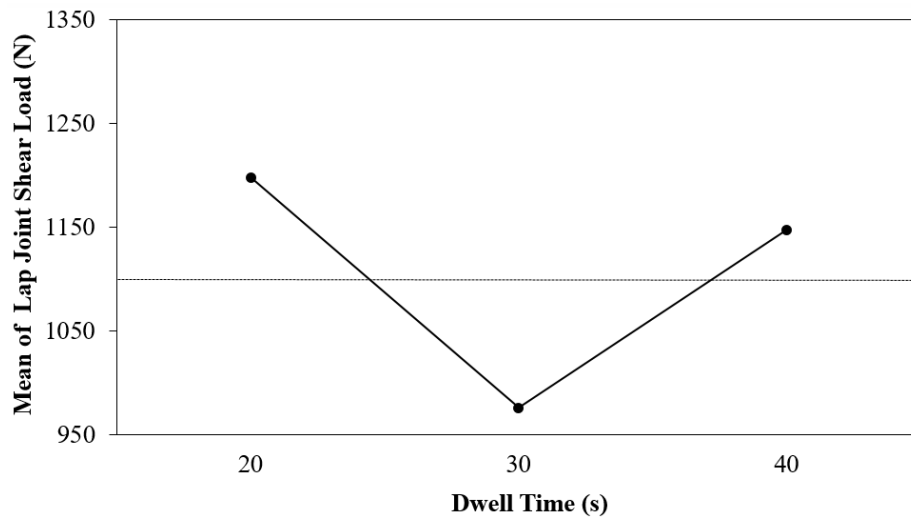


Figure 8.18 : Dwell time-lap joint shear load graph of main effects for ABS-PC joint.

8.1.4 Normal probability plot of residulas

The residual values graphs in Figure 8.19, 8.20, and 8.21 were created according to the lap joint shear load average values of ABS-ABS, PC-PC and ABS-PC joints in Table 8.1, 8.2 and 8.3, respectively. When these graphs are examined visually, it is seen that weld strengths do not show an unusual tendency in terms of independence and normality assumptions.

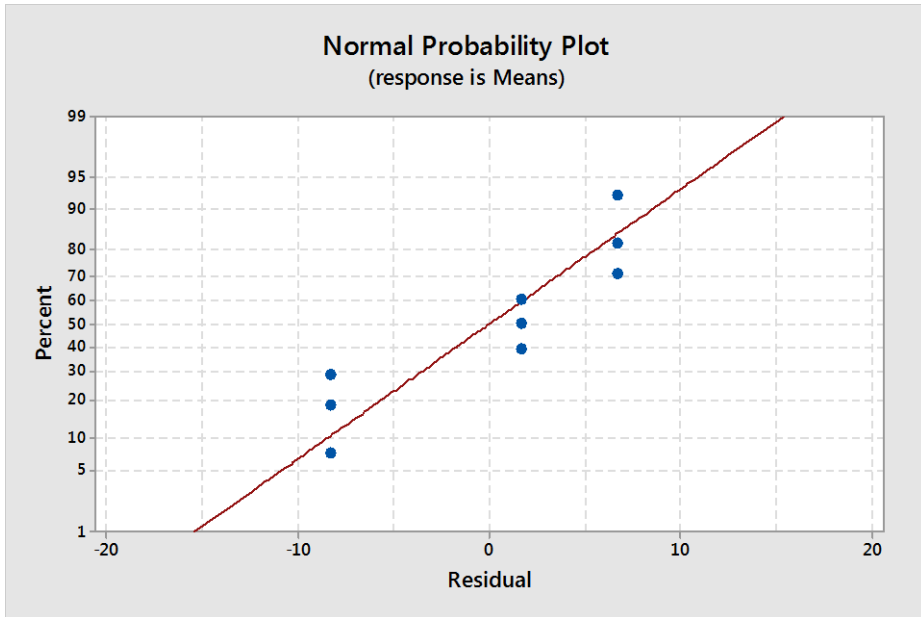


Figure 8.19 : Normal probability and residual values graphs for weld strengths in ABS-ABS joints

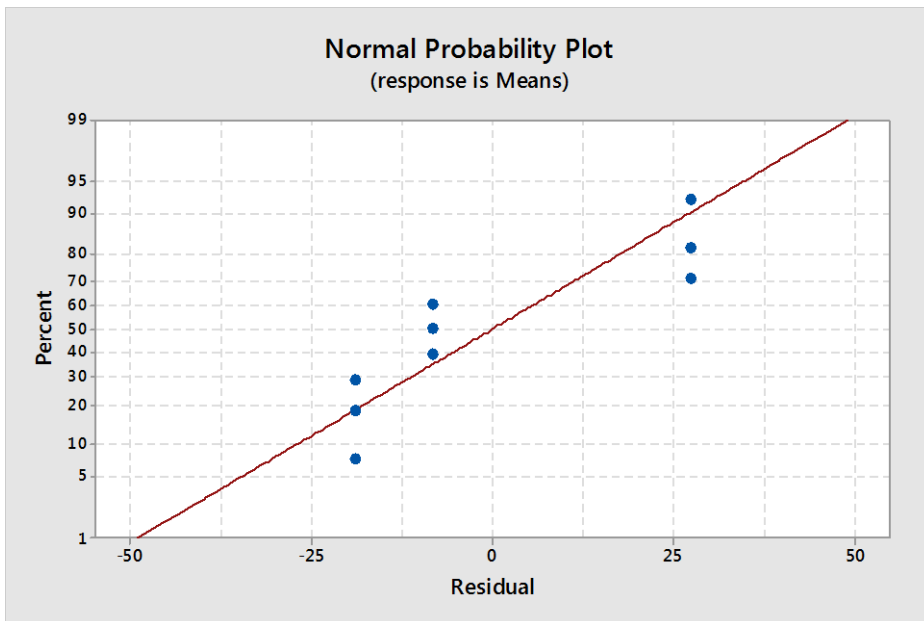


Figure 8.20 : Normal probability and residual values graphs for weld strengths in PC-PC joints

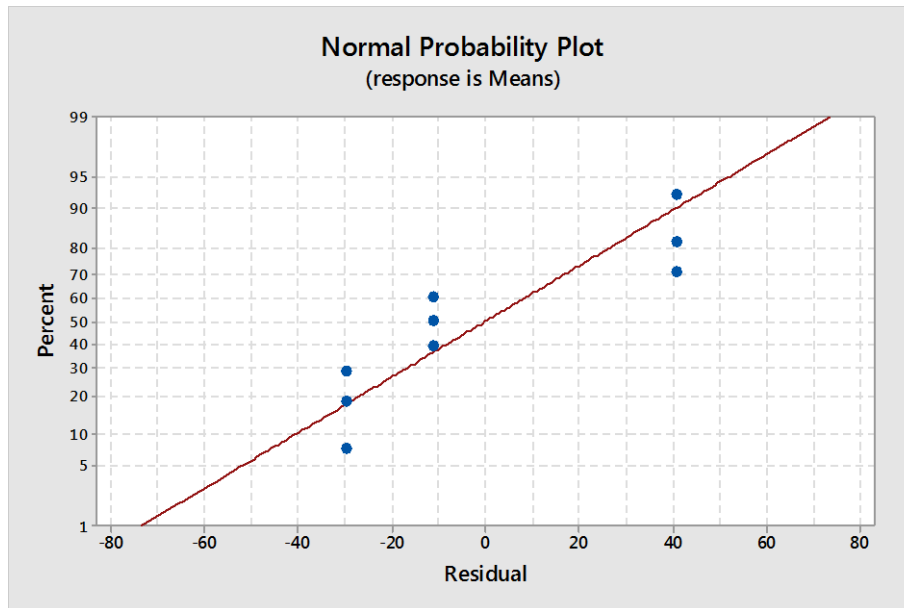


Figure 8.21 : Normal probability and residual values graphs for weld strengths in ABS-PC joints.

8.1.5 Analysis of variance (ANOVA)

Another way to reveal the influences of the process parameters on the joint strength is the statistical analysis of the experimental data consisting of two stages.

The first stage is analysis of variance (ANOVA) and the second stage is the Fisher test (F-test) which is related to the correlation of input parameters in the FSSW process [88].

In the first phase, ANOVA is used to investigate the significance of the process parameters using the relationship between processing parameters of FSSW and lap joint shear load.

The analysis of variance aims to determine which welding parameter has a significant effect on the weld strength and to calculate the effect rates by dividing the variances. This study includes process input variables (tool rotational speed, plunge depth, dwell time) and output variables (lap joint shear load). Evaluations and calculations of ANOVA results for lap joint shear load was carried out by using Minitab v17.1 software (Table 8.10, 8.11 and 8.12).

Table 8.10 : ANOVA results for lap joint shear load of ABS-ABS joint.

Welding Parameter	Symbol	Degree of Freedom	Sum of Squares	Mean Squares (Variance)	Variance Ratio	Contribution
Factor		f	S	V	F	P (%)
Rotational Speed	A	2	108,769	54,384	310	30.6
Plunge Depth	B	2	134,345	67,172	383	37.8
Dwell Time	C	2	112,217	56,108	320	31.5
Error	E	2	350	175		0.1
Total		8	355,680			100.0

Table 8.11 : ANOVA results for lap joint shear load of PC-PC joint.

Welding Parameter	Symbol	Degree of Freedom	Sum of Squares	Mean Squares (Variance)	Variance Ratio	Contribution
Factor		f	S	V	F	P (%)
Rotational Speed	A	2	425,222	212611	120	64.5
Plunge Depth	B	2	35,513	17756	10	5.4
Dwell Time	C	2	195,213	97606	55	29.6
Error	E	2	3,533	1,766		0.5
Total		8	659,480			100.0

Table 8.12 : ANOVA results for lap joint shear load of ABS-PC joint.

Welding Parameter	Symbol	Degree of Freedom	Sum of Squares	Mean Squares (Variance)	Variance Ratio	Contribution
Factor		f	S	V	F	P (%)
Rotational Speed	A	2	214,286	107,413	26	56.8
Plunge Depth	B	2	73,761	36,880	9	19.5
Dwell Time	C	2	81,469	40,734	10	21.6
Error	E	2	7,965	3,982		2.1
Total		8	377,480			100.0

8.1.6 Fisher Test (F Test)

The second step in statistical analysis is the Fisher test, which determines the significance of the process parameters.

A larger F value shows that the variation of the process parameters leads to a significant change in the effectiveness.

When the variance ratios in Table 8.13 are evaluated with Fisher test significance levels in Table 8.14, 8.15 and 8.16. Fisher test significance levels of the factors affecting the FSSW process of ABS-ABS, PC-PC and ABS-PC joints can be listed as in Table 8.13.

For ABS-ABS welds, it was found that process input variables showed a very significant influence on welding strength at the 99.5% confidence level because of their F values (310, 383, 320) which are greater than Fisher test values ($F_{0,005}(2,2) = 199$) (Table 8.14). Plunge depth has a maximum significant effect on increase in the lap joint shear load.

For PC-PC welds, their confidence levels are at 99%, 90%, and 95%, respectively. Because their F values determined from experimental results are 120, 10 and 55 which are greater than the F-values concluded from statistical calculations as seen Table 8.15. The most dominant factor was the tool rotational speed in increasing the lap joint shear load.

For ABS-PC welds, effect of tool rotational speed, plunge depth and dwell time was found statistically significant on lap joint shear load at the 95%, 90%, and 90% confidence levels because their F values are 26, 9 and 10, respectively. These values are greater than the F-values concluded from statistical calculations ($F_{0,05}(2,2) = 95.00$ and $F_{0,1}(2,2) = 90.00$) (Table 8.16). In this investigation, tool rotational speed is the most effective factor and plays a major role in affecting the lap joint shear load of the weld.

Table 8.13 : Fisher test values.

$F_{\alpha}(f_1, f_2)$	Significance level (%)	Confidence level (%)	Fisher test value
$F_{0.005}(2,2)$	0.5	99.5	199
$F_{0.01}(2,2)$	1	99	99
$F_{0.05}(2,2)$	5	95	19
$F_{0.1}(2,2)$	10	90	9

α : Significance level

f_1 : degree of freedom for variable factor

f_2 : degree of freedom for error factor

Table 8.14 : Fisher test values for the FSSW parameters of ABS-ABS joint.

Symbol	Welding Parameters	Variance Ratio	Confidence Level (%)
A	Tool Rotational Speed	310	99.5
B	Plunge Depth	383	99.5
C	Dwell Time	320	99.5

Table 8.15 : Fisher test values for the FSSW parameters of PC-PC joint.

Symbol	Welding Parameters	Variance Ratio	Confidence Level (%)
A	Tool Rotational Speed	120	99
B	Plunge Depth	10	90
C	Dwell Time	55	95

Table 8.16 : Fisher test values for the FSSW parameters of ABS-PC joint.

Symbol	Welding Parameters	Variance Ratio	Confidence Level (%)
A	Tool Rotational Speed	27	95
B	Plunge Depth	9	90
C	Dwell Time	10	90

8.1.7 Contribution rate of welding parameters

The contribution rate (P_i) is part of the total variation observed in the experiment and attributed to each factor (Equation 6.13). The contribution rate can be explained as the ratio of the sum of squares to the total sum of squares for each factor. It shows the relative power of each factor to reduce the differences (Equation 8.4).

$$P_i = \frac{SS'_i}{SS_T} \quad (8.4)$$

If the process parameter levels are fully controlled, the contribution percentage of the total variation may be reduced.

For example, the contribution ratio of the dwell time for ABS-ABS joint is calculated as follows.

$$P_C = \frac{SS'_i}{SS_T} = \frac{112217}{355680} = 0.315$$

$$P_C = 31.5 \%$$

The influence of the control factors on the FSSW processes of ABS-ABS, PC-PC, and ABS-PC joints are shown in Figure 8.22, 8.23 and 8.24, respectively. Also, The error rates were very low in FSSW of ABS-ABS, PC-PC, and ABS-PC joints. It proves that the experimental design was very successful.

In the FSSW process of ABS-ABS specimens, the total percentage of contribution rate was 99.9%. The error ratio was only 0.1%. The most effective factor was plunge depth with a contribution rate of 37.8% (Figure 8.22).

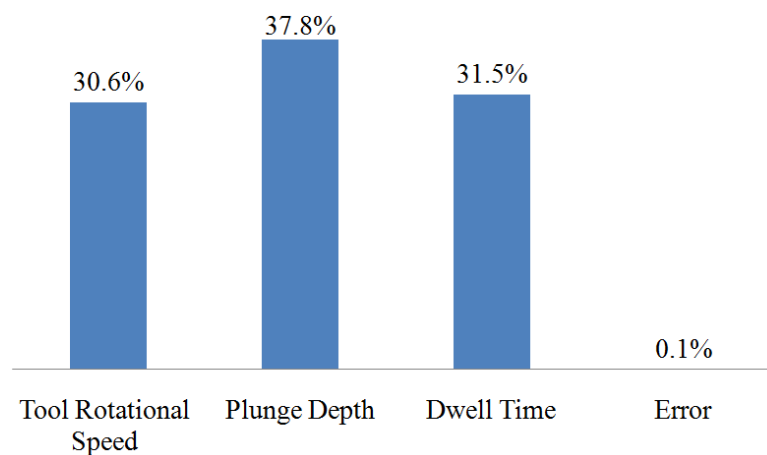


Figure 8.22 : Contribution rates of welding parameters for ABS-ABS joint.

In the FSSW process of PC-PC specimens, the total percentage contribution rate of welding parameters was 99.5%. Experimental errors was only 0.5%. According to ANOVA results, it was found that the tool rotational speed is the most important factor having a contribution rate of 64.5% (Figure 8.23).

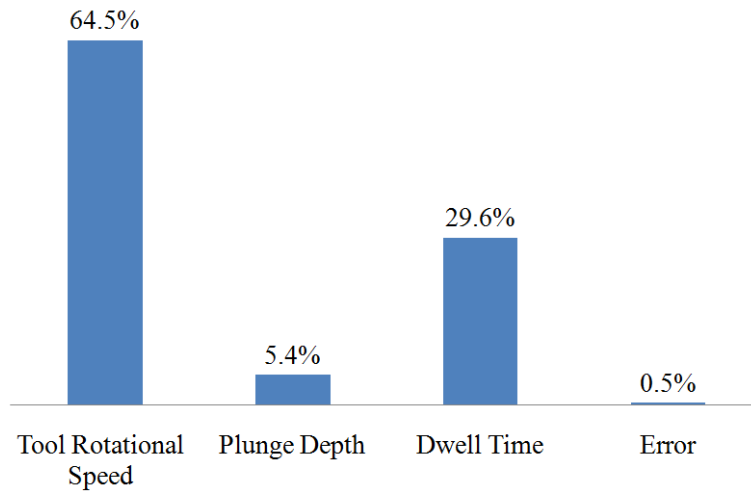


Figure 8.23 : Contribution rates of welding parameters for PC-PC joint.

In the FSSW process of ABS-PC dissimilar joint, the total percentage contribution rate of the FSSW parameters was found as 97.9%. The percentage of experimental error was 2.1%. The most important parameter is the tool rotational speed with a contribution of 56.8% (Figure 8.24).

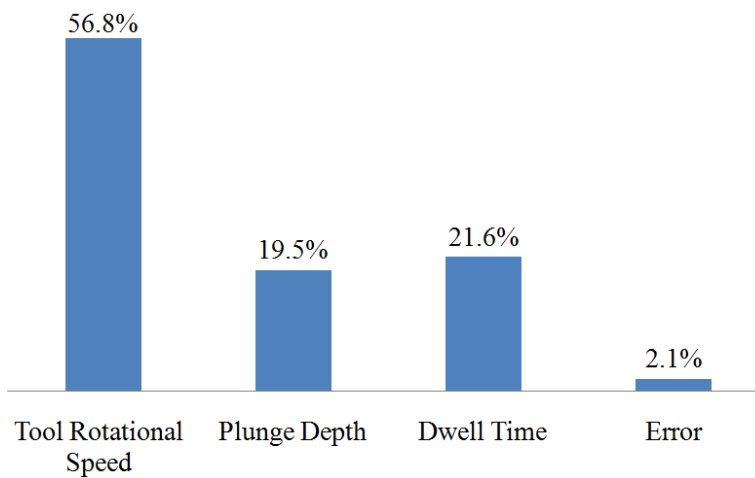


Figure 8.24 : Contribution rates of welding parameters for ABS-PC joint.

8.1.8 Optimum welding parameters

8.1.8.1 Optimum welding parameters and levels for ABS-ABS joints

In the FSSW process of ABS-ABS joint, the optimum welding parameters are found as $A_1B_3C_3$ from the Figure 8.25, 8.26 and 8.27 created by selecting the highest S/N ratios in the main effect plots (Figure 8.1, 8.2 and 8.3) and according to the S/N result table depending on the tensile test results (Table 8.4).

Optimum process parameters and their levels were listed in the Table 8.17. For the FSSW of ABS-ABS joint, if the tool rotational speed is set to level 1 and the plunge depth and dwell time are set to level 3, optimum process parameters will be obtained from the Taguchi method.

Table 8.17 : Optimum process parameters and levels for FSSW of ABS-ABS joint.

Symbol	Welding Parameters	Optimum Welding Parameters and Levels		
		Levels		
A	Tool Rotational Speed	1	1000 rpm	$A_1B_3C_3$
B	Plunge Depth	3	11.5 mm	
C	Dwell Time	3	40 s	

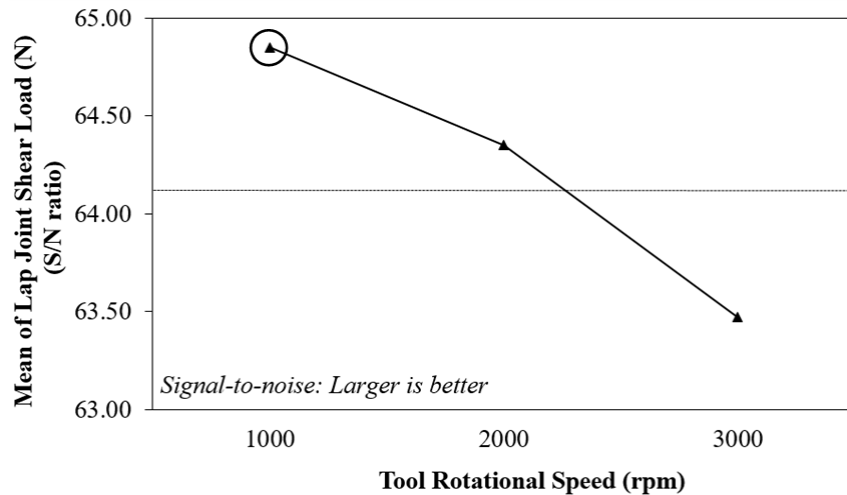


Figure 8.25 : Main effects plot of FSSW of ABS-ABS joint (optimum tool rotational speed-lap joint shear load).

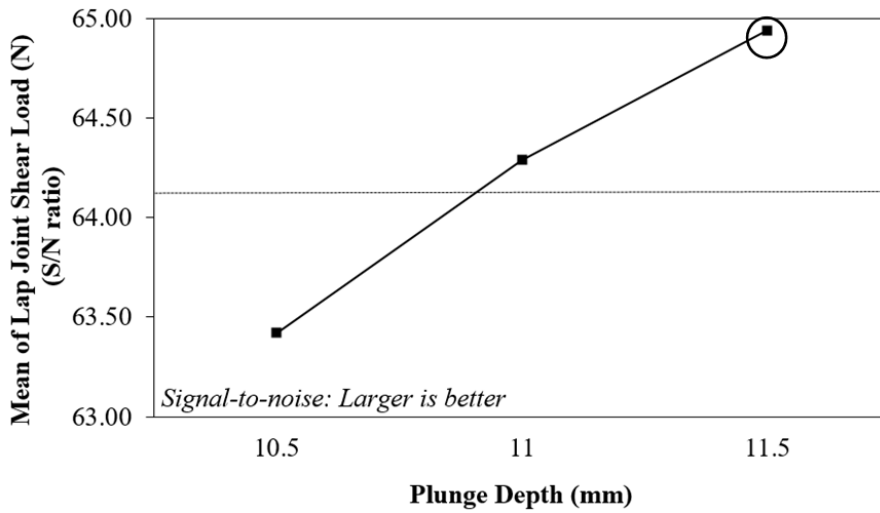


Figure 8.26 : Main effects plot of FSSW of ABS-ABS joint (optimum plunge depth-lap joint shear load).

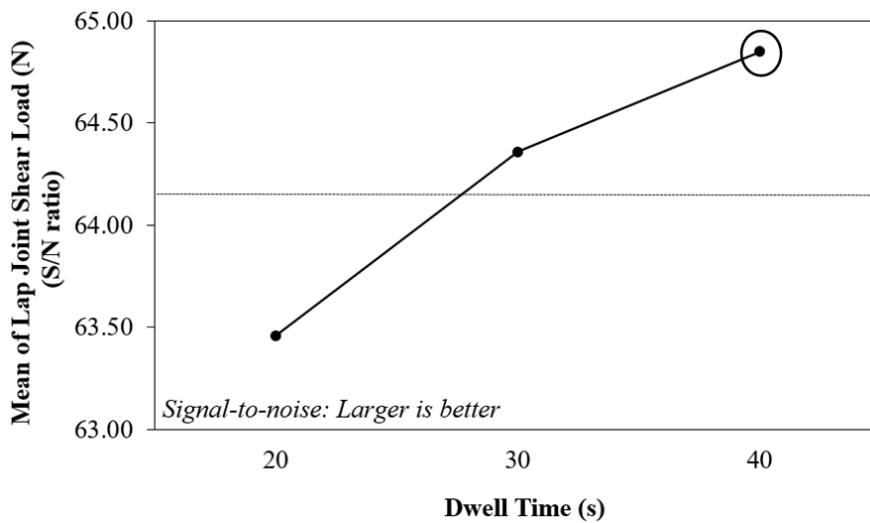


Figure 8.27 : Main effects plot of FSSW of ABS-ABS joint (optimum dwell time-lap joint shear load).

8.1.8.2 Optimum welding parameters and levels for PC-PC joints

The same way is followed to find the optimum parameters of FSSW of PC-PC joints as in the FSSW of ABS-ABS joint. Thus, the optimum welding parameters of FSSW of PC-PC joints were found $A_3B_1C_3$ by selecting the highest S/N ratios as illustrated in Figure 8.28, 8.29 and 8.30 which are created depending on the S/N ratio response table (Table 8.6) and main effects graphs of lap joint shear load-S/N ratios (Figure 8.7, 8.8 and 8.9).

Table 8.18 shows the optimum welding parameters and levels of FSSW of PC-PC joints. Optimum lap joint shear load is achieved, when the tool rotational speed is selected as level 3, the plunge depth is selected as level 1 and the dwell time is selected as level 3 in the Taguchi method.

Table 8.18 : Optimum process parameters and levels for FSSW of PC-PC joint.

Symbol	Welding Parameters	Optimum Welding Parameters and Levels		
		Levels		
A	Tool Rotational Speed	3	2400 rpm	
B	Plunge Depth	1	10.5 mm	A ₃ B ₁ C ₃
C	Dwell Time	3	40 s	

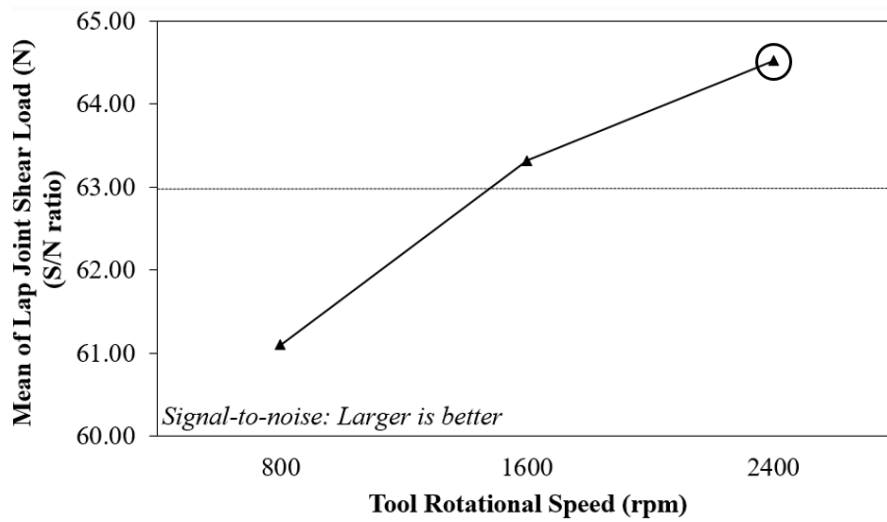


Figure 8.28 : Main effects plot of FSSW of PC-PC joint (optimum tool rotational speed-lap joint shear load).

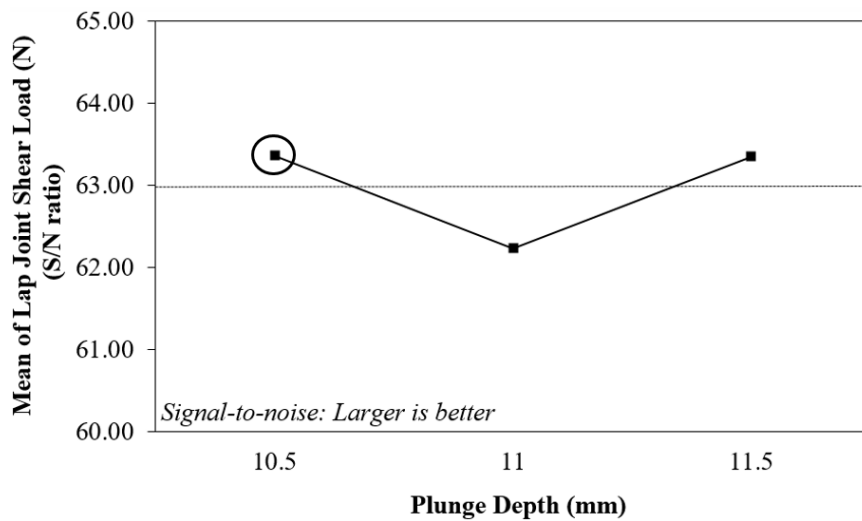


Figure 8.29 : Main effects plot of FSSW of PC-PC joint (optimum plunge depth-lap joint shear load).

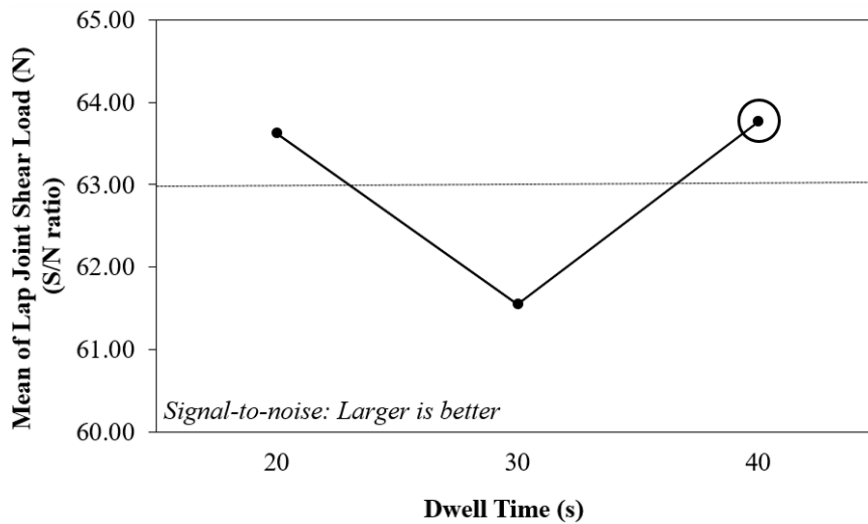


Figure 8.30 : Main effects plot of FSSW of PC-PC joint (optimum dwell time-lap joint shear load).

8.1.8.3 Optimum welding parameters and levels for ABS-PC joints

In the same way, optimum parameters of the FSSW of ABS-PC dissimilar thermoplastics are found $A_1B_1C_1$ by selecting the highest S/N ratios in Figure 8.31, 8.32 and 8.33 created according to the S/N ratio response table (Table 8.8) and main effects graphs of the lap joint shear load-S/N ratios (Figure 8.13, 8.14 and 8.15).

Optimum process parameters and levels were listed in Table 8.19. In the FSSW of ABS-PC dissimilar thermoplastics, if the tool rotational speed, plunge depth and dwell time is set to level 1 optimum lap joint shear load will be achieved according to the Taguchi experimental method.

Table 8.19 : Optimum process parameters and levels for FSSW of ABS-PC joint.

Symbol	Welding Parameters	Optimum Welding Parameters and Levels		
		Levels		
A	Tool Rotational Speed	1	800 rpm	$A_1B_1C_1$
B	Plunge Depth	1	10.5 mm	
C	Dwell Time	1	20 s	

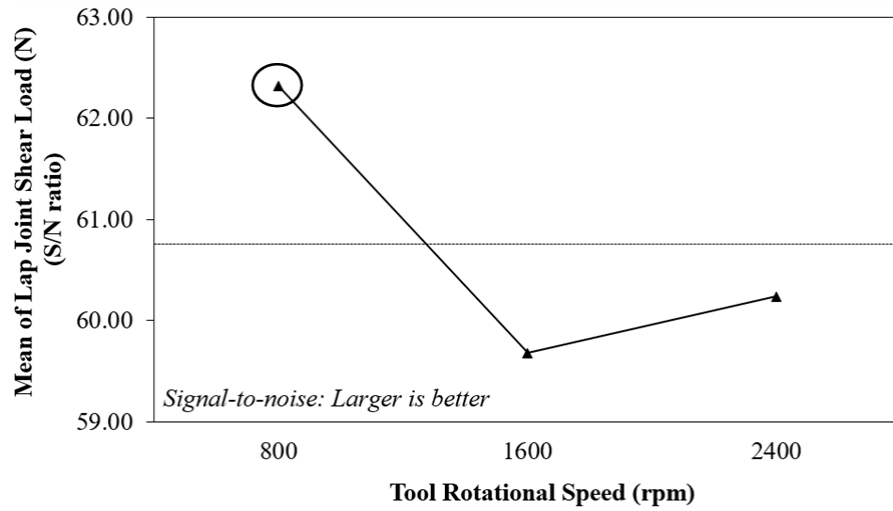


Figure 8.31 : Main effects plot of FSSW of ABS-PC joint (optimum tool rotational speed-lap joint shear load).

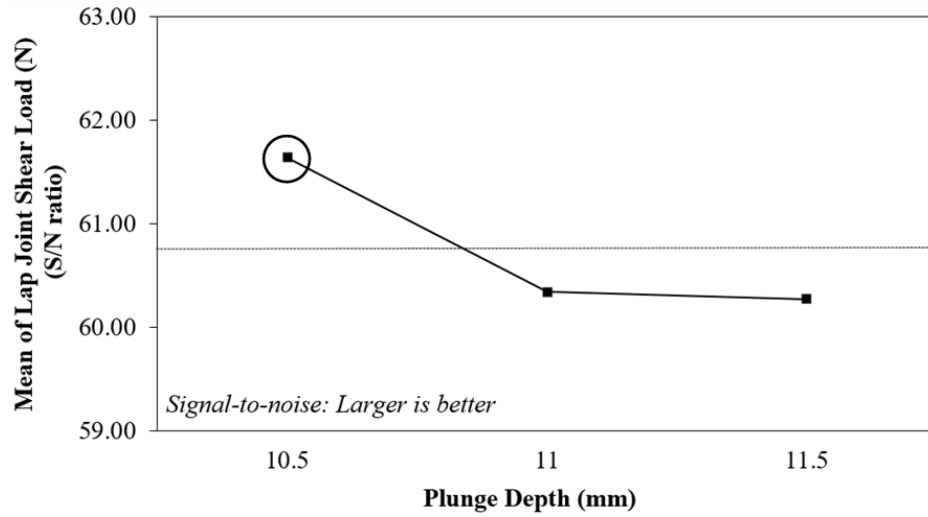


Figure 8.32 : Main effects plot of FSSW of ABS-PC joint (optimum plunge depth-lap joint shear load).

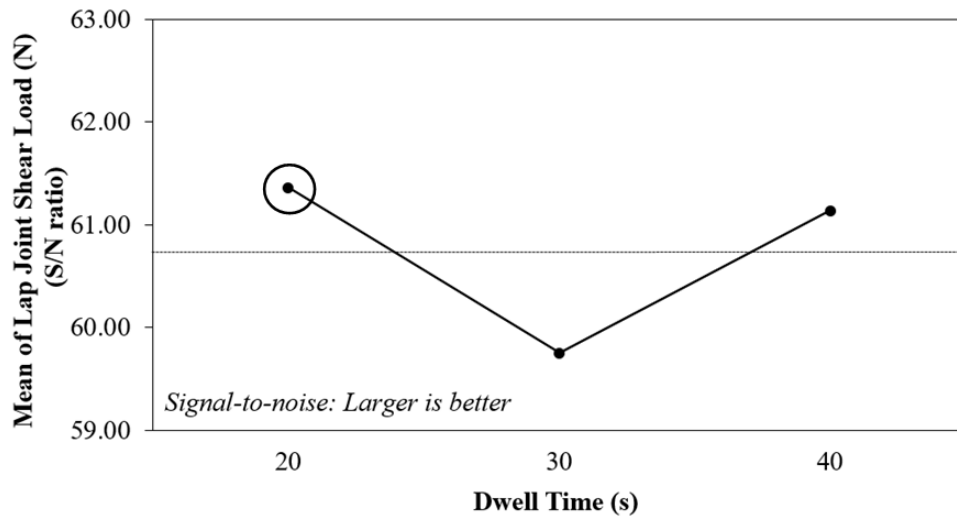


Figure 8.33 : Main effects plot of FSSW of ABS-PC joint (optimum dwell time-lap joint shear load).

8.1.9 Calculations of predicted values of optimum lap joint shear load for ABS-ABS, PC-PC and ABS-PC joints

Since optimum process parameters and levels are determined as $A_1B_3C_3$ for FSSW of ABS-ABS joint, the predicted value of optimum lap joint shear load (SL_p) is calculated using Equation 8.5.

$$SL_p = A_1 + B_3 + C_3 - 2T_m \quad (8.5)$$

$$SL_p = 1763 + 1780 + 1765 - 2(1637)$$

$$SL_p = 2034 \text{ N}$$

where T_m is the overall average of lap shear fracture loads by obtained experiments.

The same way is followed to find the predicted value of optimum lap joint shear load and S/N ratios of PC-PC and ABS-PC joints.

For FSSW of PC-PC joints:

$$SL_p = A_3 + B_1 + C_3 - 2T_m \quad (8.6)$$

$$SL_p = 1689 + 1491 + 1556 - 2(1439)$$

$$SL_p = 1858 \text{ N}$$

For FSSW of ABS-PC joints:

$$SL_p = A_1 + B_1 + C_1 - 2T_m \quad (8.7)$$

$$SL_p = 1321 + 1235 + 1198 - 2(1107)$$

$$SL_p = 1540 \text{ N}$$

y_i is substituted by SL_p in Equation 6.5 then Equation 8.8 can be written as below.

$$S/N = 10 \log \left(\frac{1}{n} \sum_{i=1}^n \frac{1}{SL_p^2} \right) \quad (8.8)$$

S/N ratios are calculated as 66.16, 65.30 and 63.75 dB for ABS-ABS, PC-PC, and ABS-PC, respectively. Calculated predicted value of optimal lap joint shear loads and S/N ratios are shown in Table 8.23, 8.24 and 8.25, respectively.

8.1.10 Confirmation experiments of FSSW of ABS-ABS, PC-PC and ABS-PC joints

As the last step, the improvement of the weld strength must be verified using the optimum process parameters. The purpose of confirmation experiments is to examine and confirm the results achieved during the analysis.

If the optimum combination of parameters and their levels coincidentally match with one of the experiments in the orthogonal array then the confirmatory experiment is not necessary [72].

In this study for ABS-ABS, PC-PC, and ABS-PC joints, confirmation experiments are not required since the optimum combination of parameters and their levels ($A_1B_3C_3$, $A_3B_1C_3$ and $A_1B_1C_1$) already match with the experiments in the Taguchi's L_9 orthogonal array, respectively (Table 7.6).

8.1.11 Initial lap joint shear loads and improvements of ABS-ABS, PC-PC, and ABS-PC joints

The main effect graphs of the S/N ratios used when finding the optimum welding parameters are also used to find the initial lap joint shear load. The initial welding parameter levels of ABS-ABS, PC-PC, and ABS-PC joints are found as $A_2B_2C_2$, $A_2B_3C_1$, $A_3B_2C_3$, and these levels correspond to the lap joint shear load which are

closest to the average levels indicated by the dashed lines, respectively (Figure 8.34-8.36, 8.37-8.39 and 8.40-8.42). Table 8.20, 8.21 and 8.22 show the initial welding parameter levels of joints (ABS-ABS, PC-PC and ABS-PC), respectively.

Table 8.20 : Initial welding parameters and levels of ABS-ABS joint.

Symbol	Welding Parameters	Initial Welding Parameters and Levels		
		Levels		
A	Tool Rotational Speed	2	2000 rpm	A ₂ B ₂ C ₂
B	Plunge Depth	2	11 mm	
C	Dwell Time	2	40 s	

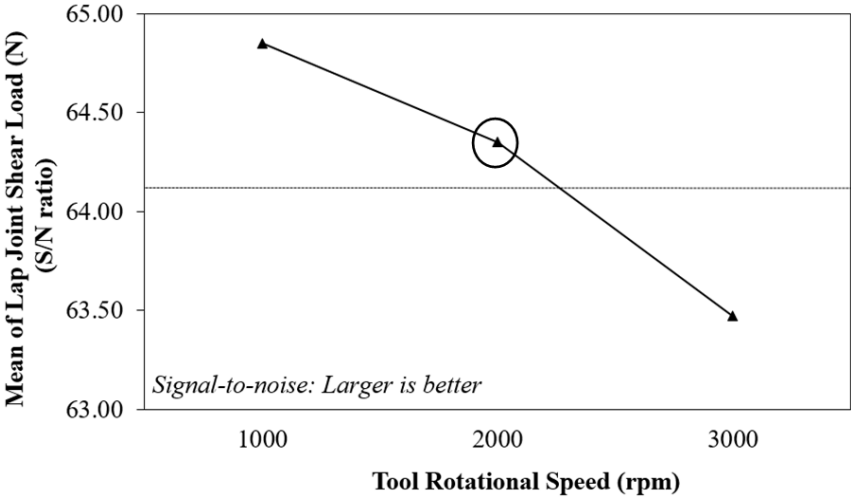


Figure 8.34 : Initial tool rotational speed-lap joint shear load graph of S/N ratios for ABS-ABS joint.

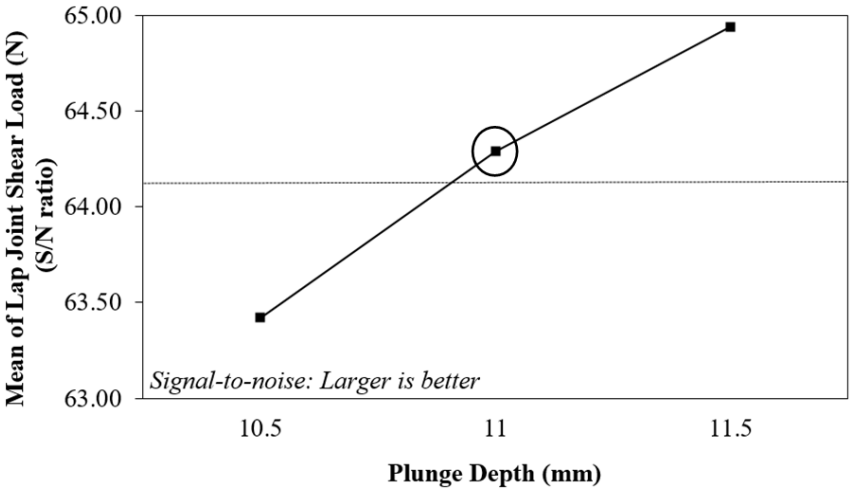


Figure 8.35 : Initial plunge depth-lap joint shear load graph of S/N ratios for ABS-ABS joint.

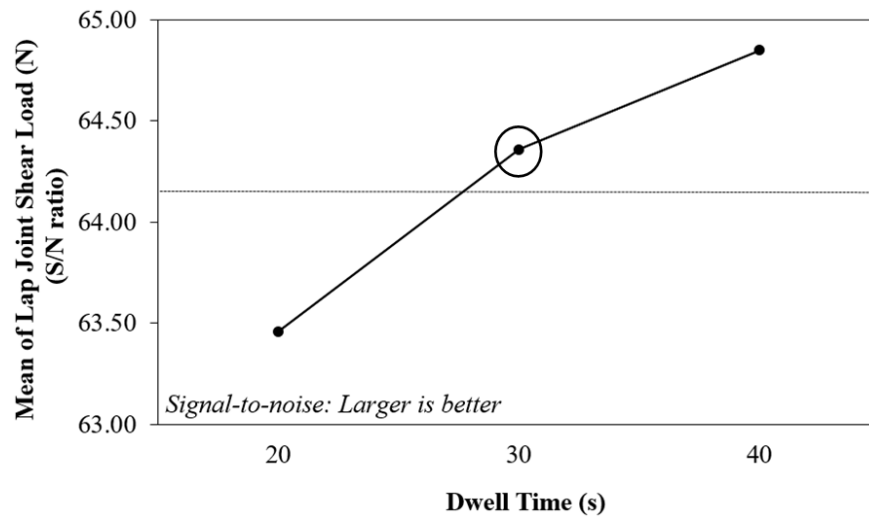


Figure 8.36 : Initial dwell time-lap joint shear load graph of S/N ratios for ABS-ABS joint.

Table 8.21 : Initial welding parameters and levels of PC-PC joint.

Symbol	Welding Parameters	Initial Welding Parameters and Levels		
		Levels		
A	Tool Rotational Speed	2	1600 rpm	A ₂ B ₃ C ₁
B	Plunge Depth	3	11.5 mm	
C	Dwell Time	1	20 s	

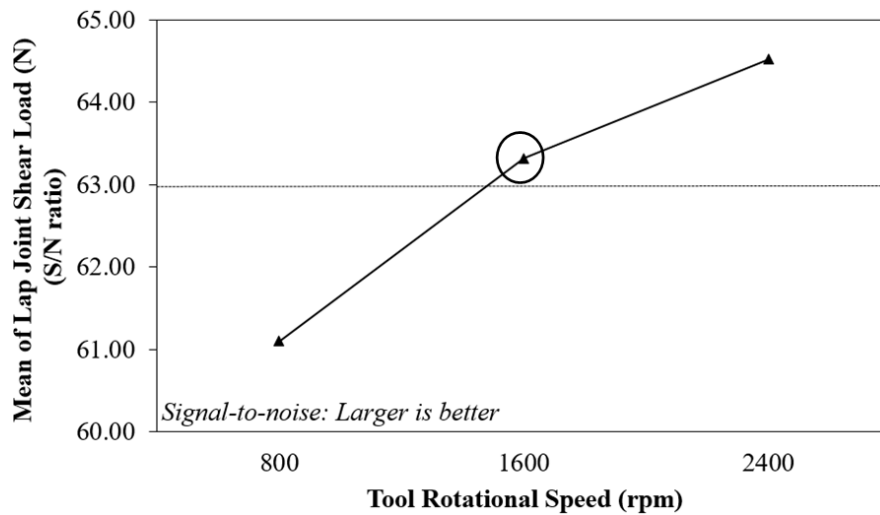


Figure 8.37 : Initial tool rotational speed-lap joint shear load graph of S/N ratios for PC-PC joint.

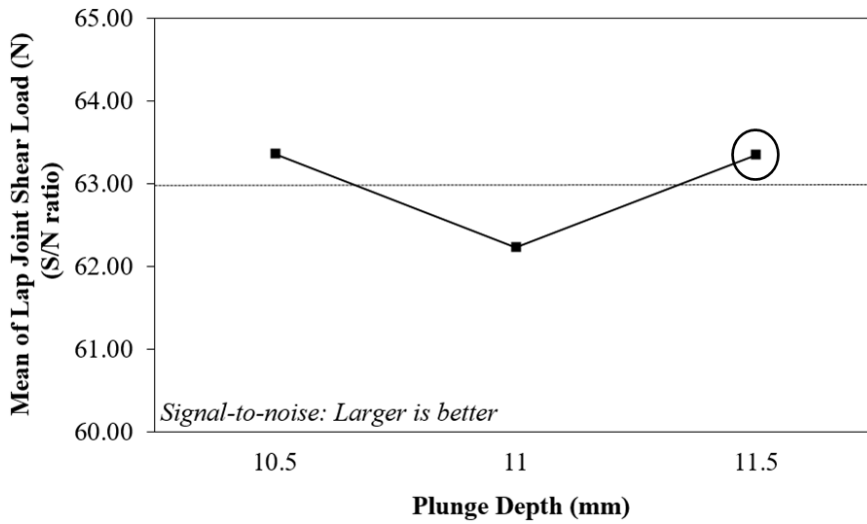


Figure 8.38 : Initial plunge depth-lap joint shear load graph of S/N ratios for PC-PC joint.

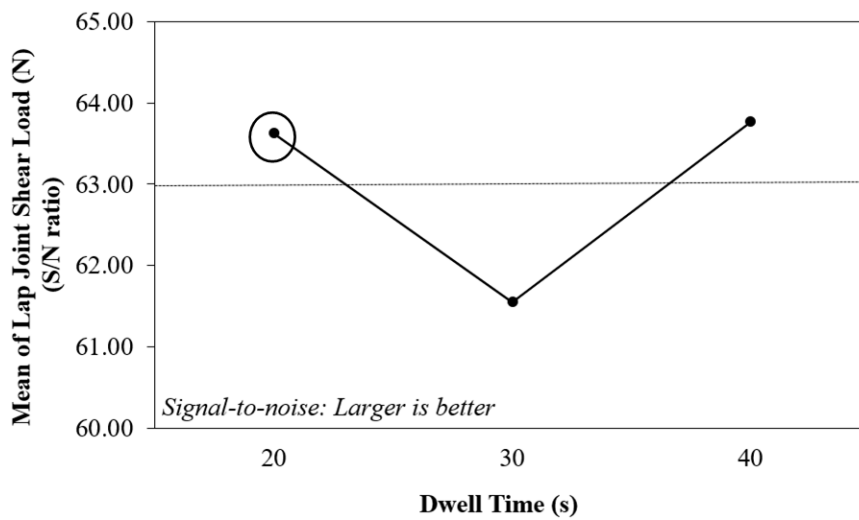


Figure 8.39 : Initial dwell time-lap joint shear load graph of S/N ratios for PC-PC joint.

Table 8.22 : Initial welding parameters and levels of ABS-PC joint.

Symbol	Welding Parameters	Initial Welding Parameters and Levels		
		Levels		
A	Tool Rotational Speed	3	2400 rpm	
B	Plunge Depth	2	11 mm	A ₃ B ₂ C ₃
C	Dwell Time	3	40 s	

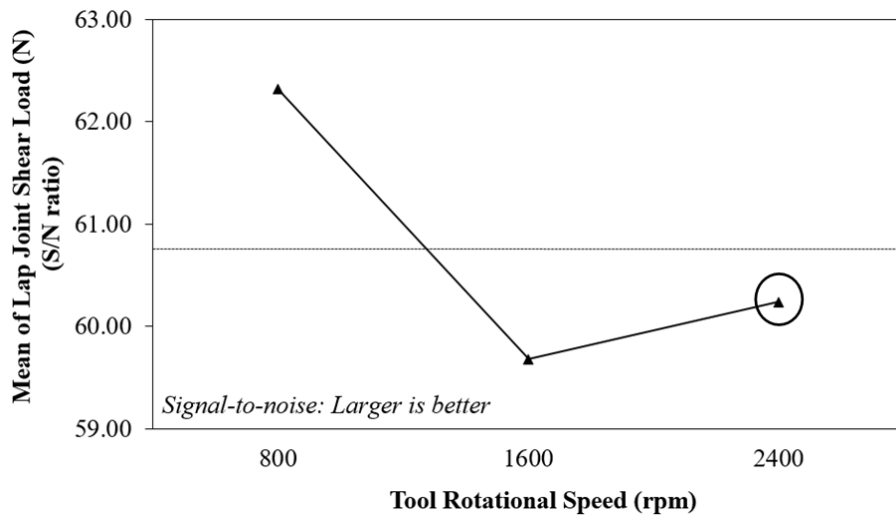


Figure 8.40 : Initial tool rotational speed-lap joint shear load graph of S/N ratios for ABS-PC joint

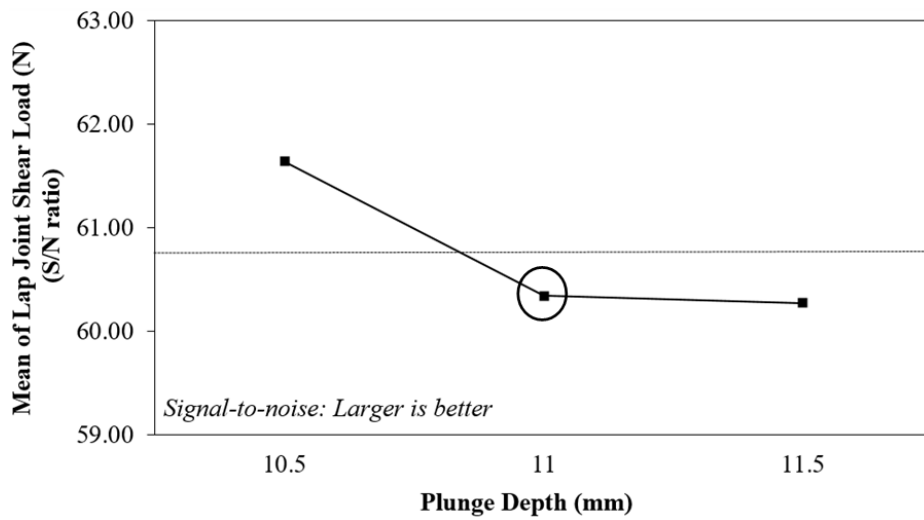


Figure 8.41 : Initial plunge depth-lap joint shear load graph of S/N ratios for ABS-PC joint.

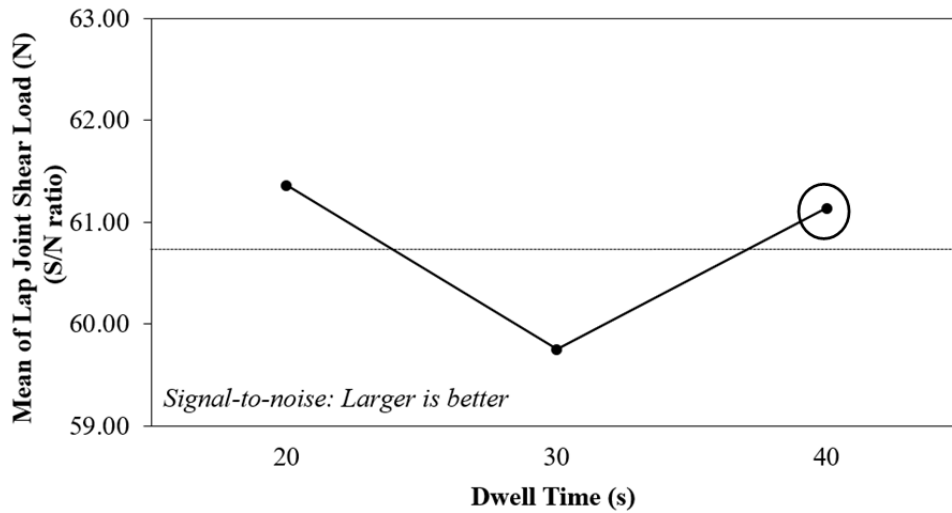


Figure 8.42 : Initial dwell time-lap joint shear load graph of S/N ratios for ABS-PC joint.

8.1.12 Calculations of initial lap joint shear loads of ABS-ABS, PC-PC and ABS-PC joints

After the initial welding parameters and levels have been determined, the way in the calculations of the optimum lap joint shear load is followed to calculate the initial lap joint shear load.

Calculation of initial lap joint shear load of ABS-ABS joint:

$$SL_i = A_2 + B_2 + C_2 - 2T_m \quad (8.9)$$

$$SL_i = 1655 + 1651 + 1656 - 2 \times 1638$$

$$SL_i = 1686 \text{ N}$$

Calculation of initial lap joint shear load of PC-PC joint:

$$SL_i = A_2 + B_3 + C_1 - 2T_m \quad (8.10)$$

$$SL_i = 1468 + 1475 + 1529 - 2(1439)$$

$$SL_i = 1594 \text{ N}$$

Calculation of initial lap joint shear load of ABS-PC joint:

$$SL_i = A_3 + B_2 + C_3 - 2T_m \quad (8.11)$$

$$SL_i = 1036 + 1040 + 1147 - 2(1107)$$

$$SL_i = 1009 \text{ N}$$

where T_m is overall average of lap shear fracture loads by obtained experiments.

S/N ratios are calculated using equation 6.5 and found 64.53, 64.05, 60.08 for FSSW of ABS-ABS, PC-PC and ABS-PC joints. Their initial lap joint shear loads and S/N ratios are shown in the Table 8.23-8.25, respectively.

8.1.13 Comparison of the results of ABS-ABS, PC-PC and ABS-PC joints

According to the results obtained from ABS-ABS, PC-PC and ABS-PC experiments, a 21%, 15%, and 57% increase in lap joint shear load was achieved. The S/N ratios were improved by 1.6, 1.2, 3.9 and the lap joint shear loads were increased by 340, 245, 572 from the initial welding parameters to the optimum welding parameters, respectively (Table 8.23-8.25).

Table 8.23 : Comparison of the results for ABS-ABS joint.

Parameter Levels	Initial Welding	Optimal Welding		Improvement
	Experimental	Prediction	Experimental	
	A ₂ B ₂ C ₂	A ₁ B ₃ C ₃	A ₁ B ₃ C ₃	21%
Lap Joint Shear Load (N)	1686	2032	2034	348
Calculated S/N Ratio (dB)	64.53	66.16	66.16	1.63

Table 8.24 : Comparison of the results for PC-PC joint.

Parameter Levels	Initial Welding	Optimal Welding		Improvement
	Experimental	Prediction	Experimental	
	A ₂ B ₃ C ₁	A ₃ B ₁ C ₃	A ₃ B ₁ C ₃	15%
Lap Joint Shear Load (N)	1594	1842	1840	245
Calculated S/N Ratio (dB)	64.05	65.30	65.29	1.24

Table 8.25 : Comparison of the results for ABS-PC joint.

Parameter Levels	Initial Welding	Optimal Welding		Improvement
	Experimental	Prediction	Experimental	
	A ₃ B ₃ C ₂	A ₁ B ₁ C ₁	A ₁ B ₁ C ₁	57%
Lap Joint Shear Load (N)	1009	1540	1581	572
Calculated S/N Ratio (dB)	60.08	63.75	63.98	3.90

8.2 Visual Examination and Morphological Analysis of Welded Joints of ABS-ABS, PC-PC, and ABS-PC

Weld morphology plays an important and decisive role in determining weld strength. It is clear that there is a strong relationship between the macrostructure of the welding zone and the mechanical properties of the welded joints.

Process parameters directly influence the morphologies of the welded specimens as well as mechanical properties. Figure 8.43 shows a schematical illustration of the cross-section of a friction stir spot welding joint.

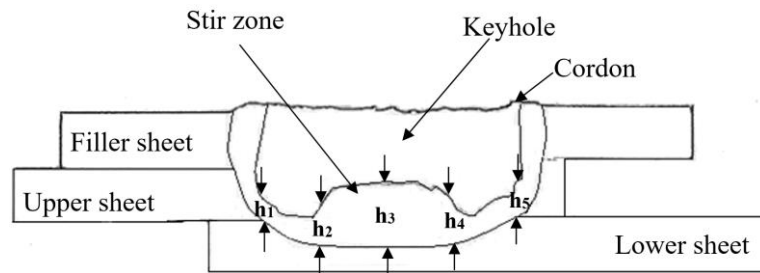


Figure 8.43 : The cross-sectional schematic view of the FSSW joint.

In FSSW, the center of the joint is called as stir zone (SZ) or weld nugget (Figure 8.43). The weld nugget means the weld bond in the FSSW joints. In addition, the cross-section area of a weld nugget provides an evaluation of the strength of weld specimens and their fracture morphology. In the welding process, the heated and softened sheet flowing radially and upward is penetrated by the rotating tool.

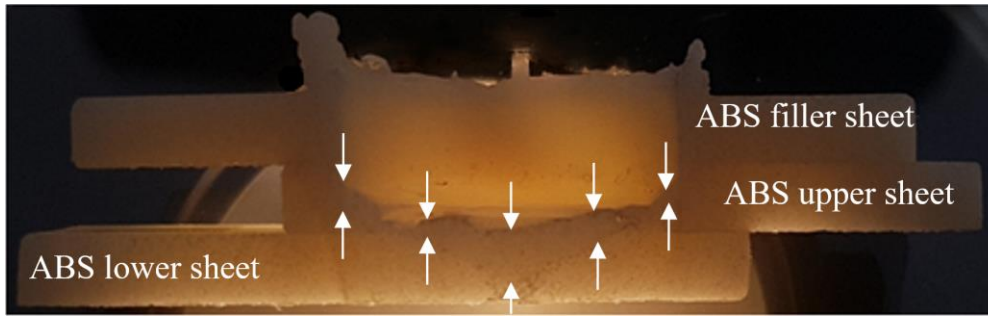
The particles of the molten materials are spun and extruded in the form of a cordon by the tool and ejected from the weld zone by inertial forces during the stirring process. Thus, the material loss increase with the forces in the weld area (Figure 8.43). A flow of the material is close to the movement of the tool. The designed threaded welding tool has capable of creating excessive friction heat and stirring, provides softening in the stirring zone and the nugget gets thicker.

A keyhole forms during the friction stir spot welding process. Upper and lower sheet materials are displaced upwards and outwards by the movement of the tool when the rotating pin forms the keyhole. After the retraction of the threaded pin tool, the keyhole remains at the weld area (Figure 8.43).

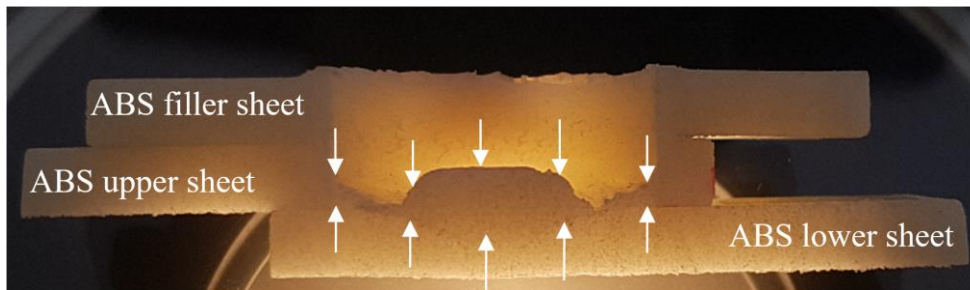
According to the cross-section of the weld specimens, measurements of the nugget heights (h_1 , h_2 , h_3 , h_4 , h_5) may indicate nugget cross-sectional area (Figure 8.43).

In order to measure the nugget heights and investigate the effects of the nugget heights on the joint strength, three welded specimens having the lowest, moderate and highest lap joint shear loads of ABS-ABS, PC-PC and ABS-PC joints are dissected by water jet cutting.

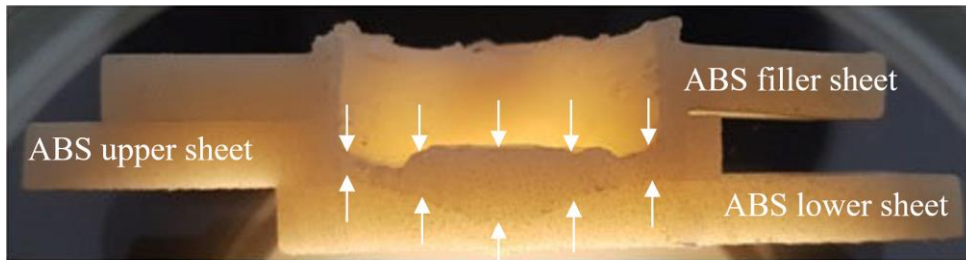
Figure 8.44 shows the cross-sectional views of ABS-ABS welded joints fabricated by using the same welding conditions for highest, moderate and lowest lap joint shear loads measured by the lap shear test.



a) Lowest lap joint shear load with 3000 rpm, 11 mm, 20 s



b) Moderate lap joint shear load with 2000 rpm, 11.5 mm, 20 s



c) Highest lap joint shear load with 1000 rpm, 11.5 mm, 40 s

Figure 8.44 : The cross-sectional macrostructures of ABS-ABS welded specimens for a) worst parameters b) moderate parameters and c) optimum parameters.

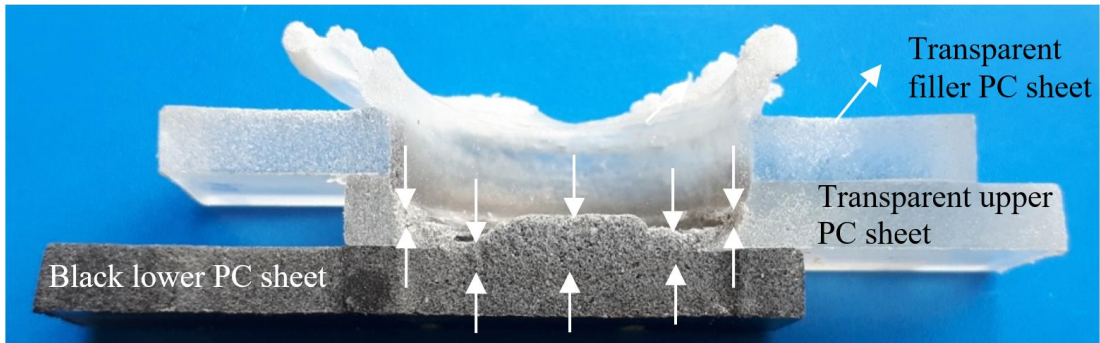
Table 8.26 : Nugget heights for ABS-ABS welded joints with the lowest, moderate, highest lap joint shear load.

Welded joints with different lap joint shear load	Nugget heights (mm)				
	h_1	h_2	h_3	h_4	h_5
Lowest	2.4	2.6	2.8	1.9	2.1
Moderate	2.3	3.4	4.8	3.3	2.3
Highest	2.5	3.5	4.9	3.4	2.4

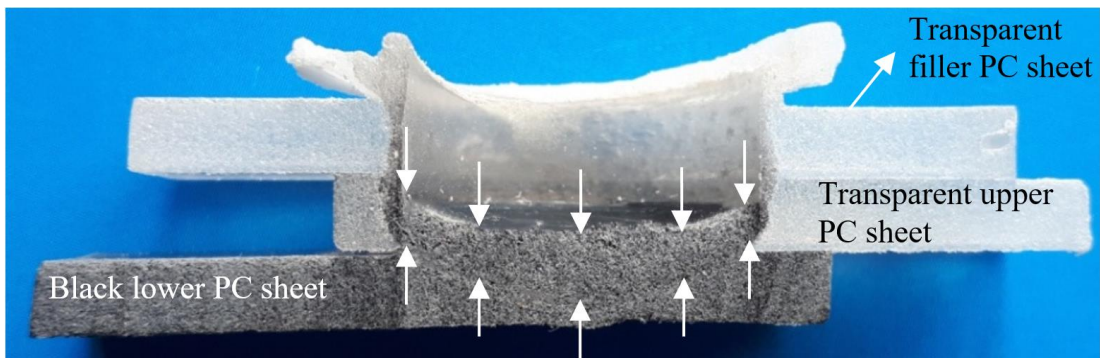
The nugget heights for three welded ABS-ABS specimens were measured from five different points to investigate differences of macrostructure characteristics (Table 8.26). The heights in Table 8.26 validate that while nugget heights are increasing, the lap joint shear loads increase. While maximum nugget heights were achieved for the welded joint by selecting lowest level of tool rotational speed (1000 rpm), high level of plunge depth (11.5 mm) and dwell times (40 s), the lowest nugget heights were obtained by selecting the highest level of tool rotational speed (3000 rpm), moderate level of plunge depth (11 mm) and lowest level of dwell time (20 s). This means that there is an expected relationship between the morphology of the welded joints and the weld strength. Also, keyhole size (Figure 8.44) in the stir zone of welded joint with the highest lap joint shear load (Figure 8.44 c) was smaller compared to the lowest and moderate welded joints (Figure 8.44 a,b). The cross-sectional appearances showed that with the decrease of the keyhole size, the lap joint shear load increased.

In PC-PC joints, to observe and evaluate produced specimens, 25.4 x 100 mm black lower PC sheet and natural PC upper sheet with transparent filler PC sheet have been overlapped by 25 mm in length. Thus, the fabricated specimens were used to investigate the effects of the nugget heights and show a mixture of the transparent PC and black PC sheets.

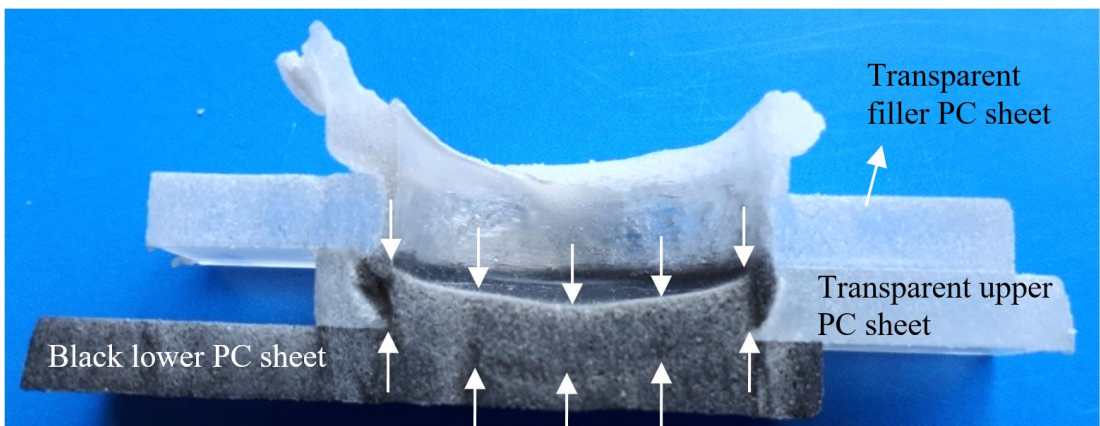
Figure 8.45 shows the cross-sectional appearances of welded joints produced by using the same welding conditions for which highest, moderate and lowest lap joint shear loads measured by the lap shear test. The nugget heights measured from five different points in stir zones for three welded specimens of PC-PC joints were tabulated in Table 8.27.



a) Lowest lap joint shear load with 800 rpm, 11 mm, 30 s



b) Moderate lap joint shear load with 1600 rpm, 11 mm, 40 s



c) Highest lap joint shear load with 2400 rpm, 10.5 mm, 40 s

Figure 8.45 : The cross-sectional macrostructures of PC-PC welded specimens for a) worst parameters b) moderate parameters and c) optimum parameters.

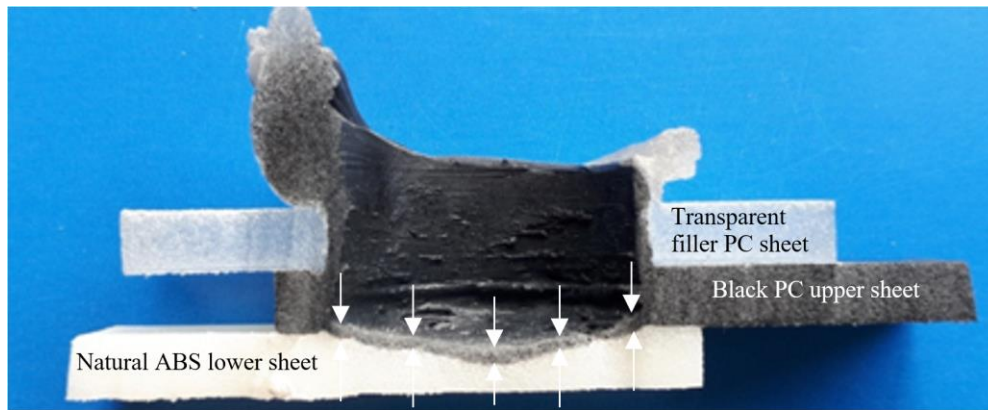
Table 8.27 : Nugget heights for PC-PC welded joints with the lowest, moderate, highest lap joint shear load.

Welded joints with different lap joint shear load	Nugget heights (mm)				
	h ₁	h ₂	h ₃	h ₄	h ₅
Lowest	1.4	2.3	3.4	2.1	1.3
Moderate	3.1	2.9	3.5	3.1	3.1
Highest	3.6	3.4	4.0	3.3	3.6

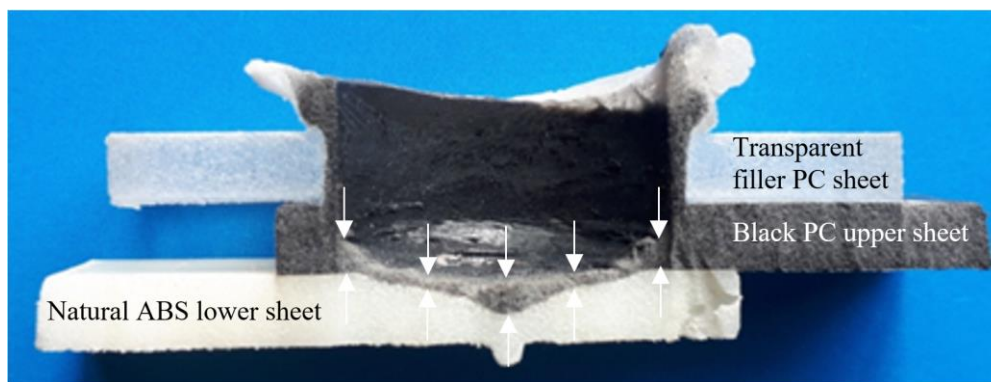
When the stir zone areas were compared, it was seen that the maximum nugget heights are obtained at optimum welding parameters. According to cross-section appearances of the FSSW joints, selection of the highest level of tool rotational speed (2400 rpm), and dwell time (40 s) and lowest level of plunge depth (10.5 mm) resulted in the highest lap joint shear load for the welded joint. However, the nugget height decreases from the cross-section of the highest lap joint shear load to the section of the lowest lap joint shear load as shown in Figure 8.45 a,b,c. In addition, keyhole size in the stir zone of welded joint with the highest lap joint shear load (Figure 8.45c) was smaller compared to the welded joint of lowest and moderate lap shear load (Figure 8.45 a,b). It is noticeable that increasing the keyhole size results in decreasing the lap joint shear load.

In ABS-PC joint similar to PC-PC joint, 25.4 x 100 mm black upper PC sheet and natural ABS lower sheet with transparent filler PC sheet have been overlapped by 25 mm in length to fabricate specimens for visual observations.

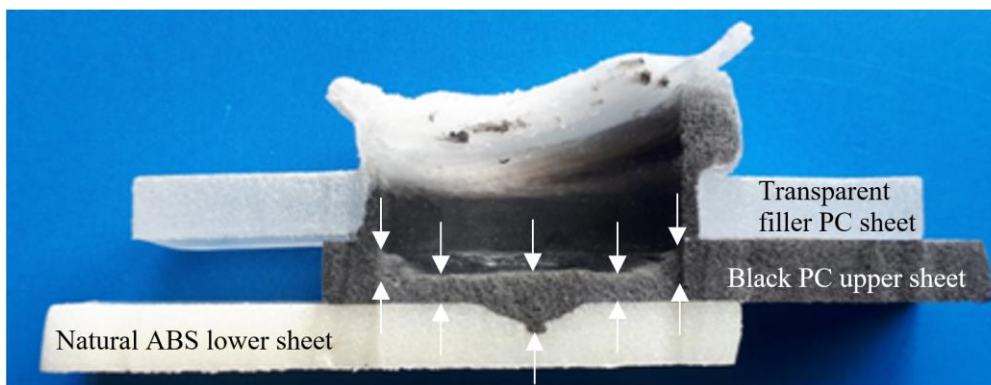
In Figure 8.46, the cross-sectional view of the ABS-PC joints and the mixing of these dissimilar materials during FSSW can be distinctly observed for the lowest, moderate and highest lap joint shear loads measured by lap shear tests. The macrostructures of three welded specimens were investigated in terms of five measurements of nugget heights from different points as shown in Table 8.28.



a) Lowest lap joint shear load with 2400 rpm, 11.5 mm, 30 s



b) Moderate lap joint shear load with 2400 rpm, 11 mm, 20 s



c) Highest lap joint shear load with 800 rpm, 10.5 mm, 20 s

Figure 8.46 : The cross-sectional macrostructures of ABS-PC welded specimens for a) worst parameters b) moderate parameters and c) optimum parameters.

Table 8.28 : Nugget heights for ABS-PC welded joints with the lowest, moderate, highest lap joint shear load.

Welded joints with different lap joint shear load	Nugget heights (mm)				
	h ₁	h ₂	h ₃	h ₄	h ₅
Lowest	1.1	0.7	1.5	0.8	1.1
Moderate	2.5	1.0	2.1	0.9	2.4
Highest	3.5	2.4	4.2	4.3	2.7

For ABS-PC joint, when the stir zone areas were compared, maximum nugget heights were achieved at optimum welding parameters. Thus, the highest lap joint shear load for the welded joint was obtained by selecting low levels of tool rotational speed (800 rpm), plunge depth (10.5 mm) and dwell times (20 s). When the welded joints are examined in terms of keyhole size, cross-section appearances of the welded joints proved that with the increase in keyhole sizes results in a decrease in lap joint shear load as seen in Figure 8.46 a, b, c.

ABS-ABS, PC-PC, and ABS-PC joints were compared visually for all three cases (lowest, moderate and highest lap joint shear loads). It was clearly seen that the welding macrostructures were influenced by process parameters. For all joints, higher nugget heights have been observed for the samples having the highest lap joint shear loads than samples having moderate and the lowest lap joint shear load, respectively. These macrostructure photographs prove the relationship between process parameters, parameter effects, morphology and hence lap joint shear load. Consequently, it was observed that the optimum process parameters positively affected weld morphologies for ABS-ABS, PC-PC and ABS-PC joints. In optimum process parameters of joints, the higher nugget heights led to increased in the lap joint shear loads (Figure 8.44, 8.45 and 8.46).

8.3 Effects of Process Parameters on Weld Strength for ABS-ABS, PC-PC, and ABS-PC Joints

8.3.1 Effect of tool rotational speed

Low tool rotational speeds generate insufficient frictional heat between the weld and base material. Therefore, lack of material flow occurs in the welding zone and causes low weld strength. However, excessive tool rotational speeds lead to overheating of

the tool and high inertial forces. So, the material gets parted by the tool and the joint strength decrease as a result of high inertial forces [66].

In the FSSW of ABS-ABS joint, it was observed lap shear fracture load decreased along with increase in tool rotational speed (Figure 8.1). The maximum lap joint shear load obtained at the tool rotational speed of 1000 rpm. The rotational speed of 1000 rpm among the designed experiment parameters had a strong joint by creating sufficient frictional heat for ABS-ABS welded specimens. High levels of the tool rotational speed of 2000 and 3000 rpm resulted in lower lap joint shear loads.

In the FSSW of PC-PC joint, there is a positive relationship between tool rotational speed and the lap joint shear load of welded specimens as shown in Figure 8.4. It can be seen an obvious improvement in the lap joint shear load with increasing the tool rotational speed. While the maximum lap joint shear load was obtained at the tool rotational speed of 2400 rpm, the minimum lap joint shear load was obtained at 800 rpm.

In the FSSW of ABS-PC joint, the maximum lap joint shear load was achieved at a tool rotational speed of 800 rpm. Moderate and lowest lap joint shear loads were obtained at the tool rotational speed of 2400 and 1600 rpm, respectively.

8.3.2 Effect of plunge depth

Increase in the plunge depth led to increased shoulder pressure between the shoulder bottom and the materials, thus, more frictional heat is generated. On the other hand, since the polymers have poor thermal conductivity, it is difficult to soften the overlapped interface by heat generated from the shoulder bottom and sufficient softening was only possible around the rotating pin [63]. In addition, increasing the plunge depth causes the enlargement of the bonded area since larger frictional heat is generated. However, excessive plunge depth leads to severe joint thickness reduction. Therefore, the joint fracture load decreases [61].

In the FSSW of ABS-ABS joint, the plunge depth dramatically affected joint strength and the lap joint shear load increased almost linearly with increase in plunge depth. The maximum lap joint shear load was obtained at 11.5 mm of plunge depth (Figure 8.2). As the penetration increases, more frictional heat is generated by the threaded tool pin and the pressure exerted by the tool shoulder. However, minimum lap joint shear load was obtained at 10.5 mm of plunge depth.

In the FSSW of PC-PC joint, while the minimum lap joint shear load was obtained at 11 mm of plunge depth, the highest lap joint shear load was obtained at 10.5 mm of plunge depth.

In the FSSW of ABS-PC joint, the plunge depth was found to be the least effective factor on the lap joint shear load and by further increasing the plunge depth from 10.5 mm to 11 mm, lap joint shear load decreases with a sharp slope compared to the lap joint shear loads at a depth between 11 mm and 11.5 mm. Thus, the maximum lap joint shear load was obtained at 10.5 mm of plunge depth.

8.3.3 Effect of dwell time

Lower dwell times lead to thin nugget thickness and less time to produce heat around the tool. When dwell time increases, the more frictional heat is generated between the sheets and the tool. The produced heat influences the material in the weld region and softens a large amount of the material [66]. In addition, increase in dwell time leads to increase in temperature and larger bonded area [65]. Dwell time has a positive influence on the weld strength. At longer dwell time, the increased bonded area diameter leads to higher lap shear tensile load. However, cavities occur at excessive dwell time. Also, the cavities are the reason for the incomplete joint between the base material and nugget. Furthermore, stress concentration is observed around the cavities and these stresses initiate the cracks very early. Prolonged tool stirring may cause strict scission of molecular chains and degrades the mechanical property of the nugget. Even though higher lap shear tensile loads can be obtained, the increased dwell time is not feasible [63].

In the FSSW of ABS-ABS joint, as shown in Figure 8.3, the increase in the levels of dwell time (from 20 s to 40 s) results in an increase in the lap joint shear load. Lower dwell times led to a reduction in the nugget height. Because the time required to produce the heat of friction was insufficient. When the longer dwell time was elapsed in the stirring zone, the nugget height increased because of the generation of more frictional heat and softening of materials. Consequently, increasing dwell time had an important effect on weld strength.

In the FSSW of PC-PC joint, while minimum lap joint shear load was obtained at 30 s, maximum lap joint shear load was achieved at 40 s. From 20 seconds to 40

seconds, it was seen that the lap joint shear load first decreased and then increased and reached its maximum value.

In the FSSW of ABS-PC joint, the highest lap joint shear load was obtained at the 20 s for dwell time. From 20 seconds to 40 seconds, the lap joint shear load first decreased and then increased.

8.4 Failure Modes of ABS-ABS, PC-PC and ABS-PC Joints

After the literature research, it was difficult to obtain high-quality joints in the FSSW process applied to polymers. In this study, although all samples were successfully welded, different welding qualities were observed in the experiments. Different failure modes have been revealed according to welding appearance and quality. Figure 8.47, 8.48 and 8.49 show the different failure modes for ABS-ABS, PC-PC, and ABS-PC joints, respectively. In fact, this classification of the welds demonstrates the relationship between process parameters and their influences on the weld strength.

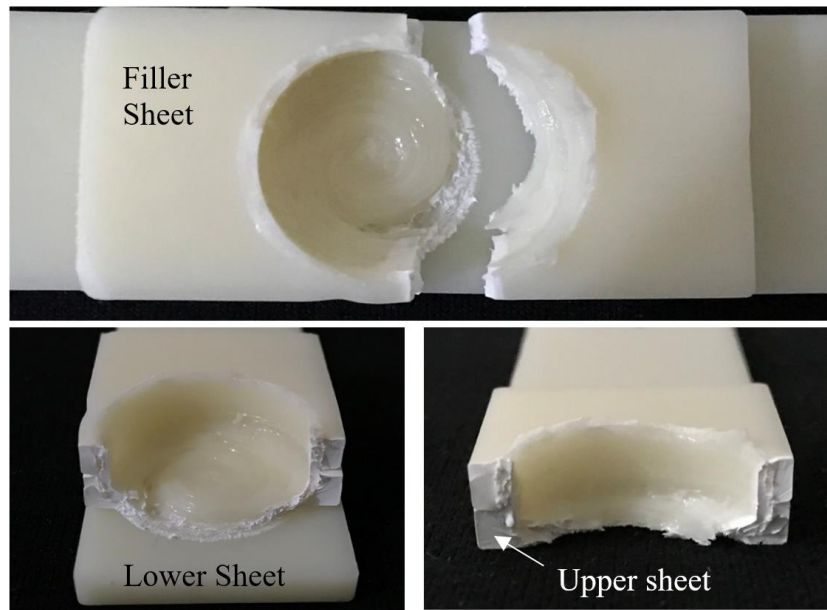
In ABS-ABS joint, three different failure modes were observed after the lap joint shear test of the samples as shown in Figure 8.47. The failure modes: upper sheet fracture, upper nugget fractures, and lower nugget fractures.

In the first failure mode, upper sheet fracture showing maximum lap joint shear load was obtained after the lap joint shear test and this type of failure was illustrated in Figure 8.47a. The separation of the stirred zone from the upper sheet shows strong adhesion in the stir zone due to the size of the nugget.

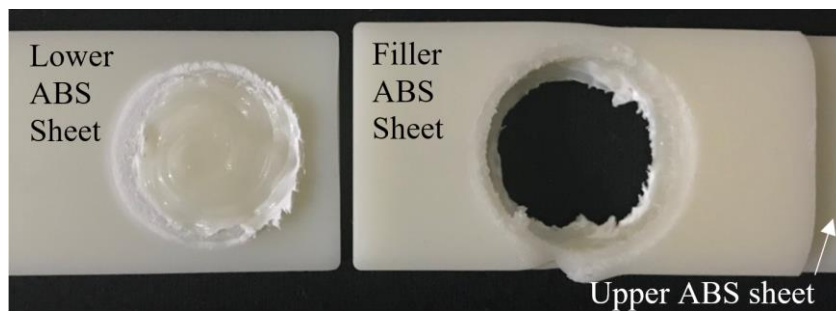
For the other failure modes (upper nugget and lower nugget failure) high lap joint shear load values were not observed like in the case of first failure mode due to the small bonded area and nugget height.

The second failure mode showed the moderate lap joint shear load and the joints were sheared off as called upper nugget failure (Figure 8.47b). This failure mode had smaller nugget heights than the first type of failure mode.

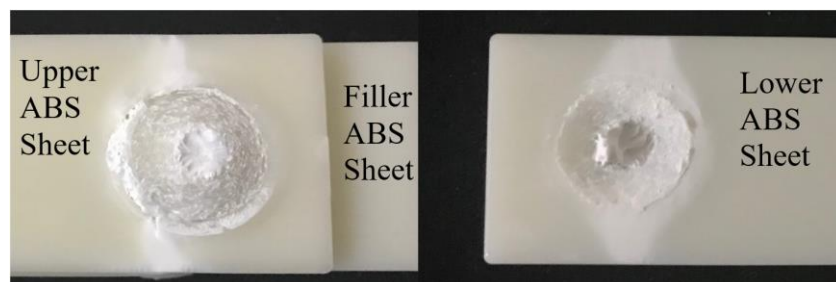
In the last type of failure mode, the smallest nugget was observed due to the insufficient dwell time (10s) to generate friction heat (Figure 8.47c). As a result, the lower nugget fracture had the lowest lap joint shear load after the tensile tests.



a) upper sheet fracture of ABS-ABS joint
(highest lap joint shear load of 2034 N with 1000 rpm, 11.5 mm, 40 s)



b) from the upper nugget fracture of ABS-ABS joint
(Moderate lap joint shear load of 1766 N with 2000 rpm, 11.5 mm, 20 s)



c) from the lower nugget fracture of ABS-ABS joint
(Lowest lap joint shear load of 1240 N with 3000 rpm, 11 mm, 20 s)

Figure 8.47 : Failure modes of ABS-ABS joints:
a) upper sheet fracture b) from the upper nugget fracture c) the lower nugget fracture.

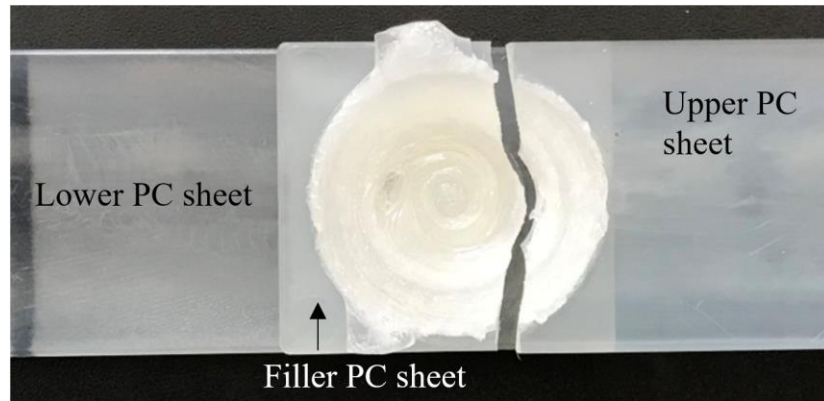
In the PC-PC joint, single lap shear tensile test is carried out to determine joint strength and then different fracture modes were identified, called as brittle fracture of upper sheet, shear fracture and cross nugget fracture from lower sheet.

Brittle fracture of the upper sheet was found in the welds under the optimum welding parameter conditions. So, the fracture was observed in the case of maximum lap joint shear load. These welds had a strong adhesion in the stirred zone.

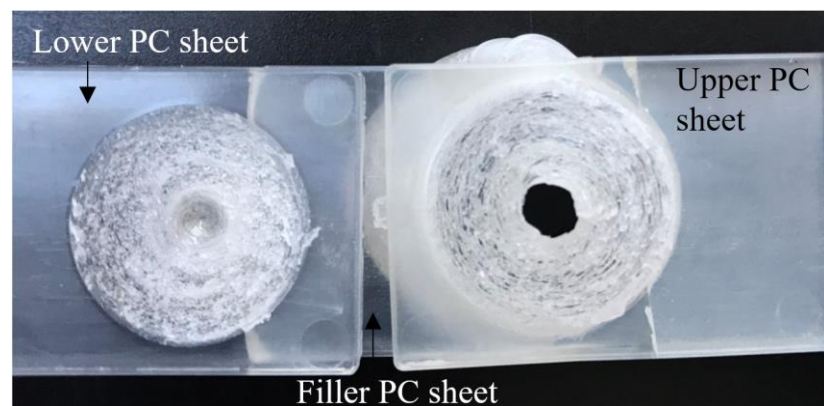
When Figure 8.45c is analyzed, cross-sectional appearances having the same welding parameters with the brittle fracture of upper sheets indicated the biggest nugget height compared to the others (Figure 8.45a, b). The maximum lap joint shear load was obtained in the brittle failure mode from the fracture surfaces in the upper sheet (Figure 8.48a).

Shear fracture is defined as shearing off at the periphery of lap interface of the joint due to tearing. Although the nugget size of the joint showed a big area, it has poor adhesion of the stirred zone (Figure 8.45b). So, moderate lap joint shear load was obtained in this type of fracture (Figure 8.48b).

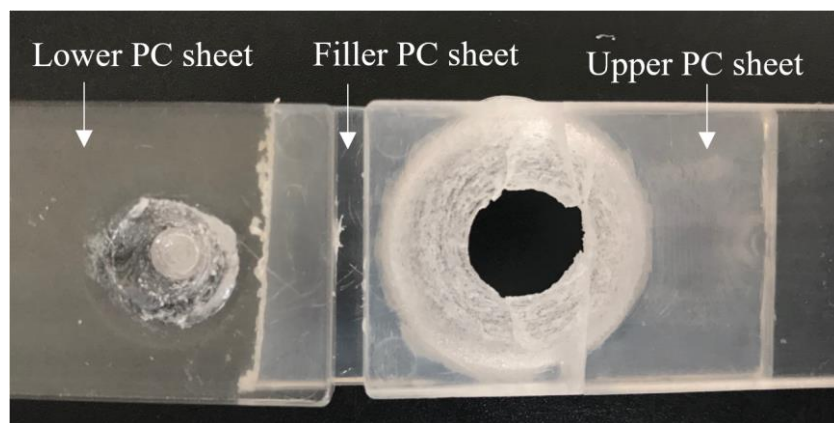
The last failure mode is cross nugget fracture from the lower sheet. It was observed thin nugget and very small bonded area compared to the shear fracture in this fracture mode. This phenomenon can be stated that obtained the cross-section sample under the same welding parameters with the cross nugget fracture from the lower sheet has the smallest nugget height (Figure 8.45a). So, minimum lap joint shear load was observed (Figure 8.48c).



a) Brittle fracture of upper sheet
(Highest lap joint shear load of 1909 N with 2400 rpm, 10.5 mm, 40 s)



b) Shear fracture
(Moderate lap joint shear load of 1718 N with 1600 rpm, 11 mm, 40 s)



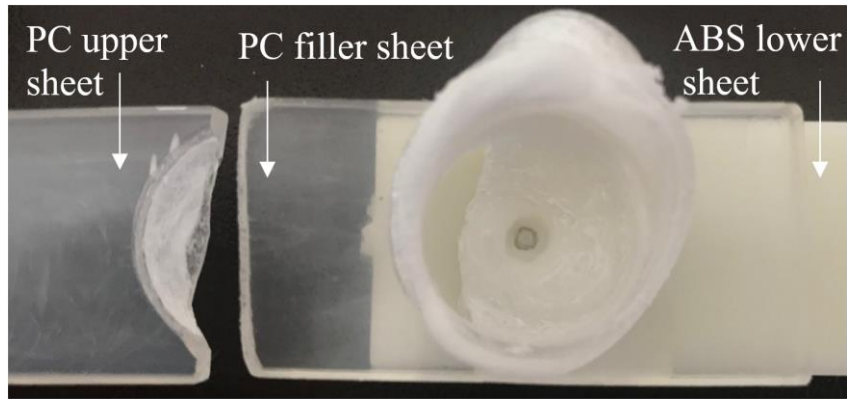
c) Cross nugget failure from lower sheet
(Lowest lap joint shear load of 1040 N with 800 rpm, 11 mm, 30 s)

Figure 8.48 : Failure modes of PC-PC joints:
a) upper sheet fracture b) the upper nugget fracture c) from the lower nugget fracture.

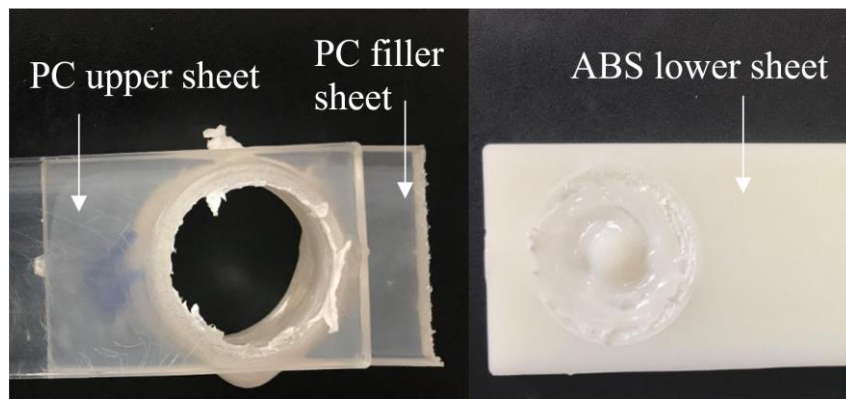
In the ABS-PC joint, two different failure modes were observed during the lap joint shear tests, namely upper sheet fracture and pull nugget from the upper sheet.

In the first type of fracture, welded PC and ABS sheets are separated from the PC upper sheet by fractured as illustrated in Figure 8.49a. This represents that the welded joints have a high lap joint shear load. Combined with the corresponding morphology (Figure 8.46c) as mentioned macrostructure analyzes, it was found that the weld nugget height was big enough, so a nugget fracture was not observed in the weld area.

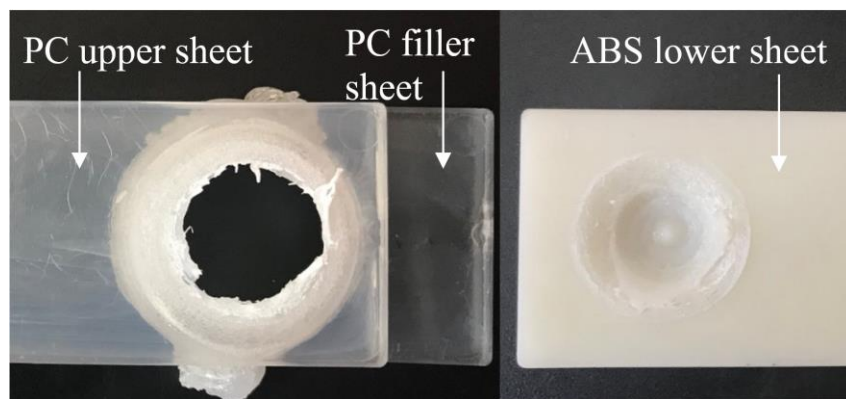
The second type of fracture, called as pull nugget from the upper sheet is shown in Figure 8.49 b,c and is defined as pulling out from the upper sheet. In this type of fracture, the weld nugget height is small and shows poor adhesion in the stir zone. Figure 8.49b has thicker nugget compared to Figure 8.49c. So, Figure 8.49b shows a good adhesion of the stir zone, when the nugget height was considered as shown in Figure 8.46b. In addition, the keyhole sizes as seen in Figure 8.49 b,c prove that lap joint shear load decrease with the increase of the keyhole in the stir zone.



a) Upper sheet fracture
 (Highest lap joint shear load of 1581 N with 800 rpm, 10.5 mm, 20 s)



b) Pull nugget from upper sheet
 (Moderate lap joint shear load of 1025 N with 2400 rpm, 11 mm, 20 s)



c) Pull nugget from lower sheet
 (Lowest lap joint shear load of 769 N with 2400 rpm, 11.5 mm, 30 s)

Figure 8.49 : Failure modes of ABS-PC joints:
 a) upper sheet fracture b) pull nugget from upper sheet c) from the lower nugget fracture.

9. CONCLUSIONS

Friction Stir Spot Welding of ABS-ABS, PC-PC, and ABS-PC joints were fabricated to find the influences of welding factors by introducing Taguchi experimental design method and optimization technique.

The friction stir spot welded ABS-ABS, PC-PC, and ABS-PC specimens were investigated to determine the lap joint shear load. As shown in the present study, the Taguchi method is applied systematically for evaluating the optimization of welded joints, reducing the number of experiments and time.

9.1. ABS-ABS joints

The following conclusions were achieved depending on the experimental results with the Taguchi study:

- The rotational speed, plunge depth and dwell time significantly influenced the ABS specimens. The most dominant parameter with a value of 37.8% was the plunge depth and this followed by dwell time of 31.5%, tool rotational speed of 30.6%, respectively.
- Experimental error was observed as only 0.1%. Therefore, it can be understood that the experimental design was very successful.
- Optimum level parameters were obtained to reach maximum weld strength by Taguchi experimental method. These are plunge rotational speed of 1000 rpm, plunge depth of 11.5 mm and dwell time of 40 s.
- The maximum lap joint shear load of 2034 N was obtained under the optimum welding parameter condition.
- The lap joint shear load of the optimum combination of parameters was predicted as 2032 N.

- Confirmation tests were not necessary because of the fact that the optimum combination of parameter levels coincidentally match with one of the experiments in the Taguchi L₉ orthogonal array. As a result of optimization, lap shear fracture load has improved 21%, which means an improvement in lap joint shear load from the initial welding parameters to the optimum welding parameters.
- The results of the experiments prove the efficiency of the robust Taguchi technique for optimization of the FSSW.
- It has been revealed that keyhole size was reduced and lap joint shear load was improved of the welded specimens by adding one layer filler sheet.
- Three different failure modes were observed: the separation of the stirred zone from the upper sheet, upper nugget fractures, and lower nugget fractures.

9.2 PC-PC Joints

The following main conclusions were obtained by the experimental and the analytic results:

- The result of ANOVA proved that the rotational speed was the most effective parameter with a value of 64.5% on weld quality and followed by dwell time with 29.6% and plunge depth with 5.4%.
- According to ANOVA results, the quadratic mathematical models allow prediction of weld parameter with a 99.5% confident interval. The experimental error was only 0.5% and this is an indication that the experimental design has been successfully implemented.
- The optimum combination of welding parameters was the rotational speed of 2400 rpm, the dwell time of 40 s, and the plunge depth of 10.5 mm.
- Improvement in S/N ratio is 1.24 dB and lap joint shear load was increased to 1840 N from the initial welding parameters to the optimum process parameters, which means also an improvement in weld strength by nearly 15 %.

- Keyhole size of welded areas was reduced with the help of an extra filler polycarbonate sheet which used in order to increase in lap joint shear load.
- The results verify that the Taguchi design methodology is very effective in optimizing the FSW process.

9.3 ABS-PC Joints

In this investigation, FSSW of PC to ABS sheets was performed by using one PC filler sheet. It was observed FSSW of these dissimilar materials is feasible. Also, the effect of friction stir spot welding parameters on weld strength was evaluated with the help of the Taguchi method.

The following conclusions can be drawn from this study based on the range of values of parameters considered:

- Results of ANOVA verified that the prediction of welding parameter with a 97.9% confident interval. The experimental error was only 2.1% and it proves that experimental design was applied very successfully.
- ANOVA results indicated that variable parameters of process including tool rotational speed, plunge depth and dwell time, dramatically affected the weld strength. According to lap joint shear load of welded specimens, it was found that the tool rotational speed is the most influencing parameter with a value of 56.8 % followed by the dwell time 21.6% and plunge depth 19.5%.
- Taguchi optimization technique was used to determine the optimum levels of welding parameters in FSSW of dissimilar materials. The optimum levels of the rotational speed, plunge depth and dwell time are 800 rpm, 10.5 mm and 20 s respectively.
- The improvement in the lap joint shear load from the initial welding parameters to the optimal welding parameters was calculated about 57% from 1009 N to 1581 N and increase in S/N ratio is 3.90 dB.
- Keyhole size was reduced compared to the classical FSSW process by adding PC filler sheet during the experiments. Also, the filler sheet provided increasing heights of nugget.

Further studies may consider evaluation of the effect of the different welding parameters on mechanical properties by using Taguchi methodology. In addition, the most common problem is the remaining keyhole in the friction stir spot welding process. Thus, different tool profiles and geometries can be used to minimize the size of the keyhole without using filler material and different welding apparatus can be designed to restrict material loss in the stirring zone.

REFERENCES

- [1] Vivaldo-Lima, E., & Saldívar-Guerra, E. (2013). *Handbook of polymer synthesis, characterization, and processing*. John Wiley & Sons, Incorporated.
- [2] Barmouz, M., Shahi, P., & Asadi, P. (2014). Friction stir welding/processing of polymeric materials. *Advances in friction stir welding and processing*. Woodhead publishing limited, Elsevier, 601-670.
- [3] Brinson, H. F., & Brinson, L. C. (2015). *Polymer engineering science and viscoelasticity*. New York, NY: Springer.
- [4] Raza, S. F. (2015). *Ultrasonic welding of thermoplastics* (Doctoral dissertation, University of Sheffield).
- [5] Ebewele, R. O. (2000). *Polymer science and technology*. CRC press.
- [6] Young, R. J., & Lovell, P. A. (2011). *Introduction to polymers*. CRC press.
- [7] Callister, W. D., & Rethwisch, D. G. (2007). *Materials science and engineering: an introduction* (Vol. 7, pp. 665-715). New York: John wiley & sons.
- [8] Fried, J. R. (2014). *Polymer science and technology*. Pearson Education.
- [9] Sercer, M., & Raos, P. (2007). *Joining of Plastics and Composites*. Universidade de Zagreb.
- [10] Chawla, K. K. (2012). *Composite materials: science and engineering*. Springer Science & Business Media.
- [11] Larson, E. R. (2015). *Thermoplastic Material Selection: A Practical Guide*. William Andrew.
- [12] Chanda, M. (2006). *Introduction to polymer science and chemistry: a problem-solving approach*. CRC Press.
- [13] Feldman, D. (2008). Polymer history. *Designed monomers and polymers*, 11(1), 1-15.
- [14] Amanat, N., James, N. L., & McKenzie, D. R. (2010). Welding methods for joining thermoplastic polymers for the hermetic enclosure of medical devices. *Medical engineering & physics*, 32(7), 690-699.
- [15] Crawford, R. J. (1998). *Plastics engineering*. Elsevier.
- [16] Moore, J. D. (1973). Acrylonitrile-butadiene-styrene (ABS) -a review. *Composites*, 4(3), 118-130.
- [17] Olivera, S., Muralidhara, H. B., Venkatesh, K., Gopalakrishna, K., & Vivek, C. S. (2016). Plating on acrylonitrile-butadiene-styrene (ABS) plastic: a review. *Journal of materials science*, 51(8), 3657-3674.
- [18] Johansson, I. (2004). Kirk-Othmer Encyclopedia of Chemical Technology. *John Willy & Sons, Inc*, 6, 812-832.
- [19] Biron, M. (2018). *Thermoplastics and thermoplastic composites*. William Andrew.
- [20] Billmeyer, F. W., & Billmeyer, F. W. (1984). *Textbook of polymer science* (Vol. 19842, pp. 361-484). New York: Wiley.
- [21] Kutz, M. (Ed.). (2011). *Applied plastics engineering handbook: processing and materials*. William Andrew.
- [22] Amancio-Filho, S. T., & Dos Santos, J. F. (2009). Joining of polymers and polymer-metal hybrid structures: recent developments and trends. *Polymer Engineering & Science*, 49(8), 1461-1476.
- [23] Strand, S. (2003, September). Joining plastics-can friction stir welding compete? In *Proceedings: Electrical Insulation Conference and Electrical*

- Manufacturing and Coil Winding Technology Conference (Cat. No. 03CH37480)* (pp. 321-326). IEEE.
- [24] Stokes, V. K. (1989). Joining methods for plastics and plastic composites: an overview. *Polymer Engineering & Science*, 29(19), 1310-1324.
- [25] Messler, R. W. (2004). *Joining of materials and structures: from pragmatic process to enabling technology*. Butterworth-Heinemann.
- [26] Vendan, S. A., Natesh, M., Garg, A., & Gao, L. (2019). *Confluence of Multidisciplinary Sciences for Polymer Joining*. Springer Singapore.
- [27] Besharati-Givi, M. K., & Asadi, P. (2014). *Advances in friction-stir welding and processing*. Elsevier.
- [28] Mahoney, M. W., & Mishra, R. S. (2007). *Friction stir welding and processing*. ASM International.
- [29] Huang, Y., Meng, X., Xie, Y., Wan, L., Lv, Z., Cao, J., & Feng, J. (2018). Friction stir welding/processing of polymers and polymer matrix composites. *Composites Part A: Applied Science and Manufacturing*, 105, 235-257.
- [30] Troughton, M. J. (2008). *Handbook of plastics joining: a practical guide*. William Andrew.
- [31] Ratanathavorn, W. (2012). Hybrid joining of aluminum to thermoplastics with friction stir welding.
- [32] Mubiayi, M. P., Akinlabi, E. T., & Makhatha, M. E. (2018). *Current Trends in Friction Stir Welding (FSW) and Friction Stir Spot Welding (FSSW): An Overview and Case Studies* (Vol. 6). Springer.
- [33] Yuan, W. (2008). Friction stir spot welding of aluminum alloys.
- [34] Yang, X. W., Fu, T., & Li, W. Y. (2014). Friction stir spot welding: a review on joint macro-and microstructure, property, and process modelling. *Advances in Materials Science and Engineering*, 2014.
- [35] Sunil, B. R. (2019). *Surface Engineering by Friction-Assisted Processes: Methods, Materials, and Applications*. CRC Press.
- [36] Pan, T. Y. (2007). *Friction Stir Spot Welding (FSSW)-A Literature Review* (No. 2007-01-1702). SAE Technical Paper.
- [37] Cox, C. D., Gibson, B. T., Strauss, A. M., & Cook, G. E. (2012). Effect of pin length and rotation rate on the tensile strength of a friction stir spot-welded Al alloy: a contribution to automated production. *Materials and Manufacturing Processes*, 27(4), 472-478.
- [38] Devaiah, D., Kishore, K., & Laxminarayana, P. (2018). Optimal FSW process parameters for dissimilar aluminium alloys (AA5083 and AA6061) Using Taguchi Technique. *Materials Today: Proceedings*, 5(2), 4607-4614.
- [39] Zhang, Z., Yang, X., Zhang, J., Zhou, G., Xu, X., & Zou, B. (2011). Effect of welding parameters on microstructure and mechanical properties of friction stir spot welded 5052 aluminum alloy. *Materials & Design*, 32(8-9), 4461-4470.
- [40] Bilici, M. K. (2012). Application of Taguchi approach to optimize friction stir spot welding parameters of polypropylene. *Materials & Design*, 35, 113-119.
- [41] Jambhale, S., Kumar, S., & Kumar, S. (2015). Effect of process parameters & tool geometries on properties of friction stir spot welds: a review. *Universal Journal of Engineering Science*, 3(1), 6-11.
- [42] Lin, P. C., Pan, J., & Pan, T. (2008). Failure modes and fatigue life estimations of spot friction welds in lap-shear specimens of aluminum 6111-T4 sheets.

- Part 2: Welds made by a flat tool. *International Journal of Fatigue*, 30(1), 90-105.
- [43] Su, P., Gerlich, A., North, T. H., & Bendzsak, G. J. (2006). Energy utilisation and generation during friction stir spot welding. *Science and Technology of Welding and Joining*, 11(2), 163-169.
- [44] Tozaki, Y., Uematsu, Y., & Tokaji, K. (2007). Effect of tool geometry on microstructure and static strength in friction stir spot welded aluminium alloys. *International Journal of Machine Tools and Manufacture*, 47(15), 2230-2236.
- [45] Mubiayi, M. P., & Akinlabi, E. T. (2015). An overview on friction stir spot welding of dissimilar materials. In *Transactions on engineering technologies* (pp. 537-549). Springer, Dordrecht.
- [46] Wang, D. A., & Lee, S. C. (2007). Microstructures and failure mechanisms of friction stir spot welds of aluminum 6061-T6 sheets. *Journal of Materials Processing Technology*, 186(1-3), 291-297.
- [47] Yang, Q., Mironov, S., Sato, Y. S., & Okamoto, K. (2010). Material flow during friction stir spot welding. *Materials Science and Engineering: A*, 527(16-17), 4389-4398.
- [48] Jambhale, S., Kumar, S., & Kumar, S. (2015). Effect of process parameters & tool geometries on properties of friction stir spot welds: a review. *Universal Journal of Engineering Science*, 3(1), 6-11.
- [49] Jambhale, S., Kumar, S., & Kumar, S. (2015). Effect of process parameters & tool geometries on properties of friction stir spot welds: a review. *Universal Journal of Engineering Science*, 3(1), 6-11.
- [50] Arıcı, A., & Mert, Ş. (2008). Friction stir spot welding of polypropylene. *Journal of Reinforced Plastics and Composites*, 27(18), 2001-2004.
- [51] Mert, Ş., & Arıcı, A. (2011). Design of optimal joining for friction stir spot welding of polypropylene sheets. *Science and Technology of Welding and Joining*, 16(6), 522-527.
- [52] Bilici, M. K. (2012). Effect of tool geometry on friction stir spot welding of polypropylene sheets. *Express Polymer Letters*, 6(10).
- [53] Bilici MK, Yukler AI, Kastan A (2014) Effect of the tool geometry and welding parameters on the macrostructure, fracture mode and weld strength of friction-stir spot-welded polypropylene sheets. *Mater Tehnol* 48:705–711
- [54] Kurtulmus, M. (2012). Friction stir spot welding parameters for polypropylene sheets. *Scientific Research and Essays*, 7(8), 947-956.
- [55] Bilici, M. K., Yüklér, A. İ., & Kurtulmuş, M. (2011). The optimization of welding parameters for friction stir spot welding of high density polyethylene sheets. *Materials & Design*, 32(7), 4074-4079.
- [56] Bilici, M. K., & Yüklér, A. I. (2012). Influence of tool geometry and process parameters on macrostructure and static strength in friction stir spot welded polyethylene sheets. *Materials & Design*, 33, 145-152.
- [57] Bilici, M. K., & Yüklér, A. I. (2012). Effects of welding parameters on friction stir spot welding of high density polyethylene sheets. *Materials & Design*, 33, 545-550.
- [58] Lambiase, F., Paoletti, A., & Di Ilio, A. (2016). Effect of tool geometry on loads developing in friction stir spot welds of polycarbonate sheets. *The International journal of advanced manufacturing technology*, 87(5-8), 2293-2303.

- [59] Paoletti, A., Lambiase, F., & Di Ilio, A. (2015). Optimization of friction stir welding of thermoplastics. *Procedia CIRP*, 33, 562-567.
- [60] Lambiase, F., Paoletti, A., & Di Ilio, A. (2017). Friction spot stir welding of polymers: control of plunging force. *The International Journal of Advanced Manufacturing Technology*, 90(9-12), 2827-2837.
- [61] Lambiase, F., Paoletti, A., & Di Ilio, A. (2017). Effect of tool geometry on mechanical behavior of friction stir spot welds of polycarbonate sheets. *The International Journal of Advanced Manufacturing Technology*, 88(9-12), 3005-3016.
- [62] Lambiase, F., Paoletti, A., & Di Ilio, A. (2015). Mechanical behaviour of friction stir spot welds of polycarbonate sheets. *The International Journal of Advanced Manufacturing Technology*, 80(1-4), 301-314.
- [63] Yan, Y., Shen, Y., Zhang, W., & Hou, W. (2018). Friction stir spot welding ABS using triflute-pin tool: Effect of process parameters on joint morphology, dimension and mechanical property. *Journal of Manufacturing Processes*, 32, 269-279.
- [64] Yan, Y., Shen, Y., Hou, W., & Li, J. (2018). Friction stir spot welding thin acrylonitrile butadiene styrene sheets using pinless tool. *The International Journal of Advanced Manufacturing Technology*, 97(5-8), 2749-2755.
- [65] Yan, Y., Shen, Y., Lei, H., & Zhuang, J. (2019). Influence of welding parameters and tool geometry on the morphology and mechanical performance of ABS friction stir spot welds. *The International Journal of Advanced Manufacturing Technology*, 1-12.
- [66] Dashatan, S. H., Azdast, T., Ahmadi, S. R., & Bagheri, A. (2013). Friction stir spot welding of dissimilar polymethyl methacrylate and acrylonitrile butadiene styrene sheets. *Materials & Design*, 45, 135-141.
- [67] Mitra, S., Acherjee, B., Kuar, A. S., & Misra, D. (2011). Experimental investigation on diode laser welding of polycarbonate to ABS. *Power*, 2(1), 0.
- [68] Koziel, S., Ciaurri, D. E., & Leifsson, L. (2011). Surrogate-based methods. In *Computational optimization, methods and algorithms* (pp. 33-59). Springer, Berlin, Heidelberg.
- [69] Saravanan, R. (2017). *Manufacturing Optimization through Intelligent Techniques (2006)*. CRC Press.
- [70] Rao, S. S. (2019). *Engineering optimization: theory and practice*. John Wiley & Sons.
- [71] Mukherjee, I., & Ray, P. K. (2006). A review of optimization techniques in metal cutting processes. *Computers & Industrial Engineering*, 50(1-2), 15-34.
- [72] Roy, R. K. (2010). *A primer on the Taguchi method*. Society of Manufacturing Engineers.
- [73] PM, G. (2004). Machinability analysis of carbon carbon composites using EDM.
- [74] Prior, J. F. G. D. (2015). Application and Optimization of Friction Stir Welding on Electrical Transformers Components.
- [75] Kadu, R., Deshpande, V.S., Thobani S. and Dorle, S.A. (2009)s, "Optimization of Boring Process parameters Using Taguchi Design of Experiment", *Udyog Pragati*, Vol.33, No. 4, pp.13-17
- [76] Antony, J., Warwood, S., Fernandes, K., & Rowlands, H. (2001). Process optimisation using Taguchi methods of experimental design. *Work Study*, 50(2), 51-58.
- [77] Kemmler, S., Fuchs, A., Leopold, T., & Bertsche, B. (2015). Comparison of Taguchi Method and Robust Design Optimization (RDO): by application of a

functional adaptive simulation model for the robust product-optimization of an adjuster unit.

- [78] Gundlach, C. (2004). *Entwicklung eines ganzheitlichen Vorgehensmodells zur problemorientierten Anwendung der statistischen Versuchsplanung* (p. 33). Kassel University Press.
- [79] Phadke, M. S. (1995). *Quality engineering using robust design*. Prentice Hall PTR.
- [80] Akbari, M., Asadi, P., Besharati Givi, M. K., & Khodabandehlouie, G. (2014). Artificial neural network and optimization. *Advances in friction-stir welding and processing*. Woodhead Publishing, 543-599.
- [81] Mishra, A. (2012). Evaluation of the impact of Taguchi methods on product process parameters optimization.
- [82] Fisher, R. A. (1925). *Statistical methods for research workers* Oliver and Boyd. Edinburgh, Scotland, 6.
- [83] Phadke, M. S. (1989). Quality engineering using design of experiments. In *Quality control, robust design, and the Taguchi method* (pp. 31-50). Springer, Boston, MA.
- [84] Davis, R., & John, P. (2018). Application of Taguchi-Based Design of Experiments for Industrial Chemical Processes. *Statistical Approaches With Emphasis on Design of Experiments Applied to Chemical Processes*, 137.
- [85] Arici, A., & Sinmazçelýk, T. (2005). Effects of double passes of the tool on friction stir welding of polyethylene. *Journal of materials science*, 40(12), 3313-3316.
- [86] Shojaeefard, M. H., Khalkhali, A., Akbari, M., & Tahani, M. (2013). Application of Taguchi optimization technique in determining aluminum to brass friction stir welding parameters. *Materials & Design* (1980-2015), 52, 587-592.
- [87] Taguchi, G., Chowdhury, S., & Wu, Y. (2005). *Taguchi's quality engineering handbook*. Wiley.
- [88] Fisher, R. A. (1935). *The Design of Experiments*. Cited according to the 8th ed.

CURRICULUM VITAE

Name Surname: Asil AYZ

Place and Date of Birth: İzmir, 21.05.1993

Education

M.Sc. : 2019, Mechanical Engineering, İzmir Katip Çelebi University

B.Sc. : 2016, Mechanical Engineering, Ege University

Professional Experiences

Research Assistant: İzmir Katip Çelebi University, Mechanical Engineering Department, (2018-Present)

Mechanical Design Engineer : Vestel, R&D (2017-2018)